NASA Contractor Report 4732

Advanced Technology Composite Fuselage—Structural Performance

T. H. Walker, P. J. Minguet, B. W. Flynn, D. J. Carbery, G. D. Swanson, and L. B. Ilcewicz
The Boeing Company • Seattle, Washington

National Aeronautics and Space Administration
Langley Research Center • Hampton, Virginia 23681-0001

Prepared for Langley Research Center
under Contracts NAS1-18889 and NAS1-20013

April 1997

Printed copies available from the following:

NASA Center for AeroSpace Information
800 Elkridge Landing Road
Linthicum Heights, MD 21090-2934
(301) 621-0390

FOREWORD

This document is one of nine complementary final technical reports on the development of advanced composite transport fuselage concepts. The work described was performed by the Boeing Commercial Airplane Group, Seattle, Washington, from May 1989 through December 1995 under contracts NAS1-18889 and NAS1-20013, Task 2. The contracts were sponsored by the National Aeronautics and Space Administration, Langley Research Center (NASA-LaRC) as part of the Advanced Composite Technology (ACT) program. Direction from NASA-LaRC was provided by M.J. Shuart, J.G. Davis, W.T. Freeman, and J.B. Nelson.

The nine documents comprising the final documentation for the NASA/Boeing ATCAS program include:

Advanced Technology Composite Fuselage

- **Program Overview** (CR-4734). *Synopsis of program approach, timeline and significant findings. Design synthesis considering manufacturing, materials, processes, structural performance, maintenance, and cost.*
- **Manufacturing** (CR-4735). *Baseline manufacturing and assembly approaches. Process and tooling developments, and manufacturing demonstration activities to address critical manufacturing issues.*
- **Materials and Processes** (CR-4731). *Baseline and alternative materials and processes. Material and process developments. Material performance.*
- **Structural Performance** (CR-4732). *Methods used for design sizing. Analysis and test activities supporting assessment of design development methodologies for critical performance issues.*
- **Repair and Damage Assessment Supporting Maintenance** (CR-4733). *Maintenance considerations in design. Detailed repair concepts for quadrant design. Fabrication, inspection, and analytical developments.*

Cost Optimization Software for Transport Aircraft Design Evaluation (COSTADE)

- **Overview** (CR-4736). *Synopsis of COSTADE initiative, including integration of cost, weight, manufacturing, design, structural analysis, load redistribution, optimization, and blending.*
- **Design Cost Methods** (CR-4737). *Components of cost analysis and their interactions. Theoretical framework for process-time prediction. Methods for developing and maintaining cost equations. Applications to ATCAS quadrant designs.*
- **User's Manual** (CR-4738). *COSTADE user instructions, including hardware requirements and installation procedures. Program structure, capabilities, and limitations. Basis of cost model and structural analysis routines. Example problems.*
- **Process Cost Analysis Database** (CR-4739). *Rationale for database framework. Database user's guide, including capabilities and limitations. ATCAS process step equations.*

Use of commercial products or names of manufacturers in this report does not constitute official endorsement of such products or manufacturers, either expressed or implied, by the Boeing Company or the National Aeronautics and Space Administration.

At completion of these contracts, Boeing program management included Bjorn Backman as Program Manager, Peter Smith as Technical Manager, and Larry Ilcewicz as Principal Investigator. Authors listed for this contractor report prepared portions of the document. The members (past and present) of the Boeing ACT contract team who contributed to the work described in this document include:

Program Management:
Phil Whalley
Ron Johnson
Ray Horton
Jordan Olson
Bjorn Backman

Technical Management:
Peter Smith

Principal Investigators:
Randy Coggeshall
Larry Ilcewicz

Structural Design:
George Truslove
Chris Hanson
Ken Griess
Mike Schram
Stephen Metschan
Mike Morris
Tuan Le

Computing Support:
Bob Lundquist
Bill Koch
Sterling Johnston

Structural Analysis:
Tom Walker
Ernie Dost
Gary Swanson
Blake Flynn
Gerald Mabson
David Carbery
Scott Finn
Dan Murphy
Bernhard Dopker
David Polland
William Avery
Jerry Bodine
Doug Graesser
Andre Williams
Mark Fedro
Peter Grant
Adam Sawicki
Pierre Minguet

Technical Aide:
Bill Waltari

Materials and Processes:
Dodd Grande
David Scholz
Karl Nelson
Tony Falcone
Brian Perkins

Manufacturing Technology:
Tom May
Kurtis Willden
Val Starkey
Tim Davies
Mark Gessel
Joe Hafenrichter
Bob Matetich
Ken Goodno
Dick Curran
Ken Dull
Rob Biornstad
Peter Lohr
Stan Stawski
Chris Harris
Greg Bell
Jan Koontz
Rob Synder
Tom Cundiff
Gary Moon

Cost Analysis:
Kent Venters
Will Gaylord
Cal Pfahl
David Tervo
Len Witonsky
Odo Bormke
Robert Humphrey
Michael Proctor
Hans Fredrikson
Dennis Stogin

Fire Worthiness:
Jim Peterson
Thomas Murray

Developmental Manufacturing:
Jose Valdez
Ponci Puzon
Bonnie Luck

Test Laboratories:
Ron Slaminko
John Schneider
Carl Preuss
Joan Dufresne
Tony Phillips
Dan Moreillon
Bill Hardrath

Business Management:
Jeff Heineman
Marge Apeles
Kira Goerlich

QC and NDE Development:
Ken Mackey
Brian Lempriere
Bill Fortig
John Linn

Weights:
Glenn Parkan

Repair Development:
Bert Bannink
Mike Evens
Sherry Marrese

Customer Support:
Dave Berg
Jeff Kollgaard

Materiel:
Maureen Hughes
Mark Jones
Steve Ruth
Doug Wood
Christal Tyson-Winston
Howard Lanie
Mark McConnell
Tom Hesketh

Industry And University Design-Build-Team Members

University of Washington:
Kuen Y. Lin
James Seferis
Zelda Zabinsky
Mark Tuttle

Stanford University:
Fu-Kuo Chang

Oregon State University:
Tim Kennedy

M.I.T:
Paul Lagace
Tim Gutowski
David Hoult
Greg Dillon
Hugh McManus

Drexel University:
Jonathan Awerbuch
Albert Wang
Alan Lau
Frank Ko

University of Iowa:
Roderic Lakes

University of Utah:
William Bascom
John Nairn

University of Wyoming:
Donald Adams
Rhonda Coguill
Scott Coguill

U. of Cal. Santa Barbara:
Keith Kedward

Univ. of British Columbia:
Anoush Poursartip

Brigham Young University:
Ken Chase

San Jose State University:
Robert Anderson

Dow-UT:
Rich Andelman
Douglas Hoon

Sikorsky Aircraft:
Christos Kassapoglou

Northrop/Grumman:
Ravi Deo
Steve Russell
Bob Ley
Ram Vastava
Ram Ramkumar

McDonnell Douglas:
Benson Black

Lockheed Aero. Systems:
Tony Jackson
Ron Barrie
Bob Chu
Dan Skolnik
Jay Shukla
Bharat Shah
Lowell Adams
Lisa Ott

Fiber Innovations:
Steve Goodwin
Garrett Sharpless

Hercules Materials Co.:
Doug Cairns
David Cohen
Roger Stirling
Lynn Muir
Will McCarvill
Yas Tokita

Alliant Techsystems:
Carroll Grant
George Walker
Tammy Harris
Todd Brown
Mark Wheeler
Jon Poesch
Vern Benson

American Airlines:
Jim Epperson
Marcus Peter

Northwest Airlines:
Jim Oberg
Erik Restad
Mark Wolf

United Airlines:
Bob Bernicchi
John Player

Cherry Textron:
Howard Gapp

Sunstrand:
Glen Smith
Hossein Saatchi
Bill Durako

ICI Fiberite:
Erinann Corrigan
Russ Holthe

G.M.I:
Roland Chemana

Intec:
Brian Coxon
Chris Eastland
Rod Wishart
Shreeram Raj
Don Stobbe

Zetec:
Chuck Fitch
Gregg Colvin

Draper Laboratory:
Ed Bernardon

Hexcel:
Stacy Biel
Julaine Nichols
Kevin Marshal

E. I. Du Pont De Nemours:
Jim Pratte
Hal Loken
Ginger Gupton

Materials Science Corp.:
Walt Rosen
Anthony Caiazzo

Structural Consultant:
John McCarty

EBCO Tooling:
Rich Roberts

TABLE OF CONTENTS

TABLE OF CONTENTS (CONTINUED)

1.0 SUMMARY

Boeing is studying the technologies associated with the application of composite materials to commercial transport fuselage structure under the NASA-sponsored contracts for Advanced Technology Composite Aircraft Structures (ATCAS) and Materials Development Omnibus Contract (MDOC). Innovative designs, advanced material forms, and automated processes with the desired cost-savings potential are being pursued. This report addresses the program activities related to structural performance of the selected concepts, including both the design development and subsequent detailed evaluation.

Design criteria were developed to ensure compliance with regulatory requirements and typical company objectives. During design sizing, attempts were made to account for the most significant aspects of each design. Accurate analysis methods were selected and/or developed where practical, and conservative approaches were used where significant approximations were necessary. Design sizing activities supported subsequent development by providing representative design configurations for structural evaluation and by identifying the critical performance issues.

Significant program efforts were directed towards assessing structural performance predictive capability. The structural database collected to perform this assessment was intimately linked to the manufacturing scale-up activities to ensure inclusion of manufacturing-induced performance traits. Mechanical tests were conducted to support the development and critical evaluation of analysis methods addressing internal loads, stability, ultimate strength, attachment and splice strength, and damage tolerance. Unresolved aspects of these performance issues were identified as part of the assessments, providing direction for future development.

2.0 INTRODUCTION

Boeing's Advanced Technology Composite Aircraft Structures (ATCAS) program (contract NAS1-18889) was initiated in May 1989 as an integral part of the NASA sponsored Advanced Composites Technology (ACT) initiative. Task 2 of Materials Development Omnibus Contract (MDOC, contract NAS1-20013) was awarded in November 1993 as an extension of this work. Combined, these two contracts addressed concept selection and technology development (referred to as Phases A and B). An additional contract (NAS1-20553) has been initiated to verify this technology at a large scale (referred to as Phase C). The goal of the ACT initiative is to develop composite primary structure for commercial transport aircraft with 20-25% less cost and 30-50% less weight than equivalent metallic structure.

The ATCAS program activities within the ACT framework have focused on fuselage structure. More specifically, the primary objective of the program is to develop and demonstrate an integrated technology which enables the cost- and weight-effective use of composite materials in fuselage structures of future aircraft. The area of study is a pressurized aft fuselage section of a wide body airplane with a diameter of 244 inches, as shown in Figure 2-1. The structure, located immediately aft of the wing-to-body intersection and main landing gear wheel well, is designated Section 46 on Boeing aircraft. This section, highlighted in Figure 2-1, contains most of the structural details and critical manufacturing issues found throughout the fuselage. It has significant variations in design detail due to relatively high loads in the forward end which diminish toward the aft end, allowing a transition to minimum gage structure.

The fuselage cross-section is divided into four circumferential segments in the baseline manufacturing approach. These "quadrants" consist of a crown, keel, and left and right side panels, as illustrated in Figure 2-2. The quadrant approach was adopted to reduce panel assembly costs (fewer longitudinal splices) and leverage the size-related efficiencies of the automated fiber placement (AFP) process for laminated skins, while maintaining design flexibility for regions with differing requirements [1, 2].

Design Build Teams (DBTs), consisting of various disciplines responsible for creating aircraft structure (e.g., design, manufacturing, cost analysis, materials, structures, quality control) were formed to identify and evaluate promising structural concepts for each quadrant. A three-step approach was used. The first step, termed *baseline concept selection*, determined the concept judged to have the greatest potential for cost and weight savings, combined with an acceptable risk The second step, termed *global evaluation*, developed preliminary designs in sufficient detail to determine significant cost and weight differences between the baseline concepts and other potentially low-cost/low-weight concepts. The most attractive concept was selected for further consideration in the third step, termed *local optimization*. In this step, the individual design elements were optimized, while still considering the impact of any design changes on overall cost.

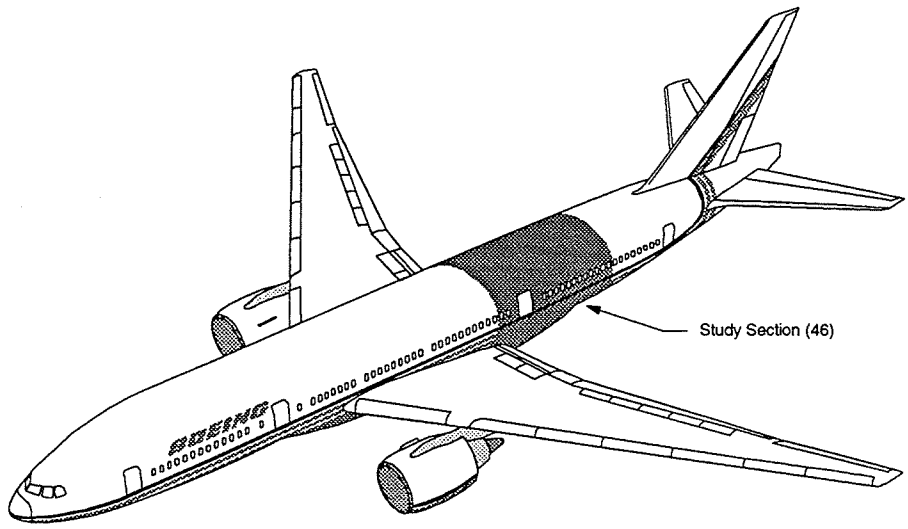

Figure 2-1. Baseline vehicle and study section.

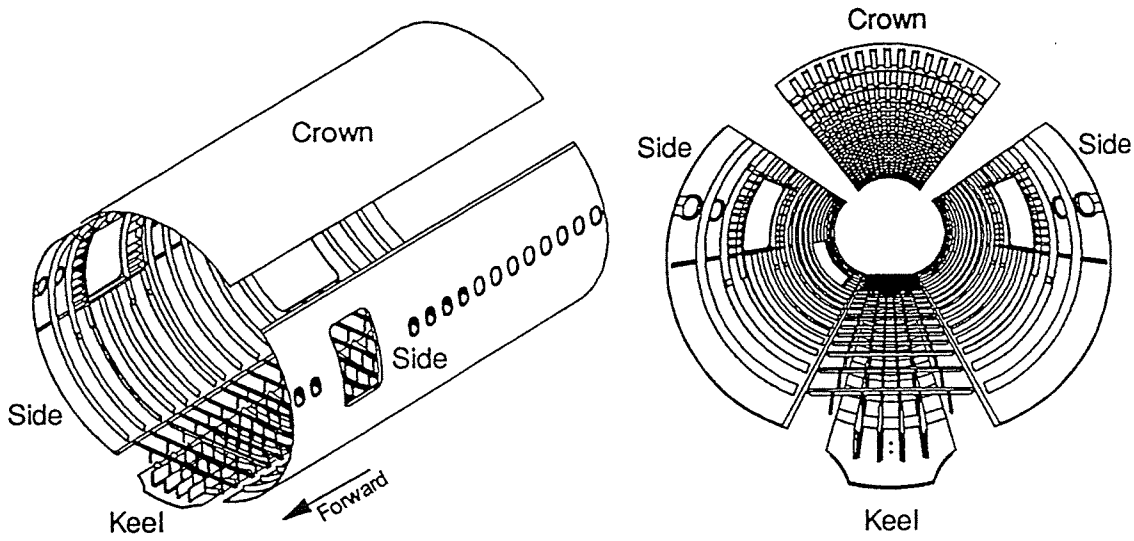

Figure 2-2. Fuselage quadrants.

Baseline concept selection and global evaluation activities resulted in the selection of a skin/stringer configuration for the crown, and sandwich construction for the keel and side quadrants [1-6]. The design process was initiated first for the crown, then the keel, and

finally the side quadrant. As a result, the relative maturity of the quadrants' structural databases are similarly staggered.

The crown panel design is depicted in Figure 2-3. The stiffened-skin design features cocured longitudinal hat-section stringers and cobonded J-section circumferential frames. The stringers spacing is 14 inches. The frames, spaced nominally at 21 inches, contain cutouts (referred to as mouseholes) to permit continuous stringers. The mouseholes necessitate fail-safe flanges on the frames to ensure bending-stiffness continuity across the frame-stringer intersection.

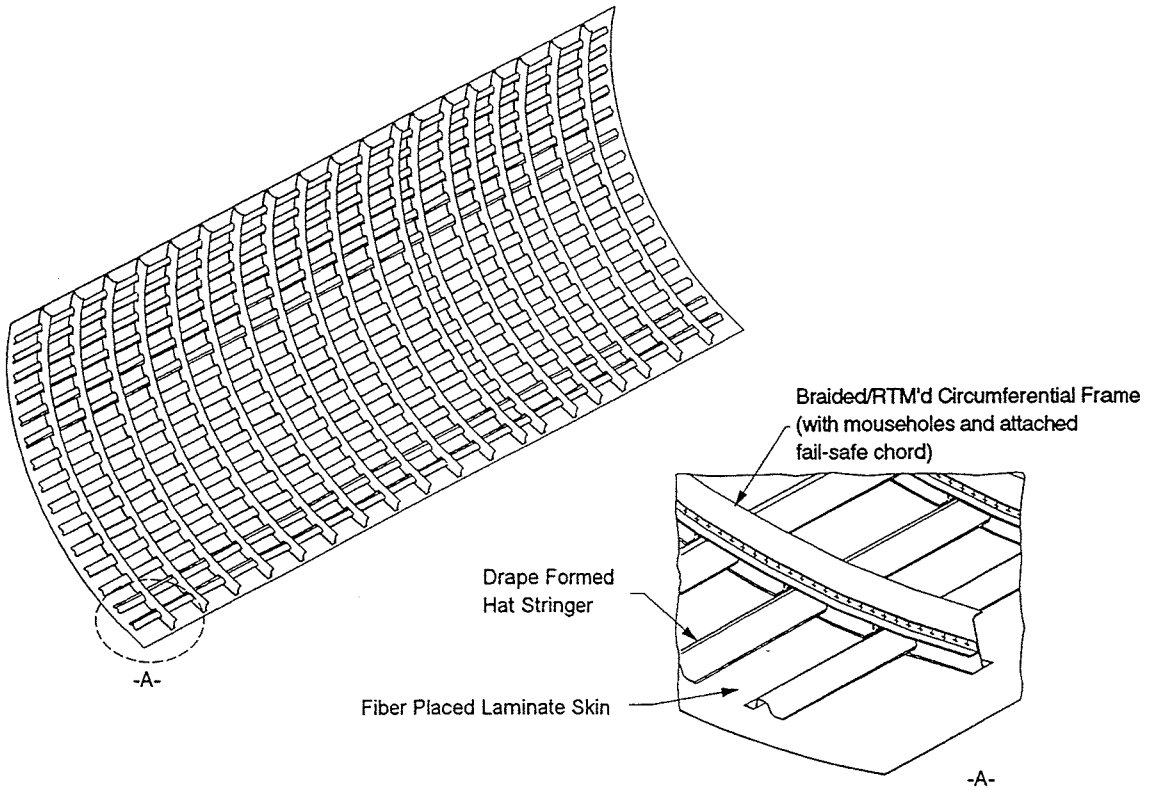

Figure 2-3. Baseline crown panel configuration.

The baseline manufacturing approach for crown panels involves AFP of skin charges on a convex mandrel. The stringers charges are fabricated using automated tape layup, which are then hot drape formed over elastomeric mandrels. The skin and stringers are cocured on a hard outer-mold-line (OML) tool with semi-rigid inner-mold-line (IML) cauls. Braided/resin-transfer-molded (RTM) frames are cobonded to the skin during cure.

The keel panel design (Figure 2-4) utilizes a thick laminate to carry the high compressive loads at the forward end, and transitions to sandwich construction further aft as the loads redistribute towards the sides. The thick laminate acts as a panelized keel beam by

distributing the equivalent material of discrete keel chords (typical of conventional fuselage structure) across a wider panel area. Ply drops and core tapers are balanced such that a constant panel thickness — and therefore constant inner panel radius — is maintained to maximize frame commonality, thereby reducing fabrication costs. Sandwich panel edges incorporate full-depth close-outs (rather than ramped-down edges) to simplify the frame interface, increase the edge bending stiffness, and provide the necessary structure for splice joint attachment. With this full-depth panel edge, the close-outs must protect the core from moisture ingression. The circumferential frames are constant J-sections. Longitudinal intercostals are required in the forward frame bays to stabilize the panel in the area of highest compression load. The attached cargo floor structure consists of discrete precured, pultruded floor beams and stanchions which are mechanically fastened to the frames.

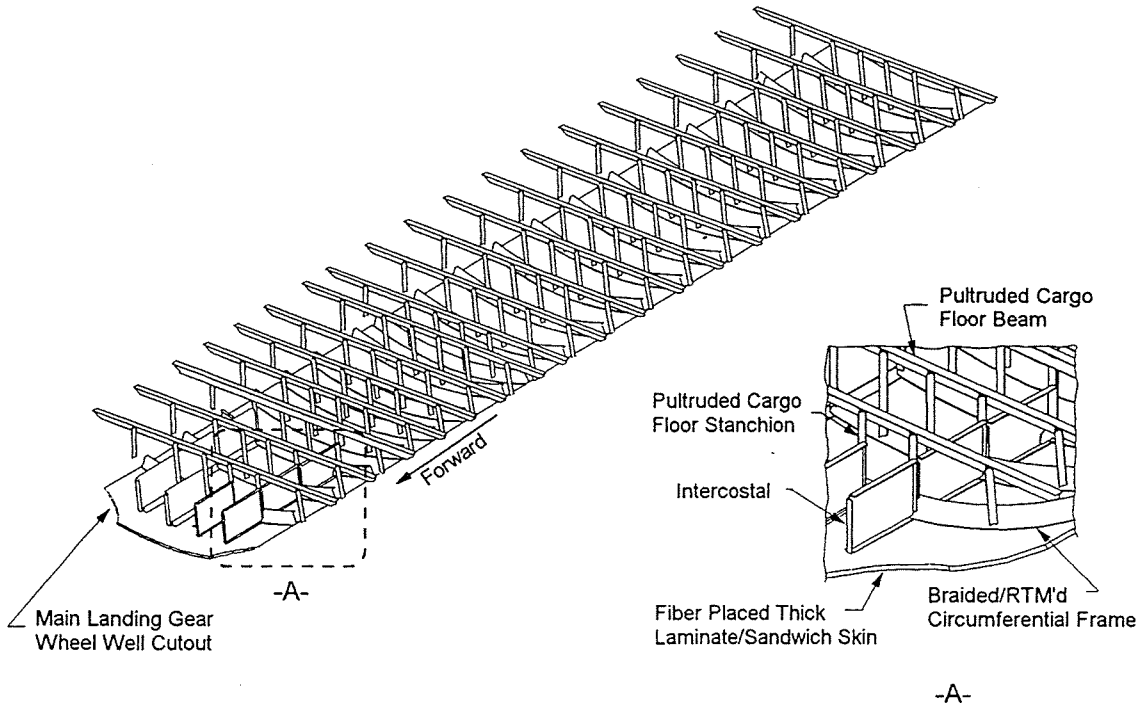

Figure 2-4. Baseline keel panel configuration.

The keel panel manufacturing approach is similar to that of the crown in the use of AFP, braided/RTM frames, OML cure tooling, and semi-rigid IML cauls. Additionally, individual honeycomb core pieces must be rough machined, heat formed to curvature, spliced together with the precured close-outs into a core blanket, and final machined prior to panel cure. The precured frames and intercostal attachment chord elements are cobonded to the sandwich panel. The intercostals are mechanically fastened to the attachment chords and cargo floor stanchions.

The side panel design is shown in Figure 2-5. Basic skin-panel design features, materials, and manufacturing approach are similar to the keel panel. Additional full-

depth close-outs are included at the window cutouts. The window and door reinforcement elements are precured and mechanically fastened to the skin panel, with the exception of the passenger-door auxiliary frames, which are cobonded during panel cure. The passenger floor structural elements are precured (pultruded or drape formed) and mechanically fastened upon fuselage-section assembly.

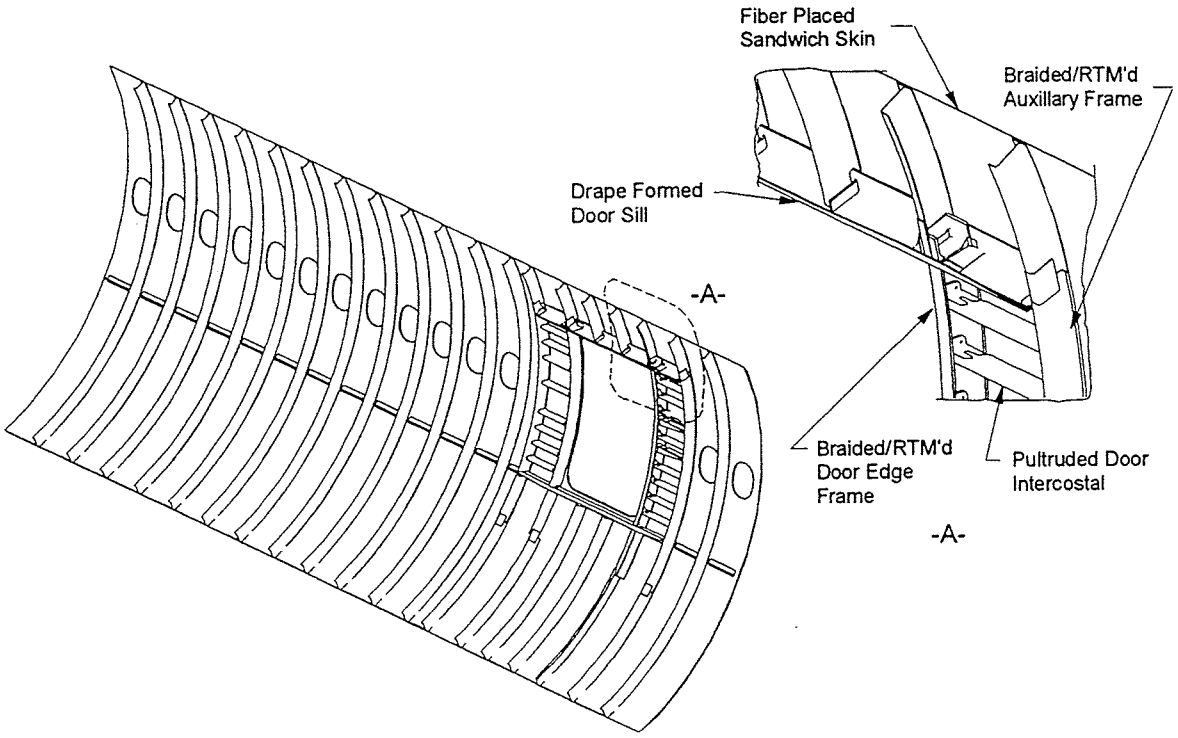

Figure 2-5. Baseline side panel configuration (passenger floor structure omitted for clarity).

Concepts for longitudinal splices between crown, keel, and side quadrants are shown in Figure 2-6. These lap splice concepts are dependent on the configuration of the panels being joined (i.e., sandwich or skin/stringer). Circumferential splice concepts are shown in Figure 2-7. Circumferential splice close-outs for the sandwich keel and side panels are solid, and incorporate partial rampdowns to accommodate external splice plates while maintaining a smooth aerodynamic outer surface. The forward keel panel splice is more complex due to the tab-out into the wheel well cutout area and the magnitude of the loads to be transferred.

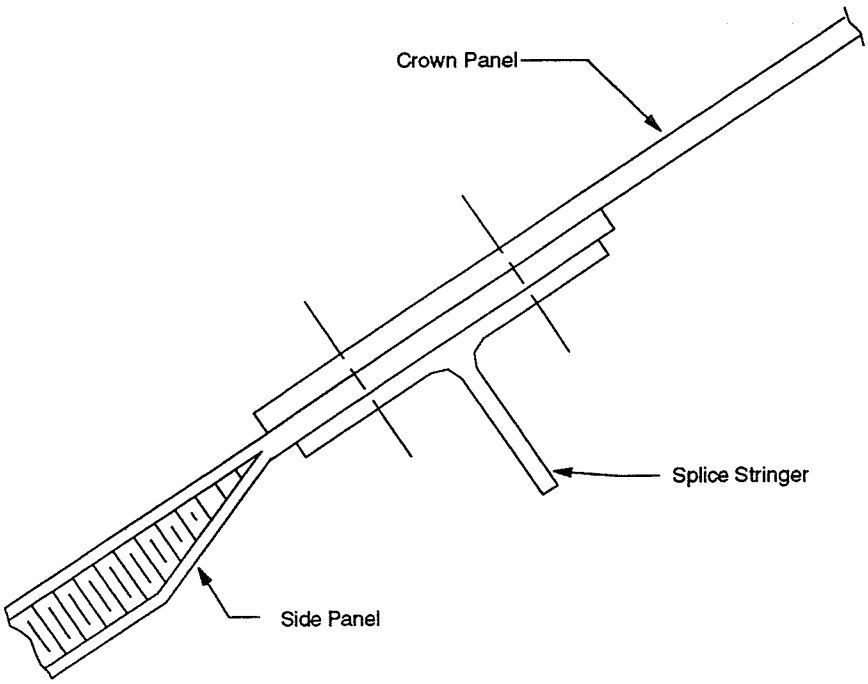

a. Crown-to-Side Panel Splice.

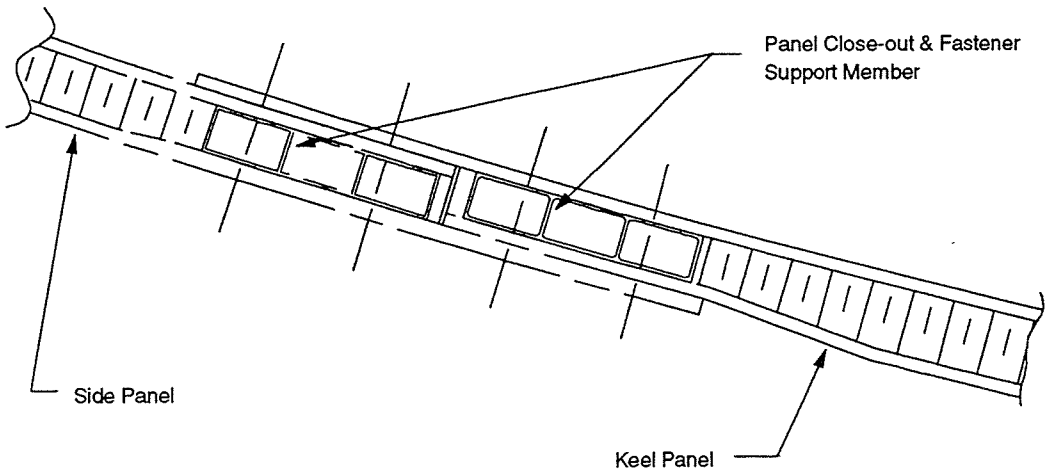

b. Keel-to-Side Panel Splice.

Figure 2-6. Baseline design concepts for the longitudinal splices.

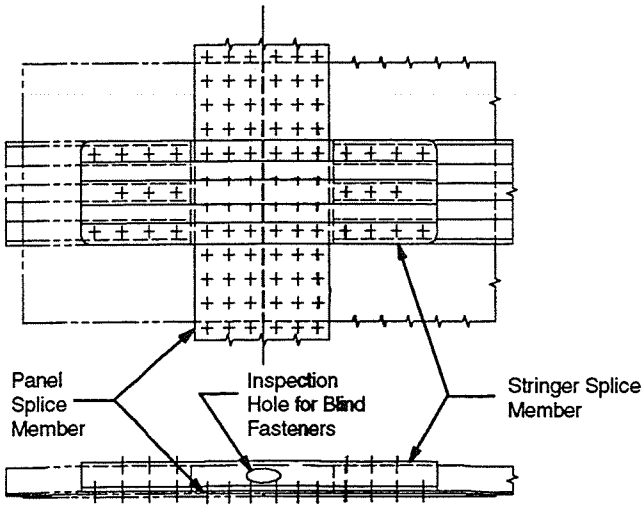

a. Crown (Skin/Stringer)
Circumferential Panel Splice

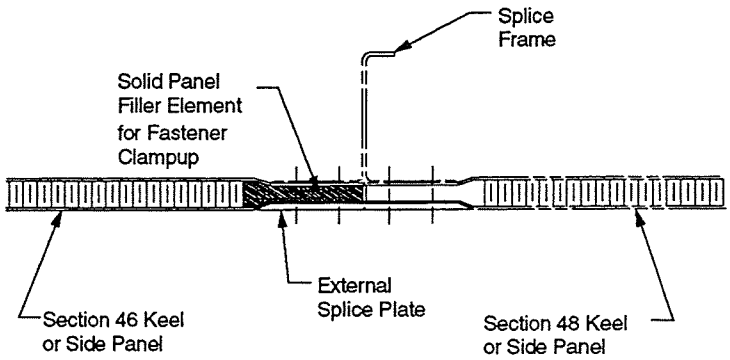

b. Aft Keel or Side (Sandwich)
Circumferential Panel Splice

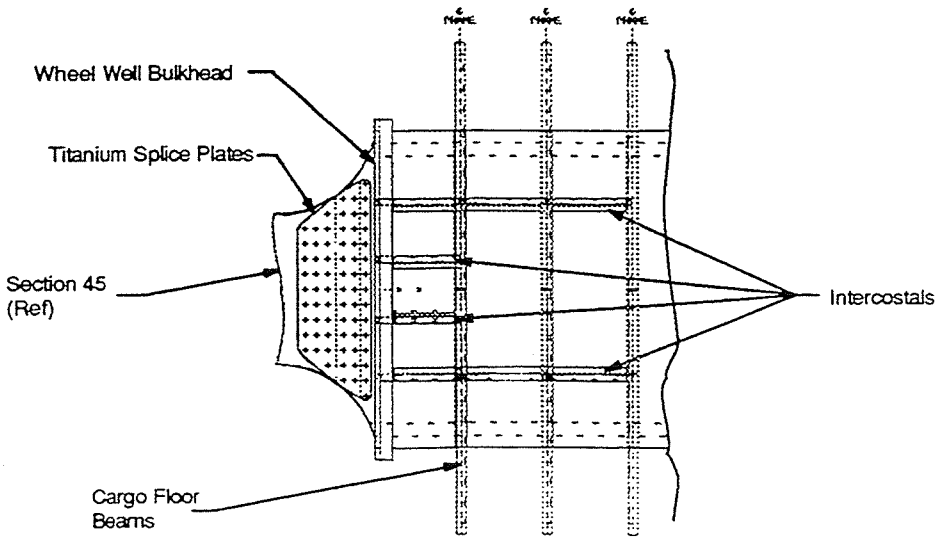

c. Forward Keel Circumferential Splice

Figure 2-7. Baseline design concepts for the circumferential splices.

Resolution of major structural performance concerns was pursued through a series of analysis and test developments. These developments were focused on critically assessing the predictive capability of design sizing tools and detailed analysis methods. Test specimens were obtained primarily from larger manufacturing scale-up and demonstration articles, ensuring consideration of typical manufacturing variations and process-induced performance traits in structural assessments. It should be noted that tests were often conducted on design configurations that differed somewhat from the concepts recommended at program's end. This is particularly true for the crown quadrant, where early designs included 22-inch frame spacing (vs. 21-inch) and significantly more axially-compliant skin and stringer laminates than later designs.

As an important prelude to the discussions of analysis and test developments contained in this document, Section 3.0 contains an overview of the sizing methodology employed in developing each quadrant, and describes the critical design drivers for each. Sections 4.0 through 8.0 discuss the program developments and unresolved issues relative to key structural concerns: internal loads, stability, ultimate strength, attachment and splice strength, and damage tolerance, respectively. In these discussions, experimental results are often compared with structural requirements. Since tests only approximate the response of the structural detail in the fuselage, the comparisons are only valid to the extent that the tests are successful at simulating the true fuselage response.

3.0 STRUCTURAL SIZING

Detailed designs of each quadrant were developed during global evaluation and local optimization to allow cost and weight assessments. During the course of the contract, the quadrant designs evolved [1], as did the criteria and methods used to develop them. Insufficient resources existed to address all structural issues or to perform sophisticated analyses for each design detail. Attempts were made to account for the most significant aspects of each design, and to use conservative approaches where approximations were necessary. The following discussions address the most recent criteria and analysis methods used to ensure structural adequacy of the developed designs. The critical design drivers determined for each quadrant using these methods are also described.

3.1 Design Criteria

3.1.1 Load Conditions

For fuselage structure, regulatory requirements address three loadings for each of ultimate and limit loads: flight loads, flight loads combined with internal pressure, and internal overpressure alone. The flight loads are determined from combinations of flight conditions, and aircraft operational configuration at the time of those conditions. They are multiplied by 1.5 and 1.0 for ultimate and limit strength evaluations, respectively. For the study aircraft, these ultimate and limit flight loads must also be combined with 13.65 and 8.85 psi of internal pressure, respectively. The ultimate and limit internal overpressure conditions for the study aircraft are 18.2 psi and 10.1 psi, respectively.

3.1.2 Aeroelastic Response

Flutter, ride comfort, and aircraft handling are strongly influenced by the fuselage bending and torsional stiffnesses (i.e., EI and GJ). Early ATCAS designs addressed these issues by placing minimum stiffness requirements relative to the metallic configurations, in an attempt to avoid significant deviations from a concept that adequately addressed them. In practice, the EI and GJ limits were accomplished by placing related requirements on the axial and shear stiffnesses (i.e., EA and Gt) of each quadrant. For the crown quadrant, the EA and Gt at each body station were required to be at least 90% of the corresponding metallic stiffnesses. This approach does not, however, account for the equally important influence of weight on the aeroelastic response. A similar requirement, therefore, was not directly applied to the keel and side quadrants, but the relationship was instead monitored. An aerodynamic analysis which includes the appropriate stiffnesses and weights is necessary to ensure that these issues are addressed, and that excessive constraints are avoided.

3.1.3 Stability

Requirements were imposed on various stability modes to ensure structural adequacy; large buckling-induced deflections and curvatures can result in structural failure, either

by in-plane material failure or through debonding of structural elements. General cylinder buckling was not allowed below ultimate load. Other requirements varied depending on quadrant configuration.

For the crown quadrant, stringer column buckling and stringer local buckling were prohibited below ultimate loads. Skin buckling, however, was permitted above 40% of ultimate load, allowing operation in the post-buckling regime.

For the keel and side sandwich configurations, facesheet dimpling, facesheet wrinkling, and skin buckling (i.e., facesheets with core) were prohibited below ultimate load. A minimum margin of safety of 20% was required for the skin buckling to account for initial imperfections. In the keel, a 10 in^2 facesheet disbond from the core was also required to be stable at ultimate load, in attempts to account for possible undetected manufacturing defects or in-service damage. This requirement was errantly omitted from side quadrant sizing activities.

Skin stability in the presence of frame-to-skin disbond was considered. The selected scenario was a complete disbonding of a single contiguous bondline. Specifically, this resulted in a requirement that the quadrant skins be stable at ultimate load with a disbond between mouseholes in the crown, a disbond of one-half of a frame in the keel (due to a mousehole cutout for drainage at the bottom centerline of the panel), and a disbond of an entire frame in the side. Due to analysis-method limitations, however, only the side-quadrant requirement was imposed during design sizing.

Several of these criteria require additional consideration and/or modification in future work. Evidence suggests that restricting skin buckling in skin/stringer configurations to loadings above 33% of ultimate load would continue to protect against separation of the stringers from the skin (see related discussion in Section 5.1.1). Requiring at least a 20% positive margin on stringer column buckling is also deemed appropriate to account for initial imperfections, since such buckling is equivalent to structural collapse. The criteria related to disbonded frames and partially disbonded facesheets were selected in a somewhat arbitrary fashion, and should be refined. The underlying issues, however, must be considered. Stability criteria for circumferential frames must also be developed.

3.1.4 Ultimate Strength

Several design criteria associated with ultimate strength were imposed. The structure was required to sustain ultimate load levels with non-visible damage, created either by hail or a tool drop, in a worst-case environment. The visibility threshold was defined to be a 0.05-inch indentation and/or a 1-inch surface crack. Ground hail was to be simulated with a 2.5-inch diameter lead impactor, and tool drops with a 1-inch diameter steel impactor. The tool-drop energy was limited to a maximum of 1200 in-lb.

Additional requirements were imposed relative to ground hail. OML surfaces of the crown and side were required to endure 500 in-lb and 300 in-lb hail impacts, respectively, without sufficient damage to necessitate immediate repair. This criteria was not imposed on the keel, since it has no significant exposure to direct ground hail impact.

The intent of these additional hail criteria was to ensure ultimate capability and avoid costly maintenance when the structure is subjected to severe hail storms.

3.1.5 Attachments and Splices

For bonded attachments, the difference in Poisson's ratio between the skin and stringers or frames was limited to less than 0.15. This parameter had been previously determined to avoid separation of bonded stringers from skins in configured compression tests. This limitation may be excessively conservative for sandwich structure, where post-buckling is not allowed.

Several requirements were imposed on mechanical joints. Fasteners were required to have minimum edge and end margins of 2.5 times their diameter plus a manufacturing tolerance of 0.05 inch. Fastener countersinks were limited to less than two-thirds of laminate or facesheet thickness to avoid knife-edges. Limits on pull-up of mismatching parts were imposed to avoid excessive assembly-induced internal stresses. Specifically, gaps of up to 0.008 inch were allowed to be pulled-up, gaps between 0.008 and 0.030 inch required liquid shims prior to pull-up, and gaps between 0.030 and 0.060 inch required a combination of liquid and solid shims. Joint strength values were selected to account for these pull-up limits.

3.1.6 Damage Tolerance

Several design criteria were imposed during structural sizing to address damage tolerance. Within this report, damage tolerance refers to residual strength in the presence of large notches, and does not address the remaining two issues typically associated with structural damage tolerance: damage growth with fatigue loading and appropriate inspection procedures and schedules to ensure the damage does not become critical prior to detection. It was perceived that addressing large notch sizes would provide equivalent or improved safety relative to current aluminum structure. The imposed requirement was to withstand 100% of limit load with a failed structural unit. Early crown design development assumed a requirement of 80% of limit load, but it was subsequently increased to 100% of limit. In the skin/stringer crown, an additional criteria was imposed, requiring the stringer-to-panel axial stiffness ratio (i.e., AE_{str}/AE_{str+sk}) to be between 40% and 60%. This ensured a balanced damage tolerant design that was not overly dependent on either the skins or stringers being intact.

For all quadrants, the damage tolerance requirements were evaluated for axially-oriented notches (referred to as *hoop damage tolerance*) and circumferentially-oriented notches (referred to as *axial damage tolerance*). In the side quadrant, where significant shear loads exist, an additional evaluation addressed notches inclined to the axial direction by 45°, (referred to as *45° damage tolerance*).

Definitions of failed structural units varied with quadrant configuration. In the crown, a failed structural unit for hoop damage tolerance was considered to be a machined through-thickness notch midway between stringers, severing a central frame and the two adjacent half skin bays. In practice, however, this was equivalent to severing a central

frame and the two adjacent *full* skin bays since the adjacent unsevered frames were assumed to provide sufficient effective stiffness to arrest damage prior to structural failure. Similarly, a failed structural unit for axial damage tolerance was assumed to be a machined notch, midway between frames, severing a central stringer and the two adjacent half skin bays. Again, in practice, this was equivalent to severing the central stringer and two adjacent *full* skin bays.

In the sandwich keel and side quadrants, there were no axial stiffening members to aid in defining a structural element. A 10-inch notch length was established for both axial and hoop damage tolerance for these quadrants based on a desire for an insensitivity of residual strength to changes in notch length. Evaluation of unconfigured compression-fracture test data for a range of laminates [7] indicated that this notch length ensured no more than a 10% strength reduction with a 4-inch increase in notch length. Smaller damage sizes (e.g., 5 inches) were used in the keel region beneath the wing-to-body fairing (approximately the forward third). This was justified by: (a) the reduced likelihood of complete penetration, due to the large thickness of the panel; (b) the typically higher intensity of inspection, due to the forward keel's critical role in maintaining aircraft structural integrity; (c) the high likelihood of rapid detection of damage, due to the keel's proximity to airline ground-service personnel; and (d) the additional protection from external damage afforded to the keel panel by the fairing.

For the hoop damage tolerance condition, the damage was assumed to be centered on a severed frame; subsequent review of the analysis methods, however, revealed that an unconservative configuration factor to account for the effect of frames was errantly used. Preliminary assessments of this effect, however, indicated that increasing the criteria from a 10-inch to a 42-inch notch (i.e., two full bays) for hoop damage tolerance would have resulted in little or no change to the keel, but might require additional plies in relatively localized areas of the side.

3.2 Crown Quadrant Analysis Methods

3.2.1 Internal Loads

Internal loads generated for the metallic version of the study airplane from linear finite element analyses were utilized to design the crown quadrant. Load cases encompassing several hundred combinations of flight conditions, payload distributions, vehicle gross weights, center of gravity locations, air speeds, and vehicle configurations were considered. Design axial (longitudinal) line loads (i.e., N_x in lb/in) for each skin/stringer segment were obtained by distributing the stringer load across the segment width, and combining them with the associated skin load. Circumferential line loads were determined assuming a perfect, uniform cylinder response to internal pressure (i.e., N_y = pressure * radius). This simplification ignores the influence of the varying properties around the circumference and the expansion restraint provided by the cargo and passenger floor structures on the hoop load distributions. Frame loads and moments were directly available from these analyses. The load distributions included the effect of compression and shear buckling on skin stiffness.

For analytical sizing, the crown quadrant was subdivided into 24 design regions over which loading and properties were considered to be constant. Additional regions were considered unnecessary since load variations in the quadrant were relatively gradual.

Three sets each of ultimate and limit flight loads (maximum axial tension, maximum axial compression, and maximum shear) were used in combination with appropriate internal pressure to size each design region. The maximum axial tension load set, for example, was determined by identifying the load case and location within the design region that produced the maximum axial tension loads. The axial, hoop, and shear loadings associated with that load case and location were then assumed for the entire design region. The maximum axial compression and maximum shear load sets were similarly determined. In general, this method allowed different locations within each design region to define each of the load sets, and flight conditions associated with each load set to vary across the quadrant. This approach also ensured that, at any location, only proper load combinations were considered to be acting together.

3.2.2 Skins

Compression and shear buckling of the skin bays were independently evaluated using closed-form solutions for orthotropic shells that accounted for transverse shear flexibility [8]. The solutions for compression addressed curved, rectangular shells. The dimensions were taken between frame centerlines and between the roots of adjacent stringer flanges, and simple supports were assumed along all four edges. Axial in-plane loadings without internal pressure were evaluated. Shear-buckling equations addressed flat square plates, and correction factors were applied to account for curvature and aspect-ratio effects. A simple interaction relationship was used to account for the combined effect of the two buckling modes. Load levels used in these calculations were compared to the ultimate loads through the minimum postbuckling criterion.

The ultimate strength capability of the skin was analyzed by determining the fiber-direction strains associated with each set of ultimate in-plane line loads using laminated-plate theory. The maximum pressure-induced hoop loads in the skin were assumed to be unaffected by the frames. No consideration was given to any reduced effectivity of the skin due to postbuckling. The "local modulus" for each fiber direction, required for determining design strain values, was determined through rotation of the laminate stiffness matrix. The design strain values as a function of laminate stiffness were determined as the lesser of those for (a) a 1-inch notch, corrected for statistical scatter (assumed to be 10%); (b) a 0.25-inch open hole, corrected for environment (assumed to be 15%) and statistical scatter; and, for compression, (c) barely visible impact damage (BVID), corrected for environment and statistical scatter [7]. A minimum gage requirement was also applied to skins to address the hail-impact criteria.

The damage tolerance assessment was performed by similarly determining the fiber-direction strains, except using each set of *limit* in-plane line loads. The hoop stiffness of the frames were ignored for these calculations. The resulting strains, considered to be far-field strains, were then adjusted to account for structural configuration [8]. These

configuration factors were extrapolations from elastic-plastic correction factors for metallic skin/stringer configurations [9]. The strains in the 0° and 90° plies were then compared with design values developed for laminates with large notches to assess axial and hoop damage tolerance, respectively. Specifically, extrapolations of experimentally-determined gross-area notched failure strains, bilinear in modulus and notch length, were used for tension strength with notches in the 15 to 45-inch range. No evaluation of axial compression damage tolerance was conducted since the reduced load levels and the stability requirements appeared to preclude it becoming a design driver for the crown.

3.2.3 Stringers

Stringer column stability was predicted using classical Euler buckling equations. The stringers were assumed to be simply-supported at the frames. An effective-skin-width approach was used to include the combined effects of load redistribution due to skin buckling and bending-stiffness effectivity of the adjacent skin [8]. Increased stringer loads resulting from shear-buckling-induced diagonal tension were included.

Stringer local stability, which addresses buckling of portions of the stringers, was evaluated using closed-form solutions which ignored transverse shear effects. The webs and caps of the hat stringers were each considered as infinitely long flat plates with simple supports on four sides. Only axial loads were considered, but additional diagonal-tension loads were included.

Stringer evaluations associated with ultimate strength and damage tolerance conditions were errantly omitted from crown design development. This omission is not anticipated to have a large effect on the quadrant's design, but no significant evaluation of this effect was conducted.

3.2.4 Circumferential Frames

A major consideration in frame sizing was the bending stiffness required to avoid general cylinder instability. A closed-form solution dependent on the frame spacing and the fuselage bending moment was used [10]. Simple checks of strains were also made using the frame loads and moments, and experimentally measured notched strengths [7]. In these checks, the effective skin width was assumed to be 21 inches (the frame spacing) for loadings with internal pressure, and 5 inches for those without pressure.

No consideration was given to frame instability modes, including frame rolling and local buckling. In addition, the frame strength for hoop damage tolerance conditions was not considered; as damage approaches the unsevered frames, high localized loading of the frame occurs, reducing the gross-area load levels necessary to cause failure.

3.2.5 Attachments

The bonded attachments of the frames and stringers to the skin were not explicitly analyzed for initial design. It was assumed that the criteria requiring a minimum postbuckling ratio and a maximum Poisson's ratio mismatch precluded element

debonding. During element and subcomponent database development, tests and analysis were used to evaluate design details.

3.2.6 Splices

The circumferential and longitudinal splices were analyzed for bearing/bypass considering only axial and hoop loading, respectively. The loading was assumed to be uniform across each design element, and approximate fastener load-sharing relationships based on past experience were used. The analysis of frame splice members and fasteners considered the transfer of both axial and bending loads in the frame.

3.3 Keel Quadrant Analysis Methods

3.3.1 Internal Loads

Loads for the keel were obtained from linear finite element analyses of a composite fuselage segment. Specifically, the model included all of Section 46 and the adjacent forward structure up to the rear wing spar. The model included composite quadrant definitions: specifically, skin/stringer crown and side, and sandwich keel. A more complete description of this model is contained in Section 4.1, [11], and "initial model" discussions in [12].

Five flight conditions were considered with this model, each with only one representative combination of payload distribution, vehicle gross weight, center of gravity location, air speed, and vehicle configuration. These flight conditions, shown in Table 3-1, in conjunction with internal pressure, had been determined to define the majority of the metallic Section 46 skin panel (i.e., skin/stringer combination). Load cases found to size the metallic circumferential frames and floor structure were not considered. As was done for the crown, circumferential line loads were determined assuming a perfect, uniform cylinder response to internal pressure. Circumferential frame loads and moments were obtained from the metallic analyses (described in Section 3.2.1), since the modeling scheme used in the composites loads model compromised the accuracy of these values. The load distributions did not include the effect of compression and shear buckling on skin stiffness.

For analytical sizing, the keel quadrant was subdivided into 152 design regions over which loading and properties were considered to be constant. The high number of regions relative to the crown were considered necessary due to the large load variations related to redistributing the high axial loads introduced at the forward end of the keel into the fuselage shell.

The procedure for determining maximum axial compression load set for each design region was identical to that used in the crown. Only the flight loads associated with the 2.5g vertical maneuver were considered, based on previous findings that this load case controls the entire quadrant's design. The other four flight conditions identified in Table 3-1, however, were additionally considered in the sizing of the longitudinal and

aft-circumferential splices. As in the crown, hoop loadings were generated from the internal pressure level, and acted throughout the quadrant. The exception was the keel tabout — the portion forward of the constant width region — which extends beyond the wheel-well pressure bulkhead and is therefore not subject to the internal pressure.

Table 3-1: Critical flight conditions for Section 46.

Flight Condition	Fuselage Response	Critical Loads
2.5g vertical maneuver	maximum positive vertical bending moment	axial tension in forward crown, axial compression in forward keel
-1.0 g vertical maneuver	maximum negative vertical bending moment	axial compression in forward crown, axial tension in forward keel
positive gust	maximum vertical shear loading (slightly lower vertical bending moments)	shear loading in side
rudder maneuver	combined bending on the fuselage	critical axial, shear loading around the passenger door structure.
abrupt down elevator	vertical bending	axial tension in the aft crown, axial compression in the aft keel

In the keel sizings, the effect of the cargo door cutout was not considered. Although the physical cutout was excluded from the composites loads model, the inertial loads due to the door's mass were imparted on the structure. To assess the approximate magnitude of the unconservatism associated with this approach, the increased loadings in the keel associated with the cargo door cutout were estimated by comparing the loading distributions on the left and right sides of the metallic aircraft. In localized regions near the forward corner of the cutout, axial load levels are likely 2 kips/in higher than the approximately 5 kips/in present without the cutout. Below the entire length of the door, the shear loads are likely 0.5 kips/in higher than the approximately 0.5 kips/in present without the cutout.

3.3.2 Sandwich

Skin buckling for the sandwich keel was evaluated in a manner similar to that used in the crown. Each in-plane load component was evaluated independently, then combined through a simple interaction equation. The compression evaluations varied, depending on the boundary conditions associated with the specific location in the keel, while the shear checks utilized the methods described for the crown.

Three general locations were considered for compression stability of the skin. In regions of the forward keel where intercostals were present, the methods used for the crown were applied, with all sides assumed to be simply supported. Near the edges of the keel, where a longitudinal splice stiffener was present, similar equations were used, except with simple supports assumed on three sides, and free conditions assumed on the edge

opposite that with the splice stiffener. In regions removed from the panel edges and the intercostals, evaluations used closed-form equations for buckling of flat rectangular plates into a cylindrical shape. The loaded ends were assumed to be simply-supported, while the longitudinal ends were assumed to be free. The increase in panel stability due to curvature was assumed to be 20%. The inclusion of transverse shear flexibility in each of these evaluations ensured consideration of the short-wave-length buckling mode, commonly termed *crimping*, that results from low transverse shear stiffness.

Facesheet wrinkling typically results in separation of the facesheet from the core and/or core crushing. This mode was evaluated using closed-form solutions for buckling of an infinite rectangular orthotropic plate on an elastic foundation. An empirical correction factor based on past metallic developments was applied [8].

Facesheet dimpling addresses the intracell buckling of sandwich facesheets over honeycomb core. It was assessed using the same methods as used for skin buckling in the vicinity of the intercostals (i.e., four sides simply supported), but assuming infinite transverse shear stiffness and no curvature. The plate was assumed to be square, with each side being the same length as the core's cell spacing. The principle loading direction was used, and any tension component in that coordinate system was ignored. A metallic empirical correction factor of 0.61 was applied to the results.

Buckling of a partially disbonded facesheet was determined using closed-form solutions for flat orthotropic plates with all four sides clamped, and no consideration of transverse shear flexibility. The disbonded region was assumed to be square with an area of 10 in^2.

The ultimate strength capability of the facesheets was evaluated in a similar manner as in the crown; fiber-direction strains were compared to notched/impacted design values. The loads were assumed to be equally divided between the two facesheets and the maximum pressure-induced hoop loads in the skins were assumed to be unaffected by the frames. The sandwich core was evaluated for flexural core crush, which can occur in curved sandwich panels with loading in the direction of curvature. The resulting through-thickness tension and compression loads were compared to associated core strengths. The bond strength between the core and the facesheets was initially assumed to be adequate for all loading conditions. Building-block tests helped validate this assumption for panel buckling and pressure pillowing load cases.

The damage tolerance assessment was performed in a similar manner as in the crown. Again, the loads were assumed to be equally divided between the facesheets, and the hoop stiffness of the frames was ignored. The factors used to adjust the skin strains for the effects of structural configurations were again extrapolations from metallic skin/stringer configurations. As mentioned in Section 3.1.6, the configuration factors used for hoop damage tolerance were later determined to be unconservative. Tension design values were again bilinear extrapolations (in modulus and notch length) of crown test results. For the compression strain design values, an inverse power law form, identical to that adopted in the Mar-Lin criteria [13], was used, with the toughness parameter and the exponent both linear functions of the laminate modulus perpendicular to the assumed notch.

3.3.3 Circumferential Frames

The keel quadrant frames were sized in a similar manner as those in the crown. The bending stiffness sufficient to avoid general cylinder instability, maximum strains considering effective skin width, and fastener bearing at the splices and cargo floor stanchion attachments were all addressed. Again, no consideration was given to frame instability modes or strength in damage tolerance scenarios.

3.3.4 Intercostals

The intercostals in the keel were sized assuming they were required to carry radial loads equivalent to 7% of the axial skin loads. This is an empirical approach for metallic keel panels, and relates to providing a node for stability deformations. The bending strains were compared with estimated allowables. The intercostal webs were checked for shear buckling using finite element models with idealized boundary conditions. Local stability of the caps was evaluated using closed-form solutions which ignored transverse shear effects. They were considered as flat plates with three sides simply supported and one side free. As discussed in Section 5.1.2, subsequent global finite element analyses indicated the initial intercostal sizing was conservative, although resources were not available to further refine the design.

3.3.5 Cargo Floor

The cargo floor beams and stanchions were sized to match the axial and bending stiffnesses of the corresponding metallic elements. This approach ensured proper functioning of the cargo handling equipment. Strains were also compared to estimated design values.

3.3.6 Attachments

The bonded attachment of the frames to the sandwich facesheets was assumed to be adequate. As discussed in Section 7.1.2, significant analysis and test efforts further addressed this issue. The flange widths of the bonded T's for connecting the intercostals to the skin were determined considering the pull-off loads generated by the assumed 7% reaction to the in-plane axial skin loads. Mechanical attachments between the intercostals, cargo-floor stanchions and circumferential frames were sized using standard bearing/bypass methods.

Attachments of the external fairing brackets were not analyzed due to resource constraints. The dominant loading is perpendicular to the panel surface, and is relatively low. Bonded and mechanically-fastened concepts were developed. The bolted attachments extended through both the sandwich and the attached flanges of the circumferential frames. Simple strength checks were conducted on the antenna attachment.

3.3.7 Splices

As in the crown, the circumferential and longitudinal splices were analyzed for bearing/bypass considering only axial and hoop loading, respectively. The loading was assumed to be uniform across each design element. Approximate fastener load-sharing relationships based on past experience were used for the longitudinal and aft circumferential splices. Load-sharing for the forward tabout splice was determined using the compatibility/equilibrium method in combination with fastener flexibilities calculated using effective thickness formulas. Standard bearing/bypass methods were then used for the critical fastener locations. The analysis of frame splice members and fasteners considered the transfer of both axial and bending loads in the frame.

3.4 Side Quadrant Analysis Methods

3.4.1 Internal Loads

As was done for the crown, internal loads generated for the metallic airplane using linear finite element analyses were utilized to design the side quadrant. Again, the load cases evaluated included several hundred combinations of flight conditions, payload distributions, vehicle gross weight, center of gravity locations, air speeds, and vehicle configurations. As was done for the crown and keel, circumferential line loads were determined assuming a perfect, uniform cylinder response to internal pressure. Only the left side quadrant was considered; resource requirements to address the cargo door cutout were beyond the scope of the program.

Internal loads for the circumferential and window frames were determined by Lockheed Martin Aeronautical Systems under their parallel NASA ACT contract (NAS1-18888). A ring model that included the floor structure was used to obtain the circumferential frame loads and moments. Detailed finite element models of a single frame bay were used to determine load distributions for the window frames. The axial load, however, was errantly applied uniformly across the panel circumference, resulting in much higher axial loads between adjacent window cutouts than occurs in the actual structure. Local load distributions for redesign of these frames at Boeing were obtained from a multi-bay finite element model using peak load levels obtained from the composites fuselage shell model (discussed in Section 3.3.1).

For analytical sizing, the side quadrant was subdivided into 220 design regions over which loading and properties were considered to be constant. The high number of regions relates to the large quadrant size and the significant load gradients near the over-wing longeron and the passenger door cutout.

The procedure for determining maximum axial tension, axial compression, and shear load sets for each design region was identical to that used in the crown.

3.4.2 Sandwich

Stability evaluations for the side quadrant facesheets, including skin buckling, crimping, wrinkling, and dimpling, were identical to those used in the keel (Section 3.3.2). Stability of disbonded facesheets was not evaluated.

The ultimate strength capability of the facesheets was evaluated in a manner similar to that used in the keel. A minimum gage requirement was also applied to the facesheets to address the hail-impact criteria. The sandwich core was evaluated for flexural core crush, as in the keel. The bond strength between the core and the facesheets was also assumed to be sufficient for all loading conditions.

Increases in facesheet thickness necessary in the vicinity of the windows were initially evaluated using RARICOM [14, 15]. This computer program uses the Rayleigh-Ritz method to determine the strain field for an elliptical cutout and a concentric skin padup in a plate subjected to uniform in-plane tension, compression, and shear loads. The resulting strains adjacent to the cutout were compared to unnotched strain data (factored for statistical and environmental effects) through an average strain criterion. Facesheet padups in areas adjacent to the door cutout were determined using semi-empirical metallic methods. Individual stress concentration factors for axial, hoop, and shear loading were applied (i.e., 4.4, 3.8, and 8.2, respectively).

The damage tolerance assessments of the side quadrant were performed identically to those of the keel, including the unconservative structural configuration factors for hoop damage tolerance. The 45° damage tolerance was also evaluated by comparing the strains in the ±45° plies with the design values.

3.4.3 Circumferential Frames

Sizing of the circumferential frames was conducted by Lockheed Martin Aeronautical Systems under their parallel NASA ACT contract, and addressed regions remote from the floor connections. Performance considerations included bending stiffness to preclude general cylinder buckling, peak strains, web shear buckling, flange crippling, frame rolling, and interlaminar tension in the radius between the web and the attached flange. As in the crown and keel, no consideration was given to frame strength in damage tolerance scenarios.

3.4.4 Passenger Floor

Strength and stiffness checks for the passenger floor were only indirectly performed. Strength and stiffness ratios between the selected materials and those used in the carbon/epoxy (T800H/3900-2) floor beams of the baseline aluminum airplane were estimated. The ATCAS floor-beam thicknesses were then obtained by applying the ratios to the thicknesses of the baseline floor beams. The stanchions for the passenger floor were sized to match the axial and bending stiffnesses of the metallic designs, and strain levels were compared with estimated design values.

3.4.5 Window Frames

Window frames were initially sized by Lockheed Martin Aeronautical Systems under their parallel NASA ACT contract. The finite element model determined strain levels and evaluated the frame's ability to preclude skin buckling near the cutout. Local buckling modes were also assessed through closed-form solutions. Redesign of these frames was accomplished at Boeing using detailed finite element models. Evaluations for that activity were limited to strain levels and the frame's ability to preclude skin buckling near the cutout.

3.4.6 Door Reinforcement

The door reinforcement elements, (e.g., edge and auxiliary frames, sills) were sized by matching the axial and bending stiffness of the metallic definitions. As discussed further in Section 6.1.3, subsequent detailed finite element analysis identified some unconservative aspects of this approach.

3.4.7 Attachments

The bonded attachment of the frames to the sandwich facesheets was assessed by Lockheed Martin Aeronautical Systems under their parallel NASA ACT contract. Mechanical attachments between (a) the floor elements and circumferential frames, and (b) the door-surround structure and the skin, were not specifically analyzed. The fastener sizes and patterns were similar to those used in the metallic design. Attachment of the window frame to the skin was checked for bearing/bypass capability. No sizing of the systems penetrations and attachments was performed due to resource constraints.

3.3.8 Splices

As in the crown and keel, the circumferential and longitudinal splices were analyzed for bearing/bypass considering only axial and hoop loading, respectively. The loading was assumed to be uniform across each design element, and approximate fastener load-sharing relationships based on past experience were used. Standard bearing/bypass methods were then used for the critical fastener locations. The analysis of frame splice members and fasteners considered the transfer of both axial and bending loads in the frame.

3.5 Design Drivers

3.5.1 Crown Quadrant

In the crown, the dominant ultimate axial loads were found to be primarily tension, and varied from approximately 7.8 kips/in at the forward end to 5.0 kips/in in the aft end, as shown in Figure 3-1. The maximum compression loads were found to be approximately 40% of the tension loads. Maximum shear loads were relatively small. A typical distribution is shown in Figure 3-2. It should be noted that these loading levels were considered during the later stages of crown development; early designs were based on

lower loads associated with a slightly different airplane configuration. The ultimate hoop load level associated with the overpressure condition (18.2 psi) was 2.2 kips/in.

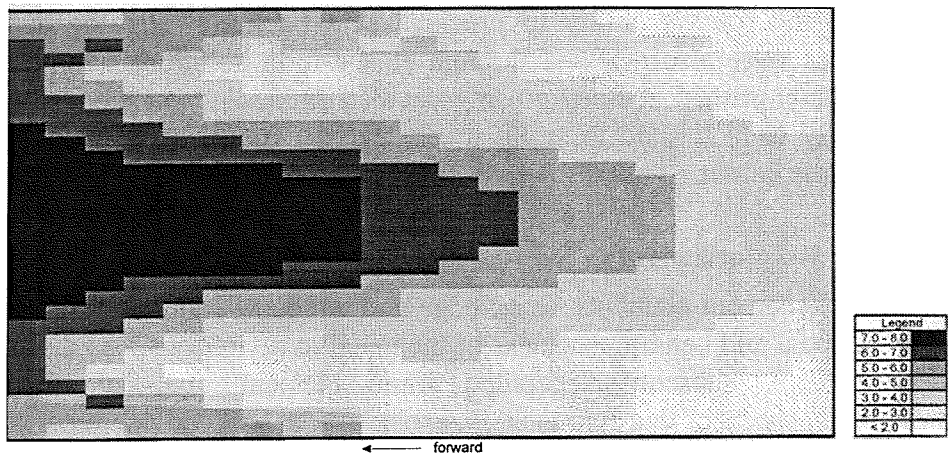

Figure 3-1. Maximum tension loads (kips/in) in the crown quadrant.

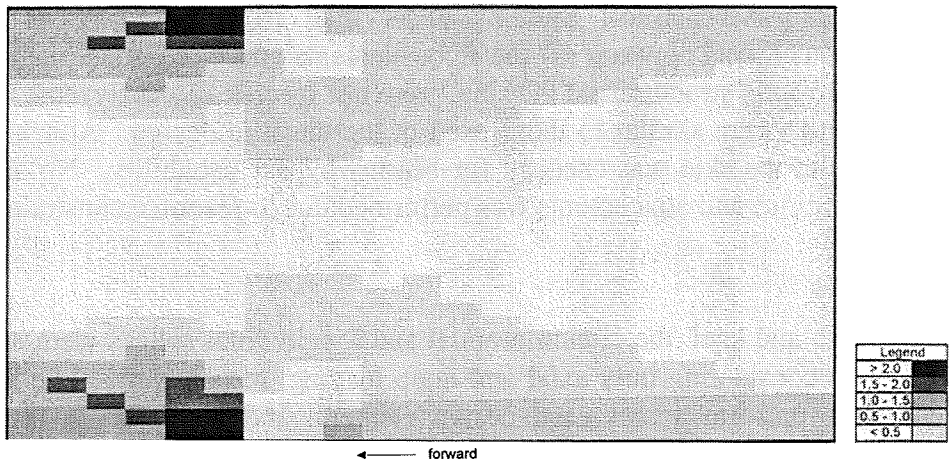

Figure 3-2 Crown-quadrant shear loads (kips/in) associated with maximum tension loads.

Margins of safety for the structural performance characteristics that controlled the crown quadrant design are shown in Figures 3-3 through 3-7. The forward end was controlled by axial tension damage tolerance near the top centerline, and skin buckling toward the panel edges. Skin buckling also controlled the edges of the aft end, with hoop damage tolerance and skin/stringer Poisson's ratio mismatch also influencing that region. The lack of a controlling performance characteristic for the top centerline in the aft end is likely a result of either a non-converged optimization or competing constraints in adjacent design elements.

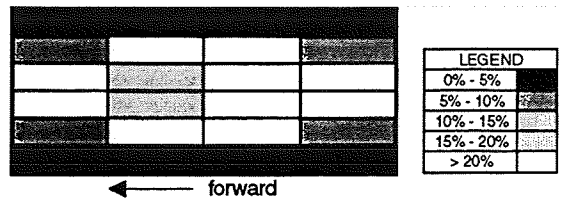

Figure 3-3. Margins of safety for skin buckling in the crown quadrant.

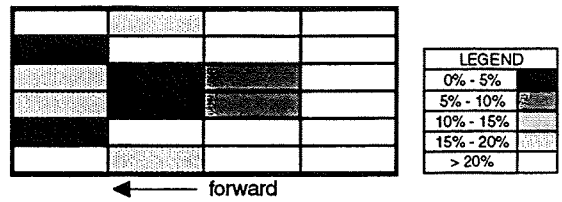

Figure 3-4. Margins of safety for axial tension damage tolerance in the crown quadrant.

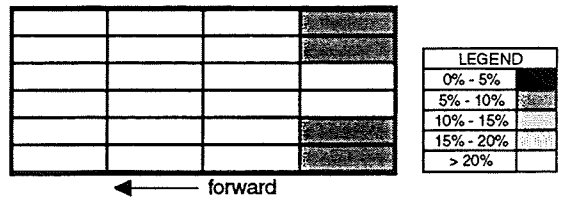

Figure 3-5. Margins of safety for hoop tension damage tolerance in the crown quadrant.

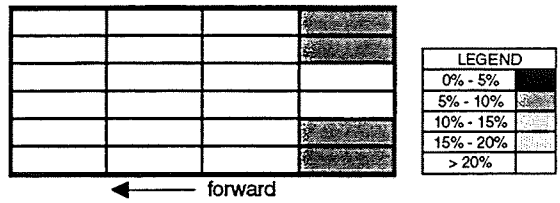

Figure 3-6. Margins of safety for skin/stringer Poisson's ratio mismatch in the crown quadrant.

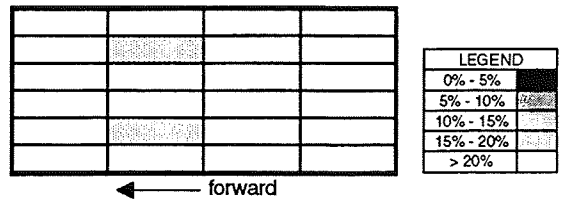

Figure 3-7. Margins of safety for minimum shear stiffness in the crown quadrant.

The bending stiffness requirements for the circumferential frames necessary to preclude general cylinder instability controlled their design. Since the frames were constrained to a constant thickness along their length, fastener bearing considerations at the longitudinal splice also had some influence.

Bearing/bypass considerations controlled most of the longitudinal and circumferential splice designs, although additional plies were required in some regions to avoid excessive fastener countersink.

3.5.2 Keel Quadrant

In the keel, the dominant ultimate axial loads were found to be primarily compression, and varied from approximately 34.5 kips/in. at the forward end to 3.5 kips/in in the aft end, as shown in Figure 3-8. Maximum shear loads in the majority of the panel ranged from near zero to 4.3 kips/in, as shown in Figure 3-9. Peak shear loads near the forward tab-out reached 7.8 kips/in. The ultimate hoop load level associated with the overpressure condition (18.2 psi) was 2.2 kips/in.

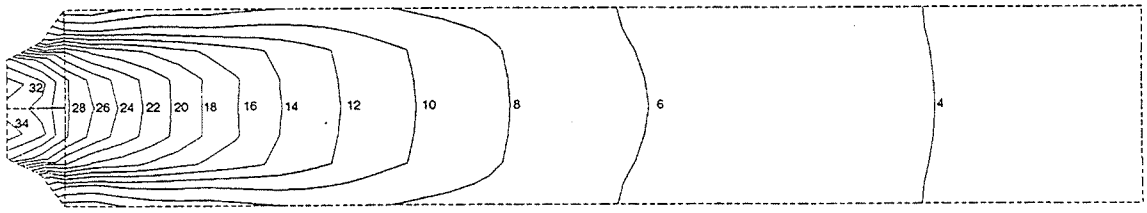

Figure 3-8. Maximum compression loads (kips/in.) in the keel quadrant.

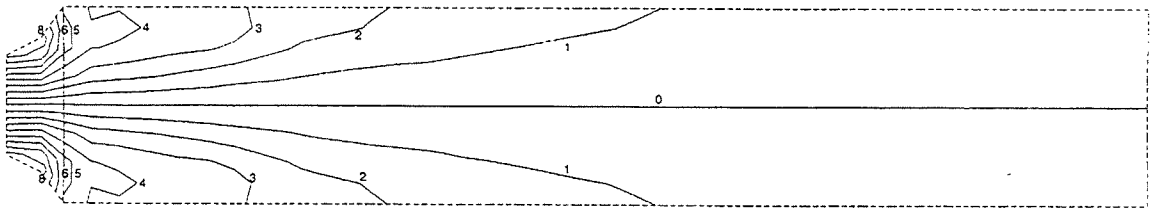

Figure 3-9. Maximum shear loads (kips/in.) in the keel quadrant.

As shown in Figures 3-10 and 3-11, the forward keel design was controlled by ultimate compression strength and, to a lesser extent, compression damage tolerance. The aft keel was controlled primarily by compression damage tolerance. Limitations on the skin/frame Poisson's ratio mismatch and skin buckling also influenced the design in localized regions of the mid-keel. Note that some additional margin may be possible with thicker gages in the mid and forward keel due to apparent improvements in compression properties with increasing skin thickness.

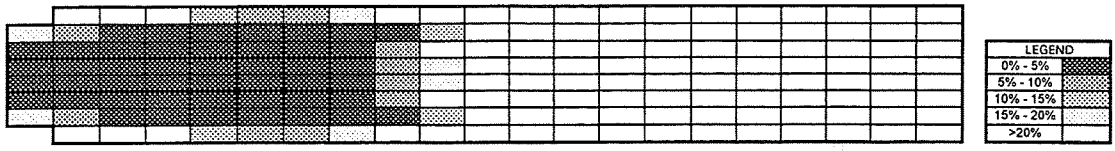

Figure 3-10. Margins of safety for ultimate compression strength in the keel quadrant.

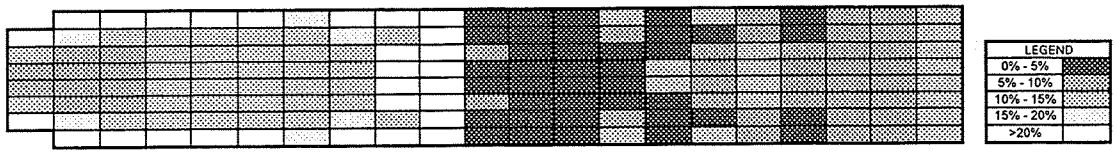

Figure 3-11. Margins of safety for compression damage tolerance in the keel quadrant.

As in the crown, the bending stiffness requirements for the circumferential frames necessary to preclude general cylinder instability controlled their design. Fastener bearing considerations at the longitudinal splice and the cargo-floor stanchion attachments also had some influence, since the frames were constrained to a constant thickness along their length.

Intercostal designs were controlled by the web shear buckling, element crippling, and maximum bending strains. The cargo floor and stanchion designs were controlled by matching of metallic stiffnesses. Bearing/bypass considerations dominated the design of the splices, as sufficient facesheet thicknesses existed to address maximum countersink requirements.

3.5.3 Side Quadrant

In the side, tension, compression, and shear loads were all found to be important. The quadrant load distributions are shown in Figure 3-12 through 3-14, respectively. In the majority of the quadrant, ultimate axial tension and compression levels are below 5 kips/in and shear levels are below 3 kips/in. The overwing longeron and the passenger door cause significant stress concentrations, with maximum ultimate tension and compression loads of 23 kips/in and shear loads of 5.6 kips/in. The ultimate hoop load level associated with the overpressure condition (18.2 psi) was 2.2 kips/in. Note that the load levels within the window-belt are not accurate since the cutouts were not explicitly modeled. Instead, the axial and shear stiffnesses of the skin elements were adjusted to simulate the reduced load-carrying capacity of the cutout region. Related discussions are contained in Section 4.1. Concentrations in the vicinity of the cargo door cutout

contained in the right side quadrant (not studied under ATCAS) are expected to be larger those associated with the passenger-door or window cutouts.

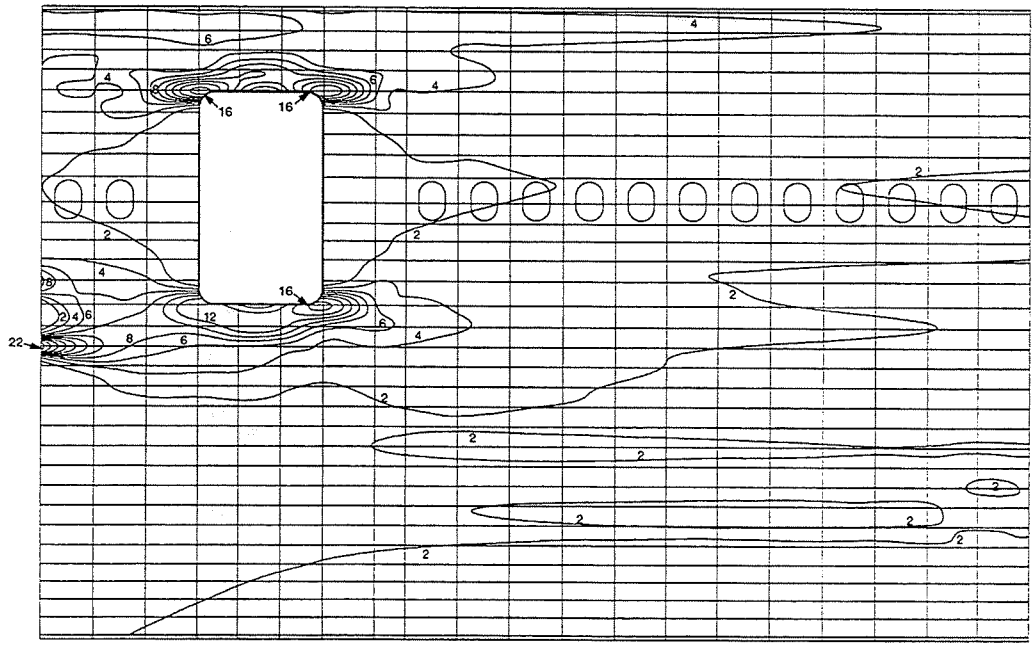

Figure 3-12. Maximum tension loads (kips/in) in the side quadrant.

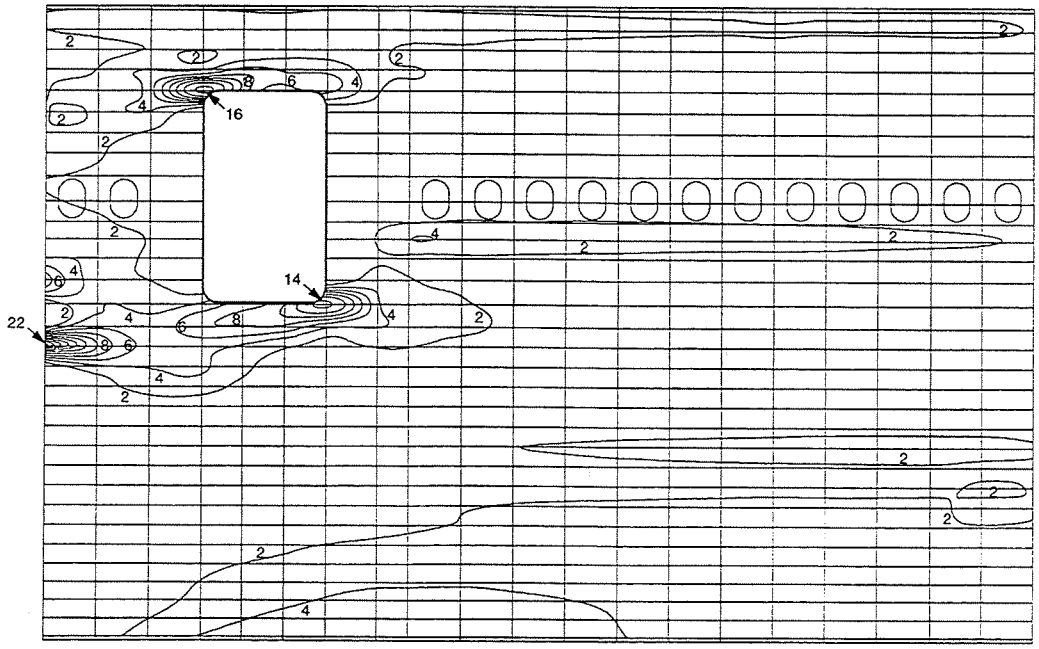

Figure 3-13. Maximum compression loads (kips/in) in the side quadrant.

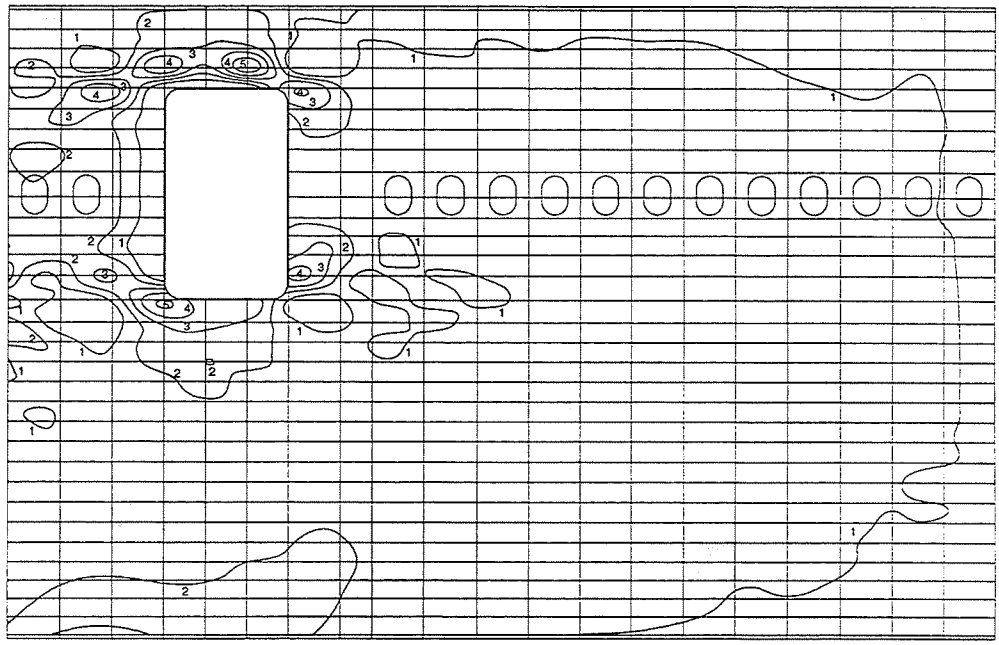

Figure 3-14. Maximum shear loads (kips/in) in the side quadrant.

Several structural issues influenced the side quadrant design. Figures 3-15 through 3-17 illustrate the margins of safety for skin buckling, compression damage tolerance, and tension damage tolerance, respectively. Margins in the window-belt region were not accurately determined in this particular analysis, and are therefore not shown. As can be seen, skin buckling was important primarily in the middle portion of the lower side and in the mid-to-upper portion of the forward side. Compression damage tolerance was important in the lower-aft end, while tension damage tolerance was critical in the middle of the upper side. It should be noted that these latter two figures include both axial and 45° damage tolerance margins. Localized regions near the passenger door corners and along the quadrant's upper edge were also influenced by ultimate compression and ultimate tension strength, respectively. As indicated in Figure 3-18, the majority of the aft end was controlled by minimum-gage requirements.

The circumferential frame design was controlled by the required stiffness to preclude general instability. Local buckling of the frame cap also played a role in determining the frame geometry.

The passenger floor stanchion sizing was controlled by the matching of the metallic stiffnesses; the resulting strain levels were low relative to the estimated design values. The window frame design was controlled primarily by peak strains, but also somewhat by fastener bearing.

As in the crown, bearing/bypass considerations controlled most of the longitudinal and circumferential splice designs, although additional plies were required in some regions to avoid excessive fastener countersink.

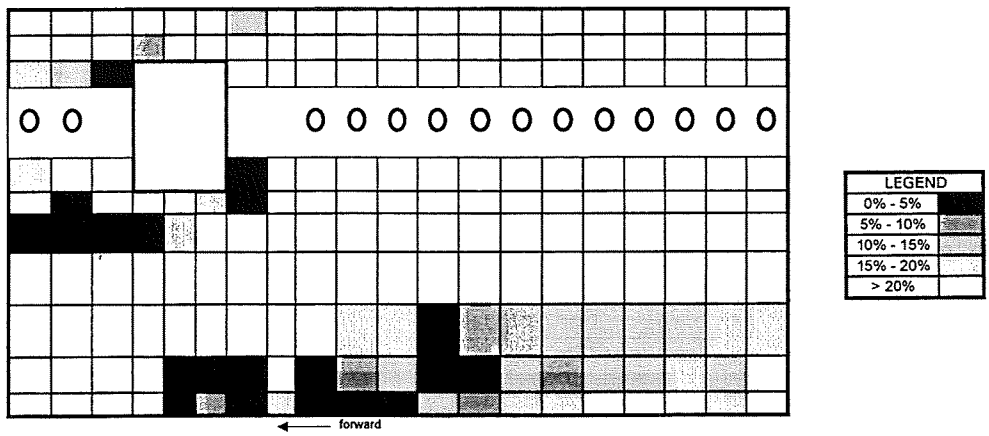

Figure 3-15. Margins of safety for skin buckling in the side quadrant.

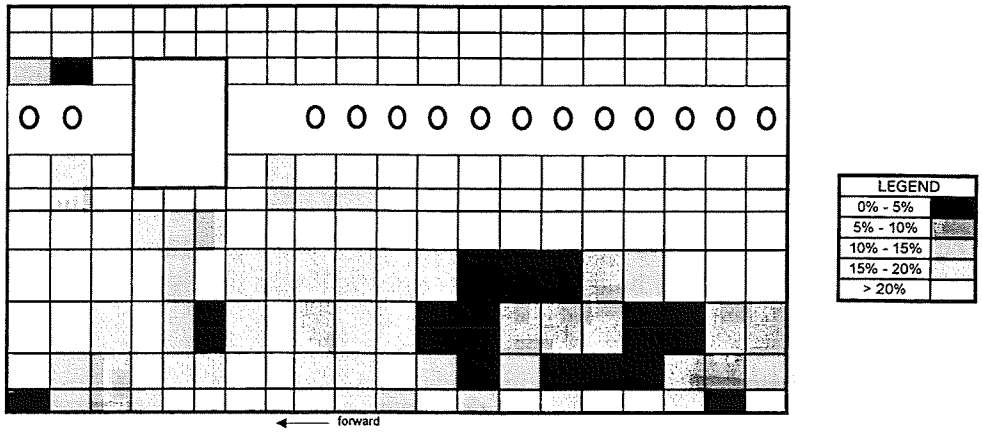

Figure 3-16. Margins of safety for compression damage tolerance in the side quadrant (includes both axial and 45° checks).

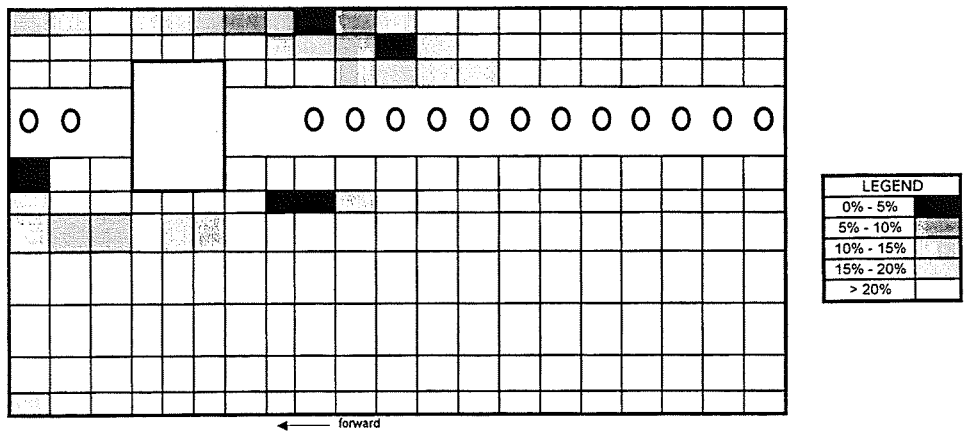

Figure 3-17. Margins of safety for tension damage tolerance in the side quadrant (includes both axial and 45° checks).

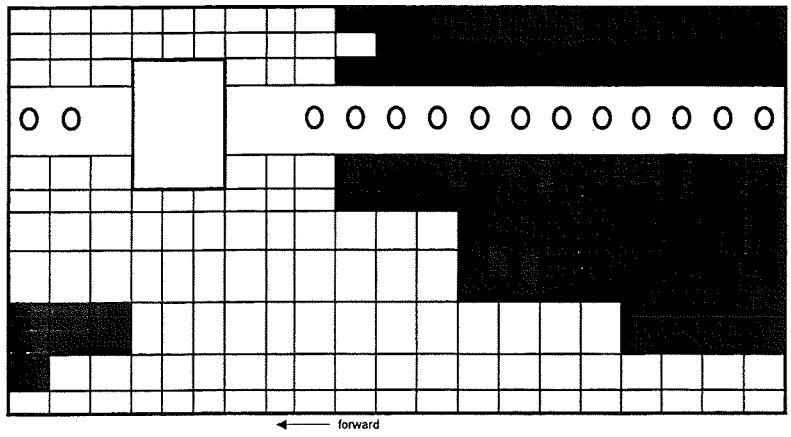

Figure 3-18. Regions of the side quadrant controlled by minimum-facesheet-thickness requirements.

4.0 INTERNAL LOAD PATHS

Internal loads must be determined to provide a basis for detailed assessment of structural capability. This requires consideration of external pressure distributions on the aircraft as well as the mass and stiffness distributions. The process is inherently iterative with design development since the structural configuration and load distributions are codependent. In the fuselage study section, significant load gradients are present due to the presence of large cutouts (e.g., doors, wheel wells).

4.1 Related ATCAS Developments

The composites loads model mentioned in previous discussions was developed under a closely coupled NASA contract (Task 3 of NAS1-19349) to assess global fuselage response. Detailed descriptions of this work are contained in [11] and [12]. The model has gone through several improvements in the course of its development, and the latest version is shown in Figure 4-1. All primary structural elements were represented, with the exception of the passenger doors and the cargo door cutout. The passenger door was assumed to only react internal pressure, and the load resultants were applied to the door stops. The cargo door was not included due to limited resources to address associated complex issues.

The skin was modeled using 4-noded quadrilateral elements (2 per bay). The bending stiffness of the elements in the side and keel was increased to accurately reflect the effect of the sandwich configuration. The hat stringers in the crown quadrant were modeled as offset beams, while the frames throughout the entire model were simulated as beams supported by plate elements, representing the shear attachment to the skin. In the crown, these plate elements were sized to account for the existence of the stringer mouseholes. The intercostals in the forward keel were discretely modeled using plates to avoid inaccurate axial load pickup. The window cutouts and window frames were discretely modeled. Padups for the longitudinal splices were included to capture their effect on axial load distributions. Fillets at the door corners were modeled to avoid artificial concentrations. A refined mesh and a splice plate were modeled in the forward keel to properly address the load introduction at this critical location. All materials were modeled using an orthotropic constitutive law.

Results from the composite loads model were compared with those from the metals model for the 2.5g vertical maneuver flight condition. Load distributions were in general agreement, and localized differences in load levels appeared to be within acceptable limits for this stage of development.

Sensitivities of the internal loads to significant quadrant stiffness changes were evaluated using the composites loads model [12]. The two crown-quadrant concepts evaluated differed primarily in their axial laminate stiffnesses; the *Soft Crown* represented an early crown design with approximately 33% lower axial stiffness than the more recent *Hard Crown* concept. The two side-quadrant designs considered in the study differed in

several ways; the *Thick Side* was an earlier, less optimized design with a larger sandwich-panel thickness than the *Thin Side* concept. The 2.5g vertical maneuver loading condition was used for the study.

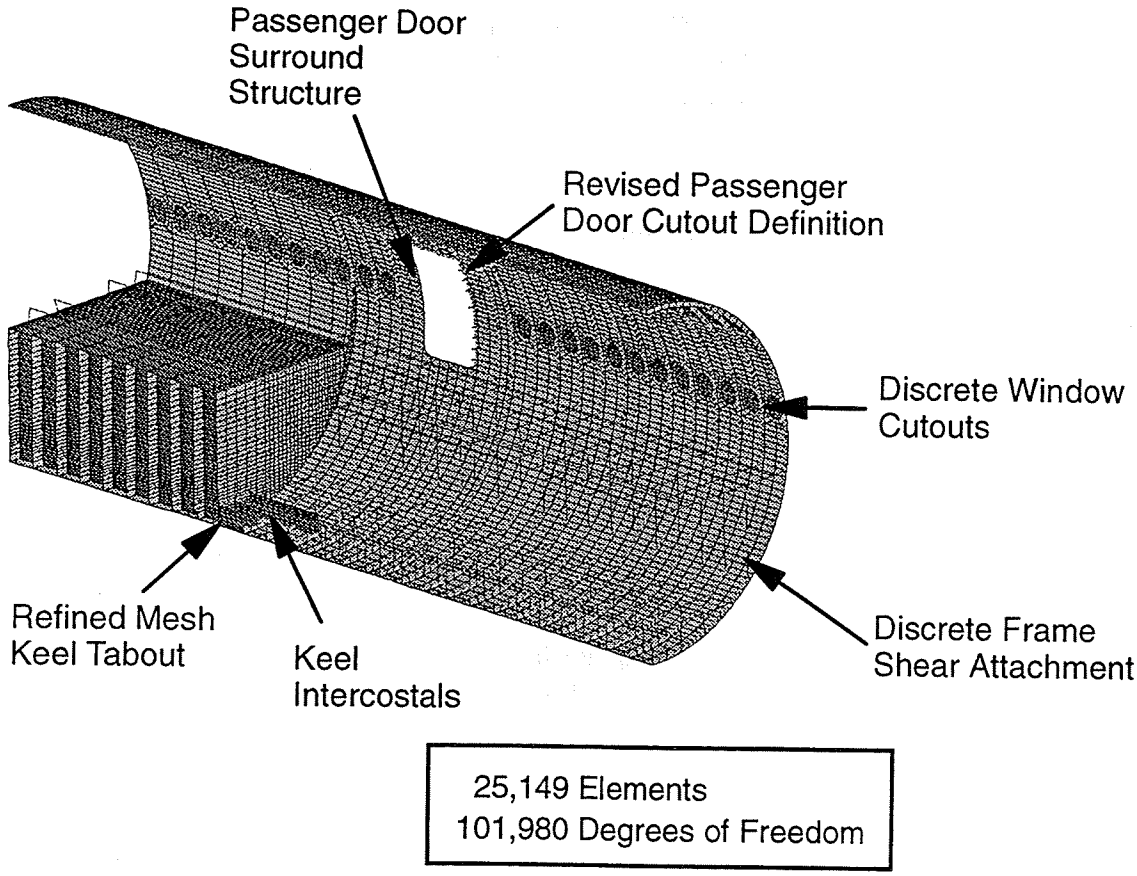

Figure 4-1. Composites loads model.

The configuration changes resulted in increased axial loading of the forward crown, and altered load redistribution near the passenger door cutout and the forward keel due to the neutral axis shift. The detailed effects on the forward keel quadrant loading are shown in Figure 4-2. The significant variations in load levels for the non-varying keel design indicate the dependence of individual quadrant loadings on the definition of other quadrants.

Two load redistribution panels (denoted FK1 and FK2) were analyzed and tested to explore the relationship between ply drops, specimen geometry, layup, and load redistribution in compression loaded structure. They were designed to support optimization of the forward keel ply-drop methodology and to assess predictive capabilities with finite element analyses. The panels varied in width (10 to 14 inches) and facesheet thickness (50 to 36 plies per facesheet) along their length such that the facesheet cross-sectional area remained approximately constant. They were equal in size but incorporated different ply drop schemes. In FK1, plies of a given orientation were

dropped in approximate proportion to their presence in the thickest layup, maintaining a nearly constant axial modulus along the panel's length. In FK2, the 0° and 90° plies were preferentially dropped, creating a higher-shear-stiffness laminate in the thinner region.

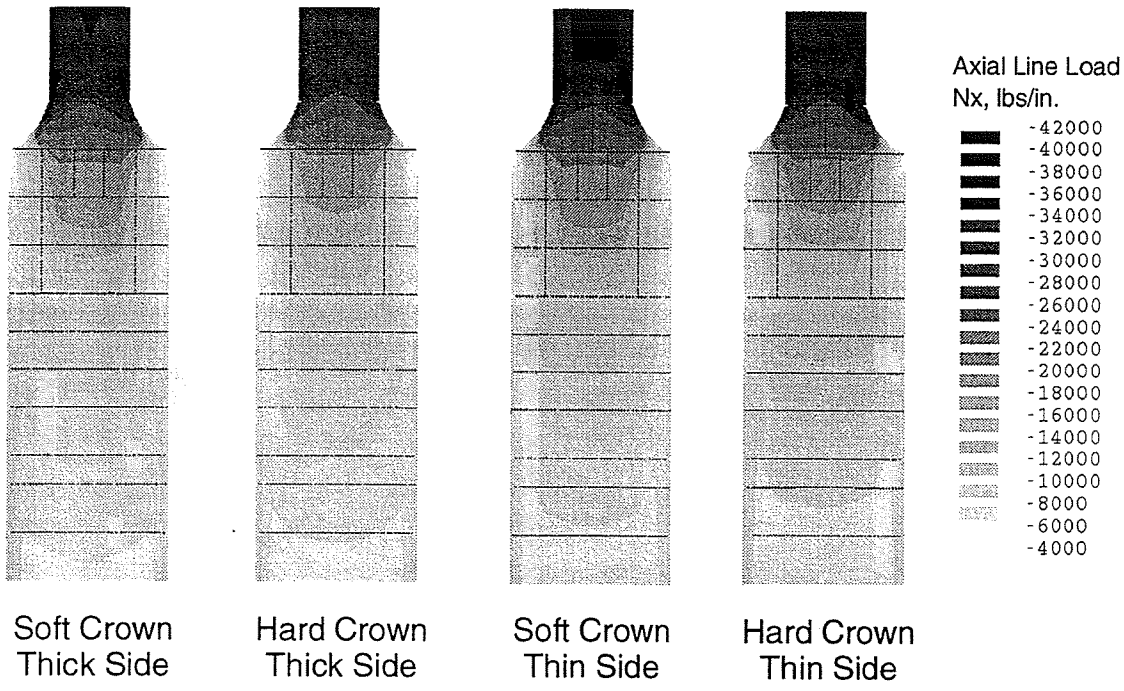

Figure 4-2. Forward keel load changes with varying crown and side quadrant definitions.

In general, the correlation between pre-test finite-element predictions and measured strains was very good, and establishes confidence in the analytical models of the FK1 and FK2 test specimens. It should be noted, however, that these models were significantly more detailed than is typical for internal loads modeling. Local gradients due to specimen geometry and laminate tapering (ply drops) were accurately predicted and, in the case of FK2, variations in strain between the outer and inner facesheets were fairly well predicted. Most of the less-accurate predictions were confined to the areas where the most severe manufacturing anomalies occurred.

A similar modeling approach was extended to the fuselage configuration [12]. Early analyses indicated representations of the forward keel splice plate and a large section of the side quadrant were necessary to obtain accurate predictions of load redistribution within the panel. Analyses of the two ply-drop philosophies addressed with panels FK1 and FK2 revealed that maintaining ±45° plies along the edge of the keel quadrant resulted in a more effective redistribution of the concentrated tab-out load into the lower side panels. Additional configurational variations were evaluated in attempts to increase the load diffusion from the keel to the side quadrants [12] in vertical bending load cases. Keel load reductions greater than 10% (as measured approximately 10 feet aft of the forward end), however, were not achieved. This is likely due to the natural tendency for

loads induced by vertical fuselage bending to be greatest in the structure furthest from the neutral axis (i.e., the keel and crown).

In initial versions of the composite loads model, the window cutouts were not explicitly modeled. Instead, the axial and shear stiffnesses of the skin elements were adjusted to simulate the reduced load-carrying capacity of the cutout regions. Comparison of strain levels determined using this approach with those obtained from later models that did explicitly include the cutouts are shown in Figure 4-3 for the *positive gust with internal pressure* load condition. The results indicate that load distributions away from the immediate vicinity of the window region can be adequately obtained using the reduced-stiffness method. Including the individual window cutouts, however, provides excellent visualization of the local load concentrations associated with the cutouts, despite having insufficient refinement to ensure accurate absolute magnitudes. Moreover, the ability to assess the extent of the redistribution zone allows boundary conditions for local analyses to be selected with higher confidence.

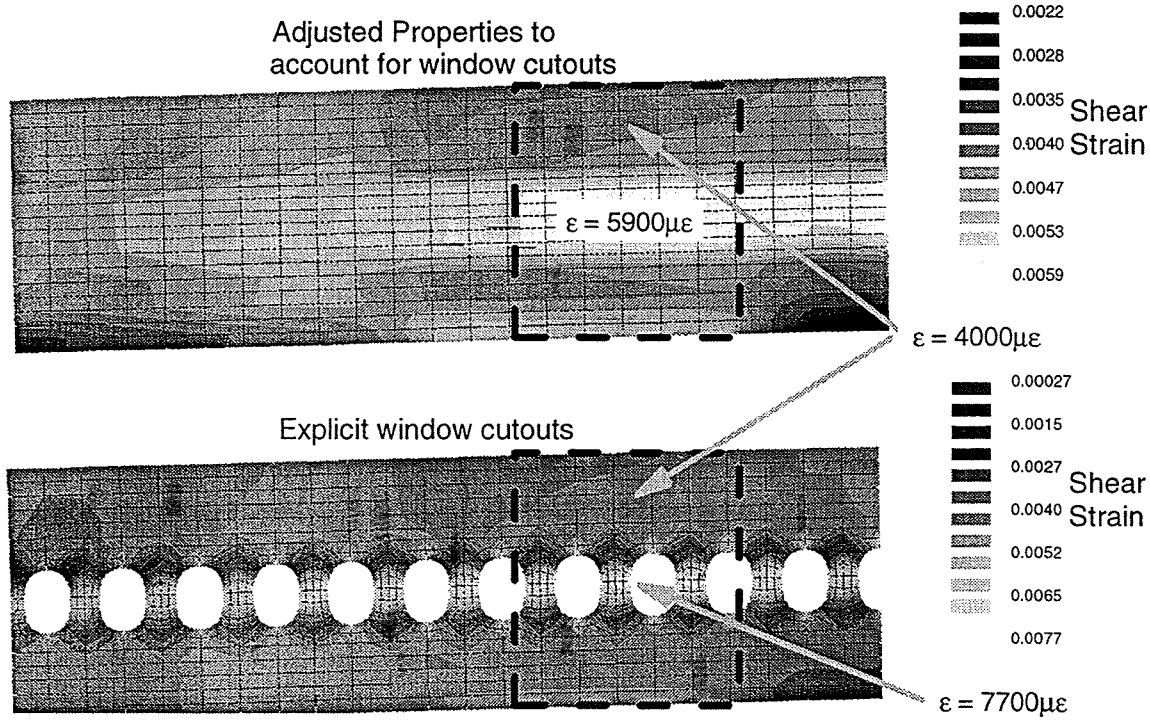

Figure 4-3. Effect of explicit modeling of the window cutouts on strain distributions.

A pressure-box test of a side panel with 3 frames and 2 windows, designated SW4, was conducted in December, 1995 at NASA Langley Research Center (LaRC). The primary goal of this test was to obtain load distributions in the vicinity of window cutouts for assessment of predictive techniques. Applied loads included internal pressure and axial tension loads, separately and combined. Tests were conducted for the nominal configuration and for simulated wide-frame-spacing. This latter condition was

approximated by removing the central frame's web and cap. Good correlation was observed in preliminary comparisons of measured and predicted strains. More detailed comparisons, however, have not yet been conducted.

4.2 Outstanding Issues

Several important issues relative to internal load distributions remain unresolved. Internal loads that reflect the current composite design definitions have not been used to resize the quadrants. This would likely result in only minor modifications to the keel quadrant, which already reflects composite loads, but may have a larger impact on both the crown and side quadrants, which were sized to metallic load levels. A full compliment of load cases, reflecting all combinations of flight conditions and mass distributions, have not been addressed in the development of composite internal loads. While consideration of all load cases is impractical in the preliminary design environment, a more thorough review of critical load cases for the metallic structure could lead to the judicial selection of several additional cases that design relatively localized regions. In addition, load cases that are critical to the frame and floor designs could be added.

The relationships between modeling approaches used in internal-loads models and the predicted global load distributions have not been thoroughly assessed. The relatively coarse discretization and linear solution sequences necessitated by schedule and budget constraints limits the accuracy of these models in predicting the effects of nonlinear responses and design details (e.g., post-buckled skins, pressure-pillowing, ply-drop schemes).

A critical assessment of current capabilities for predicting load distributions has not been conducted. Composite materials exhibit low transverse shear stiffness, which results in a range of ineffectivity for added plies and discontinuous stiffening elements. In addition, tests of notched laminates suggest that the selected materials may exhibit non-local response [7], which is characterized by broader, less severe concentrations than predicted using classical constitutive laws. Experimental measurements of load transfer in stiffening elements, through ply drops, and around large cutouts for assessing predictive capability are very limited. Pressure-box tests of ATCAS crown panels included measurements that might support assessment of load transfer in stiffening elements, but have not been evaluated in that regard.

A forward keel panel, designated FK5, has been fabricated and delivered to NASA LaRC for compression testing, and will provide valuable data for assessing load redistribution in the vicinity of the forward keel tabout and major ply tailoring. Test results obtained from the window-belt pressure-box panel (SW4) provide load-redistribution data for internal pressure and axial loads. An additional side panel with 5 frames and 4 windows, designated SW6, has been partially fabricated and will be delivered to NASA LaRC for testing in the D-box test fixture [16], and will provide cutout load redistribution data in the presence of internal pressure, axial tension, axial compression, and in-plane shear (separately and combined).

Load levels and distributions in circumferential frames are not well defined. Determination of detailed frame loads distributions from loads-model results is necessary to ensure their adequate design. The pressure-box tests of undamaged panels conducted to date can likely provide data to support the assessment of the actual distributions for both skin/stringer and sandwich configurations, and determination of both local and global modeling strategies to adequately predict them. Testing Panel SW6 in the D-box will also provide supporting data for sandwich designs.

5.0 STABILITY

Several possible stability modes must be addressed during fuselage structural evaluations. General cylinder buckling and skin buckling must be considered in all ATCAS quadrants, as well as local and torsional buckling of the circumferential frames. In the skin/stringer crown, local and column buckling of the stringers must be assessed. In the sandwich side and keel quadrants, stability considerations include facesheet disbonds, facesheet dimpling and wrinkling, and crimping.

5.1 Related ATCAS Developments

5.1.1 Crown Quadrant

Building-block tests were conducted to evaluate several compression-stability aspects of the ATCAS crown quadrant designs, as shown in Figure 5-1. Crippling tests were conducted on 36 single stringer/skin elements representative of a range of crown-panel design options to provide insights into local stability of the stringers [17]. Six of these addressed the blade stringer used along the crown/side longitudinal splice, while the remainder addressed hat stringer sections. Test variables included cross-sectional geometry, material, impact damage, impact location, and specimen length.

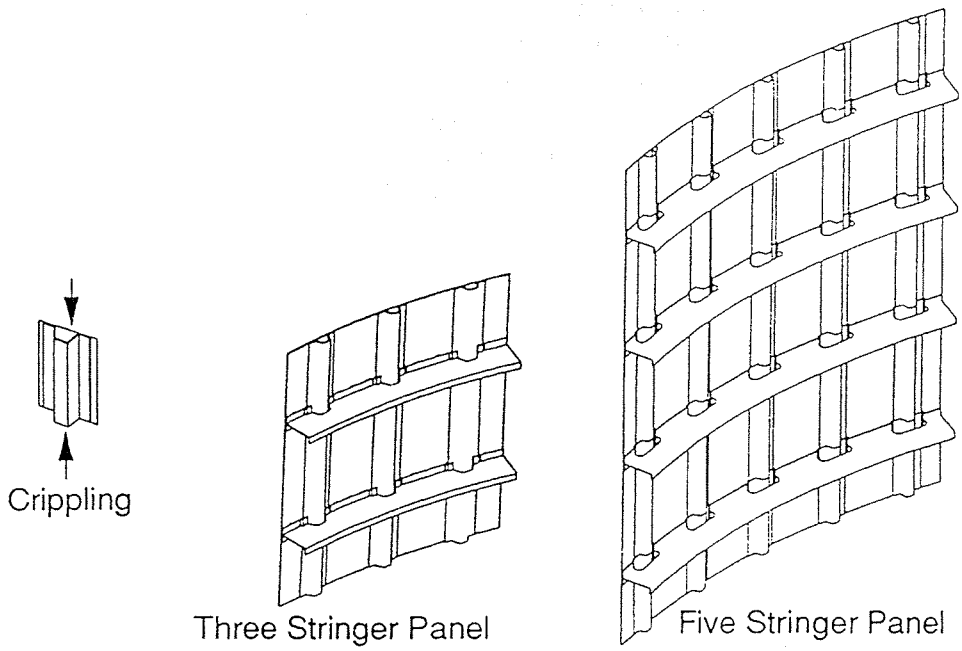

Figure 5-1. Building-block tests for crown-quadrant stability issues.

Significantly different undamaged and damaged responses were observed between AFP and hand-laid-tape crippling elements. The AFP specimens exhibited initial buckling

and final failure at loads approximately 20% below those of the tape specimens. Some of the difference in initial buckling was attributed to reduced compression and shear stiffnesses of AFP laminates measured in separate tests [7, 17]. The undamaged failures of both materials were sudden and catastrophic, and were located within the outer quarter of the specimen length. Buckling predictions using finite strip methods [18] were approximately 20 to 25% above measured values, typical of that found in similar studies. Obtaining this level of accuracy, however, was dependent on properly accounting for the stiffness increase and thickness reduction in the skin beneath the hat caused by stringer-mandrel expansion during cure.

Specimens that had been subjected to stringer-cap impact damage exhibited sublaminate buckling at, and failed through, the damage site for both material forms. Despite this similarity, however, the maximum loads and failure modes differed significantly. The tape specimens exhibited approximately 40% greater load-carrying capability than the tow specimens. Severe local deflections at the damage site formed as the tape specimens were loaded to failure. The failure event in these specimens was sudden, crushing the skin and stringer material, and separating the stringer from the skin. In contrast, the damage in the AFP specimens progressed from the stringer cap down both of the webs and was arrested at the attached flanges. Prior to failure of these specimens, severe sublaminate buckling was observed in both the stringer cap and web, and significant overall specimen bending was evident.

Five 3-stringer, 2-frame panels (two flat, three curved) were tested to assess skin buckling [17]. The two flat panels, one with blade stringers, one with hat stringers, and both with skin impact damage were tested in compression to failure. Their configurations did not represent specific crown designs. The impact damage did not appear to significantly affect the failures, which were caused by crippling at the panel end and stringer separation from the skin, for the blade- and hat-stiffened panels, respectively. Transverse deflections due to overall panel buckling were observed on both panels prior to failure.

The three curved panels contained hat stringers, and were compression tested to failure. The general test specimen configuration and the design details of each source panel are shown in Figures 5-2, 5-3, and 5-4. These panel configurations represented early crown design options, with low axial skin stiffness, although the failsafe frame chords were not included on the test panels. Figure 5-5 contains the specific source panels for the specimens, and the impact energies and locations.

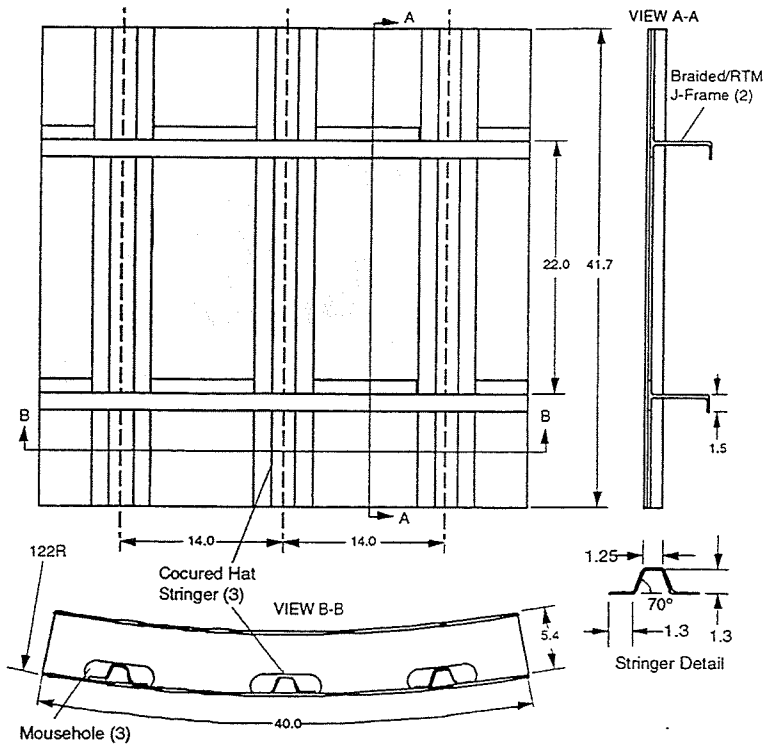

Figure 5-2. Three-stringer crown compression panel configuration.

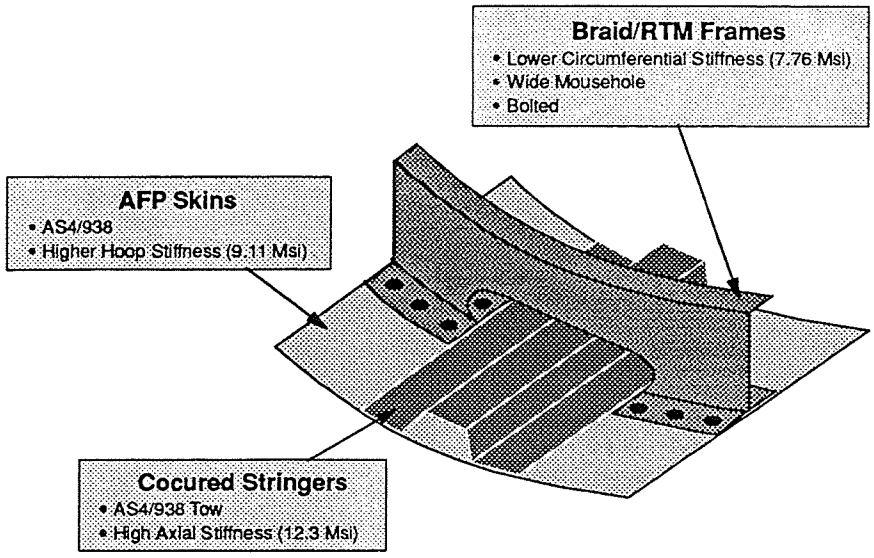

Figure 5-3. Panel 11b structural configuration.

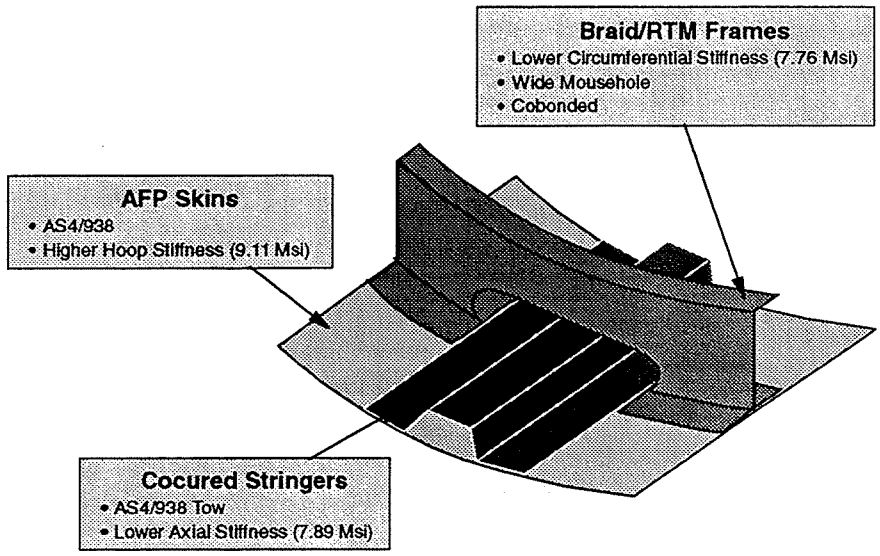

Figure 5-4. Panel 11a structural configuration.

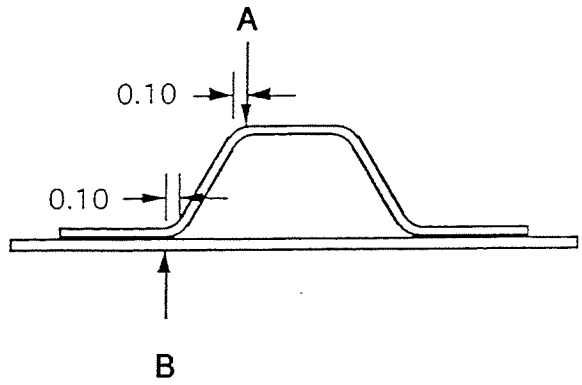

Source Panel	Description	Impact Energy and Tup Diameter at Location A		Impact Energy and Tup Diameter at Location B	
11a	Soft Stringer Soft Skin	None		None	
11a	Soft Stringer Soft Skin	200 in.-lbs.	1 in.	500 in.-lbs.	2.5 in.
11b	Hard Stringer Soft Skin	200 in.-lbs.	1 in.	200 in.-lbs.	1 in.

Figure 5-5. Impact damage specifications for 3-stringer crown compression panels.

Skin buckling in these panels was bounded by simple curved-shell predictions assuming all sides simply supported and all sides clamped. The clamped boundary condition that the hat stringers impose on the skin was evidenced by the inward buckling of the skin on both sides of the central stringer. Beam-column effects due to out-of-plane forces imparted on the stringer by the buckled skin apparently contributed to a stringer-separation failure that occurred well below the predicted overall panel buckling load. This separation, in fact, did not occur at the bondline, but within the skin's surface ply, consistent with bonded joint fracture toughness tests [7]. The BVID seemed to have only a small effect on panel failure, yet this may have been influenced by the direction of the panel secondary bending. Failure of the damaged panels initiated at the site of the stringer-flange impact. The undamaged panel failed at a similar location at an approximately 7% higher load than its damaged counterpart, indicating that the effect of this specific skin damage is relatively small. The stringer-cap damage did not have a significant effect on the panel failure since the compressive strains there were relieved by the beam-column deflections. Differing mode shapes in larger panels, though, may aggravate rather than relieve these strains. The post-buckling ratio for these panels calculated using the measured skin-buckling load was approximately 30%, while that determined using the all-sides-simply-supported predictions was approximately 22%.

Compression tests were also conducted on a single 5-stringer, 4-frame panel that represented early design concepts for the forward crown [19]. The test panel configuration and design details are shown in Figure 5-6. The panel successfully sustained 125% of the ultimate axial load without damage. In addition, the panel sustained 100% of ultimate load with BVID created by the events described in Figure 5-7. The damage did not appear to influence the overall panel response. The frames maintained the nodal lines for the buckled skin, despite the large mousehole cutouts. No evidence of stringer twisting was observed in either of these tests. The panel successfully sustained 110% of the limit axial load with a simulated 1-bay frame disbond located as shown in Figure 5-7. This disbond simulation was accomplished by removing the outer portion of the frame web between two mouseholes, decoupling the frame's bending stiffness from the skin in that region. The skin at this location buckled outward during the test, while panel areas remote to the disbond buckled inwards, as was observed in the undamaged test. This response resulted in stringer twisting.

The final test of this panel was conducted after repair of the simulated frame disbond. The frame repair resulted in initial panel buckling loads and post-buckled shapes nearly identical to those of the undamaged panel. Failure of the panel occurred at approximately 4000 $\mu\varepsilon$ through BVID "location 1" (see Figure 5-7) at 185% of ultimate load, and was accompanied and/or caused by skin/stringer separation. The failure was immediately preceded by a buckling mode change that resulted in a buckling-node shift to the impact location and significant rolling of an adjacent frame. The post-buckling ratio for these panels calculated using the measured skin-buckling load was approximately 39%, while that determined using the all-sides-simply-supported predictions was approximately 28%.

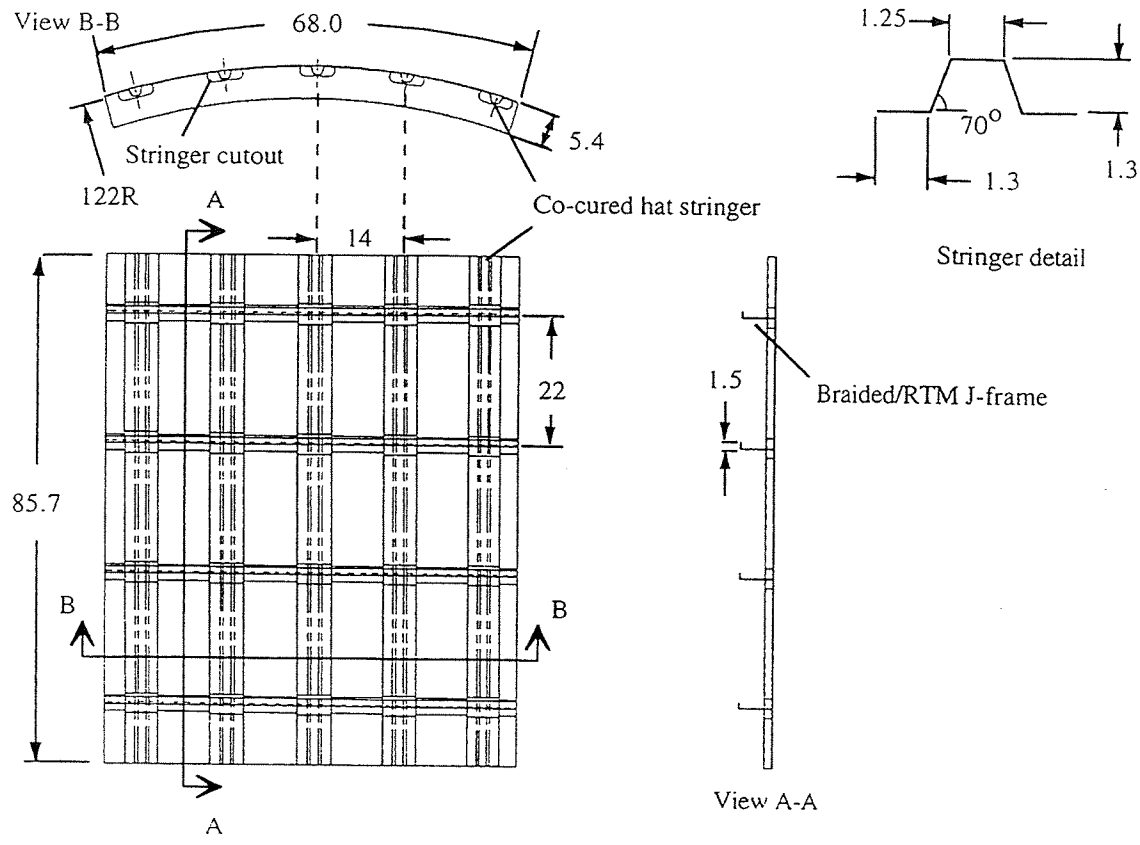

Figure 5-6. Crown 5-stringer compression test panel description.

Several important related developments were achieved under Task 3 of contract NAS1-19349, and are mentioned here for completeness. Current design guidelines for postbuckling ratio were evaluated by reviewing available test results of stiffened panels subjected to compression and/or shear loading. A wide range of test panel variables were represented, including stringer cross-sections (hat, blade, J, and I), skin thickness (0.035 to 0.28 inch), stringer spacing (4 to 14 inches), and stringer attachment (bonded, cocured, integral, and bolted). In many cases, panels contained BVID. In some cases the panels were subjected to hot/wet conditioning and/or cyclic loading prior to testing. Several panels contained embedded defects which were assumed to be non-detectable by available non-destructive evaluation (NDE) methods.

The design criterion prohibiting skin buckling below 40% of ultimate load was found to be overly conservative for panel configurations with low skin-buckling strains (i.e., below 1000 με for compression and 2000 με for shear), and unconservative for those with higher skin-buckling strains. A modified design criterion was proposed based on a power-law relationship between post-buckling ratio and skin buckling strain.

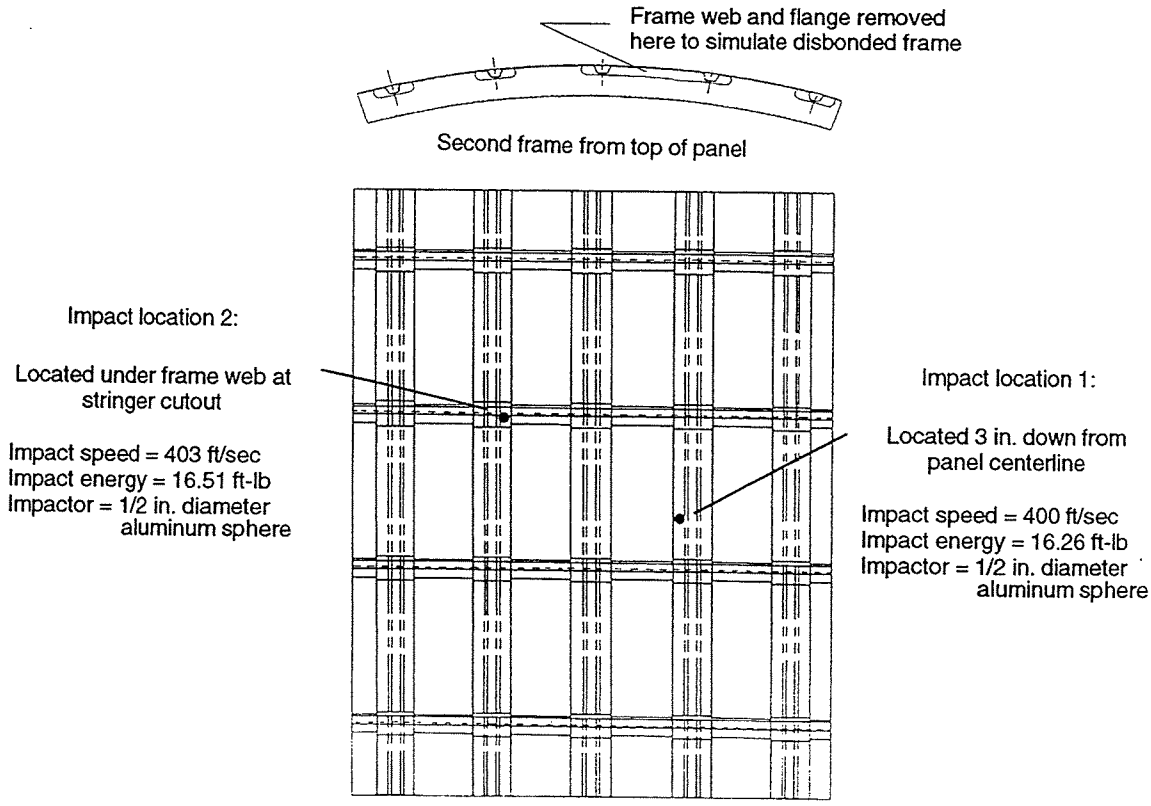

Figure 5-7. Impact damage specifications and delaminated-frame simulation for crown 5-stringer compression panel.

The accuracy of the closed-form solutions used to predict skin-bay buckling in skin/stringer configurations was also evaluated under this same contract. Multi-bay finite element analyses indicated that the closed-form methods assuming simple supports on all four sides significantly underpredict the skin buckling loads of some structural configurations, for compression and/or shear loading. The additional fixity provided by the attached stringer flanges was found to be responsible for much of the difference. A Rayleigh-Ritz-based computer program was developed to predict the buckling loads and modes for a flat plate consisting of up to three adjacent regions of differing thickness and stiffnesses. The results from this method compared favorably with those from the multi-bay finite element model.

5.1.2 Keel Quadrant

A detailed finite element analysis of the forward keel was conducted [12] to verify designs derived using the sizing methods described in Section 3.3. The model, shown in Figure 5-8 included a 12-ft longitudinal segment of the keel quadrant, extending from the forward tab-out to the seventh frame station aft of the wheel-well bulkhead. The portion of the side quadrant between the splice with the keel and the over-wing longeron was also included to ensure accurate boundary conditions for the keel panel itself. Linear

eigenvalue solutions and nonlinear analysis confirmed the adequacy of the intercostals in providing buckling nodes. The design was also found to have stability-related capability approximately 10% above that expected (i.e., a 30% positive margin of safety versus the criterion-enforced 20%). Detailed review of results also indicated that the intercostal design methodology was somewhat conservative; the modeled intercostals maintained buckling nodes but had strains lower than predicted in the sizing activity.

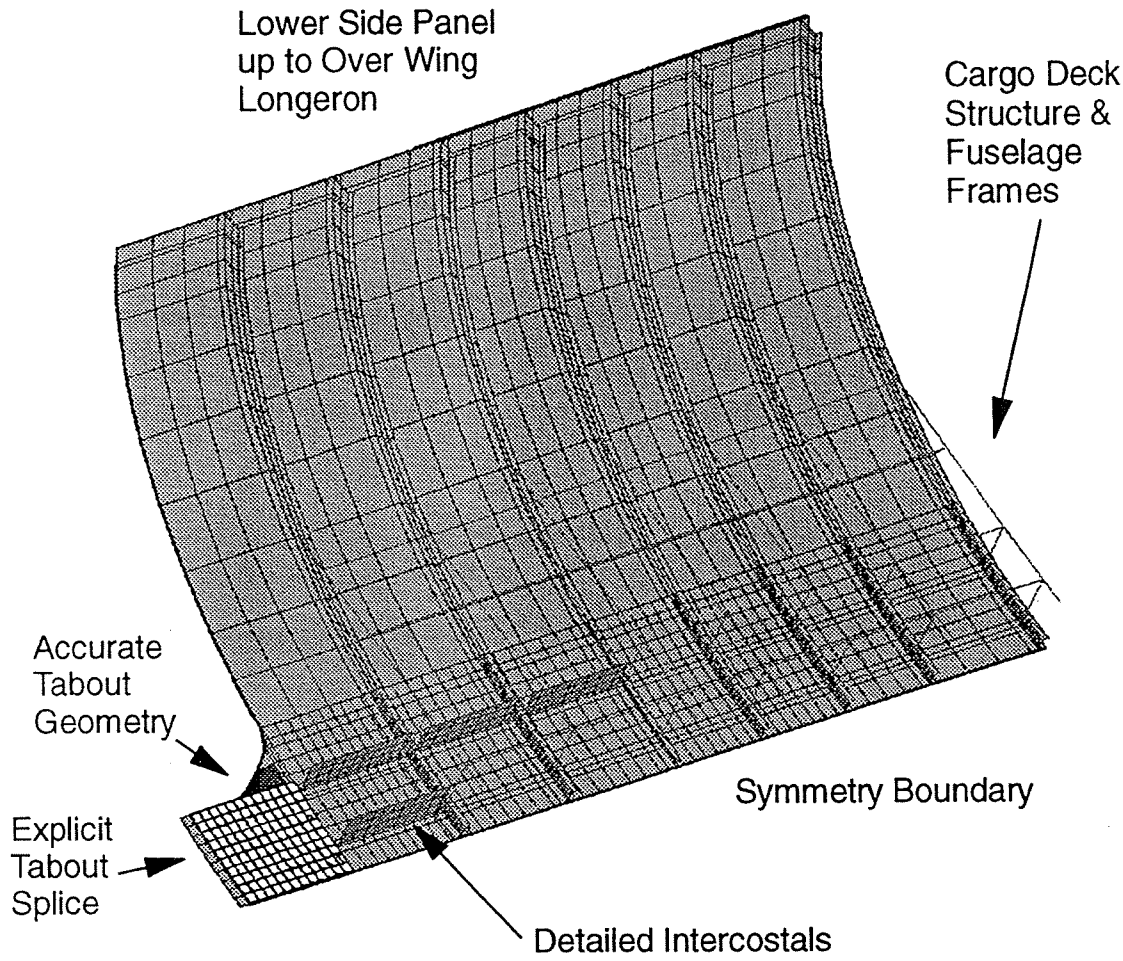

Figure 5-8. Finite element model to evaluate forward keel.

A series of tests were conducted to evaluate the stability of aft keel design concepts and predictive methods. Five flat 15- by 30-inch sandwich specimens and one curved 30- by 44-inch specimen represented a range of facesheet materials, material forms, layups, and core materials [20], as shown in Table 5-1. Each was loaded in compression with their ends potted (an approximate 90% fixity) and unrestrained edges. Significant nonlinear behavior was observed for each at the maximum load level. To preserve test specimens for additional testing, not all were brought to failure; rather, the strain data was extrapolated using a force/stiffness technique to estimate buckling loads. These estimates are compared in Figure 5-9 with predictions made using finite element analyses and the

closed-form sizing methods. The consistent over-prediction by the closed-form methods for the smaller tests is likely related to being based on an infinitely wide plate (i.e., no anticlastic curvature), which is more representative of a fuselage, but not necessarily of a finite width coupon. Finite element predictions, in general, were more accurate than those obtained using the closed-form methods. However, both the finite element analysis and closed-form sizing method underpredicted the observed behavior for the larger test (i.e., AK22), by 8% and 3%, respectively.

Table 5-1. Aft keel stability test specimen definition.

Source Panel	Facesheet Material	Core Material	Curvature	Specimen Size (in.)	Quantity
AK7	T300/F584 Tow	HRP-3/16-8.0	none	15 x 30	2
AK8	T300/F584 Tow	TPC-3/16-5.5	none	15 x 30	1
AK10a	AS4/8552 Tape	HRP-3/16-8.0	none	15 x 30	1
AK10b	AS4/8552 Tape	HRP-3/16-8.0	none	15 x 30	1
AK10c	AS4/8552 Tow	HRP-3/16-8.0	none	15 x 30	1
AK22	AS4/8552 Tow	HRP-3/16-8.0	r = 122 in	30 x 44	1

Note: Layup of all facesheets: [+45/0/-45/90/0/+45/-45/0/90/-45/0/+45]
All cores are 0.75-inch thick

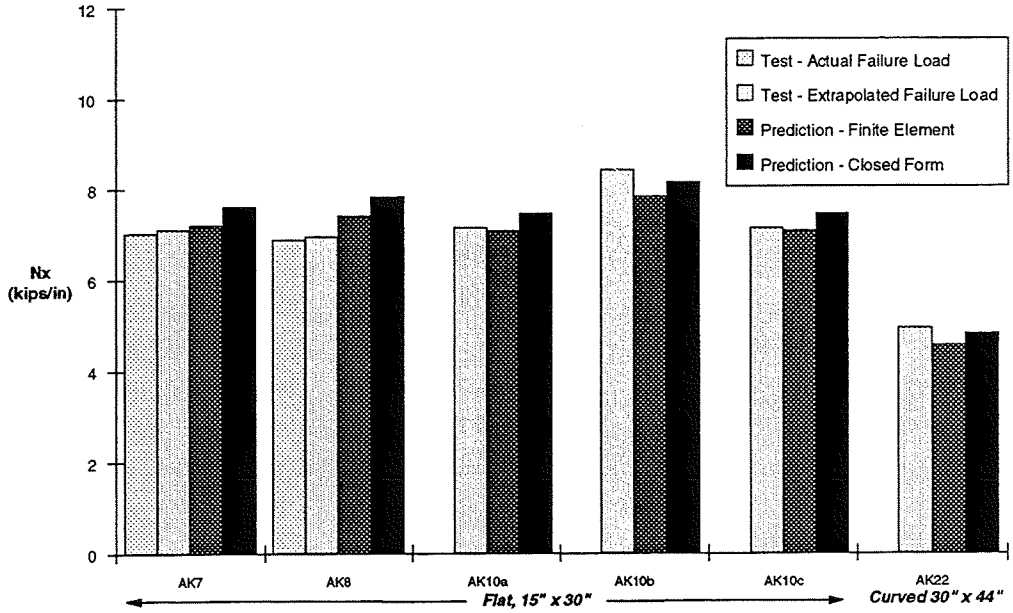

Figure 5-9. Comparison of aft keel stability test results with finite-element and closed-form predictions.

A detailed assessment of stability in the presence of ply drops and variable axial loads was conducted by Material Science Corporation, under ATCAS subcontract [21].

Several approaches to account for transverse shear were evaluated using detailed finite element models of three different frame bays. Results indicated thick shell elements with transverse shear flexibility can provide a reasonable approximation of global panel response, and geometrically nonlinear solutions are necessary to obtain accurate core shear stresses. The results were also used to determine the panel widths necessary to obtain reasonable stability predictions with the closed-form compression-sandwich-stability solutions used in quadrant sizing.

5.2 Outstanding Issues

A number of stability-related issues require additional attention. Shear and combined compression/shear stability are issues of major concern. This loading dominates the side quadrant, and little experimental data exists to critically assess predictive capability. Shear tests of both skin/stringer and sandwich configurations are necessary to address the lower portions of the crown and the upper portion of the side, respectively. Combined compression/shear tests of sandwich designs are required to address the lower side.

Several criteria must be more thoroughly studied and, if indicated, appropriately updated. The effects of these updates on the quadrant designs must be evaluated, and predictive methods must be experimentally validated for the new design spaces. Specifically, existing evidence suggests a reduction of the minimum postbuckling ratio to 33% of ultimate load is acceptable for skin/stringer configurations. The ability of the designs to avoid skin/stringer separation and to maintain buckling nodes at the frames must be assessed if such a criterion is pursued. In addition, requiring a minimum 20% positive margin of safety for stringer column buckling appears prudent, since such instability is typically catastrophic. This 20% margin accounts for any initial imperfections, and has proven effective for other Boeing applications. A more thorough assessment of potential manufacturing defects and in-service damage is needed, specifically to address disbonding of frames and/or stringers from the skin, and disbonding of facesheets from the core. Improved criteria and corresponding design-sizing methods related to the effects of this disbonding on stability are also needed.

The effect of impact damage on stability response also requires further study. Modeling of damage as soft inclusions has proven relatively successful. This approach should be extended to thoroughly assess critical impact locations in the quadrant structural arrangements. In particular, such damage in the skin may influence the minimum postbuckling-ratio criterion. It may also influence crippling and stringer column stability.

Similarly, the effect of pressure-induced out-of-plane deformations on compression and shear stability should be assessed experimentally, primarily for skin/stringer configurations where these deflections are more pronounced. These deformations act as initial imperfections; the membrane tension, however, may counteract this effect to some extent.

The relationship between tests of differing scales must be more thoroughly assessed to determine the value of conducting small-scale tests. The ATCAS stability database contains significant relevant data, but has not been evaluated in that regard.

Stability modes for circumferential frames must be addressed, including developing sizing methods and supporting test data. Of particular concern is the frame rolling mode, which is strongly dependent on structural configuration (e.g., connections to stringers).

Finally, several methods used to size the structure need improvement. The boundary conditions assumed in sizing for skin buckling require verification, particularly for sandwich structure. Curvature-correction factors used in cylindrical stability calculations for sandwich structure require further definition. The assumption that the intercostals must withstand 7% of the inplane loads to provide a stability node is conservative, and should be modified to provide an acceptable sizing guideline. Each of these issues can likely be accomplished primarily using detailed finite element analyses with limited supporting tests.

6.0 ULTIMATE STRENGTH

This section specifically addresses the strength capability of the skins and structural elements (e.g., frames, floors, intercostals) in the presence of ultimate loads. Other important components of ensuring adequate structural performance at ultimate load levels are discussed in *5.0 Stability,* and *7.0 Attachments and Splices.* In contrast to damage tolerance evaluations, ultimate strength addresses likely service damages in combination with load levels much higher than those actual expected in flight.

6.1 Related ATCAS Developments

6.1.1 Crown Quadrant

Four configured crown panels, designated Panel 11b, Panel 12, TCAPS-1 and TCAPS-5, were tested in an undamaged state in a pressure-box fixture. This test fixture was designed to simultaneously apply axial tension loads and internal pressure while providing boundary conditions representative of fuselage structure [22]. The test panels represented a range of aft crown design options, and contained 3 frames and 4 stringers, as shown in Figure 6-1.

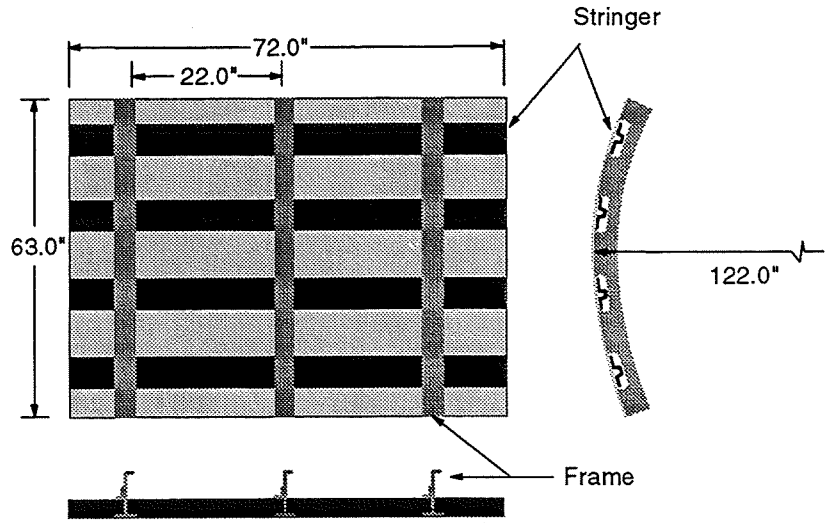

Figure 6-1. Pressure-box test panel geometry.

Differences in design detail are highlighted in Figures 6-2, 6-3, and 6-4. Panel 11b included all-graphite skins with a relatively high hoop modulus, and mechanically-fastened frames with mouseholes that extend beyond the full width of the stringers. Panel 12 and TCAPS-1 differed from Panel 11b in that the stringers had a lower axial modulus and the frames were cobonded. The geometry of all but one of the Panel 12 mouseholes was modified prior to test, as shown in Figure 6-5, based on analytical indications of reduced frame-peeling stresses at the mousehole frame-flange end. TCAPS-5 featured a graphite-glass intraply hybrid skin with a relatively low hoop

modulus and higher-stiffness bolted frames. Glass-fabric padups beneath the TCAPS-5 frame allowed a direct mechanical attachment between the frame and the stringer flange, and the mousehole configuration to be significantly narrower.

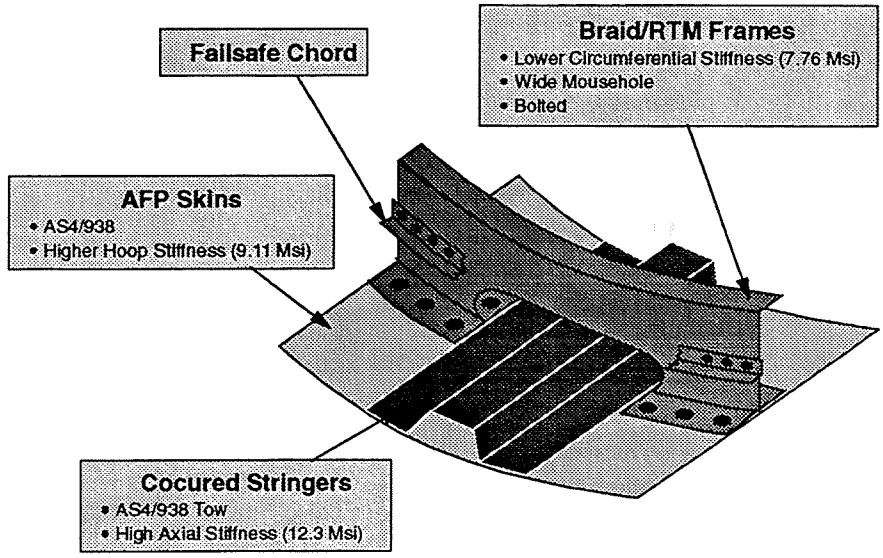

Figure 6-2. Panel 11b structural configuration (failsafe chord shown as discontinuous for clarity).

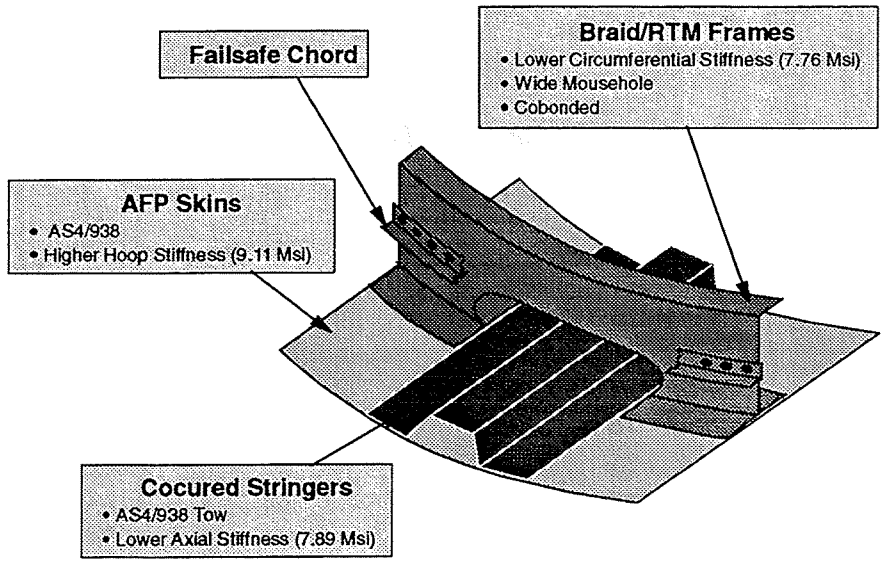

Figure 6-3. Panel 12 and TCAPS-1 structural configuration (failsafe chord shown as discontinuous for clarity).

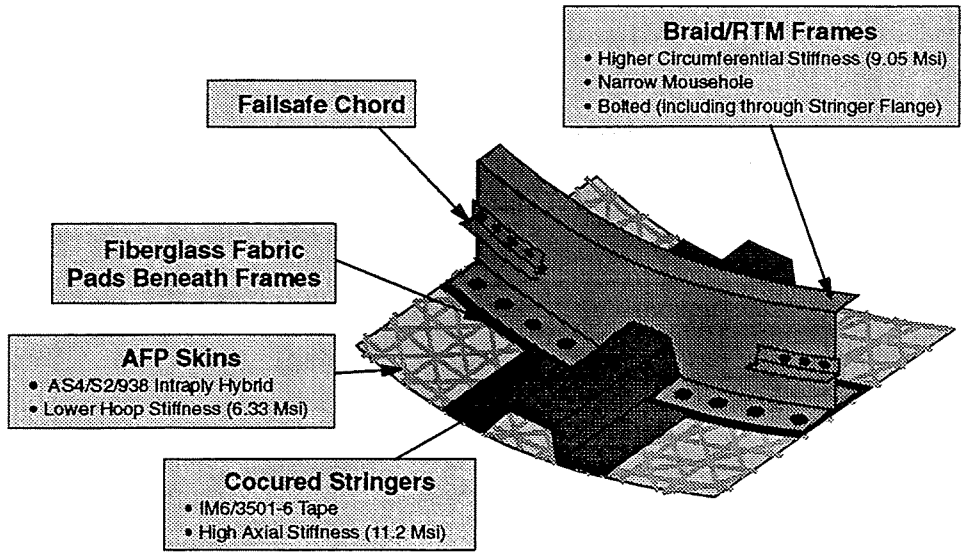

Figure 6-4. TCAPS-5 structural configuration (failsafe chord shown as discontinuous for clarity).

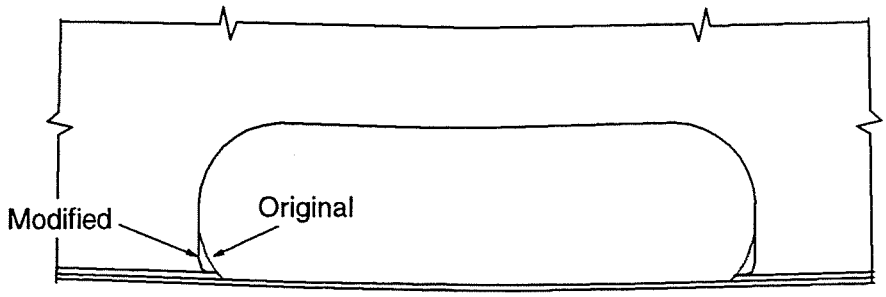

Figure 6-5. Modified mousehole geometry for Panel 12.

Panel 11b and TCAPS-5 successfully sustained the ultimate overpressure condition of 18.2 psi with 1.1 kips/in axial tension (representing the bulkhead reaction of the internal pressure). There were no indications of any damage formation for these bolted-frame panels. Further discussions of TCAPS-5 are contained in [23].

Panel 12 successfully sustained two ultimate load conditions: 13.8 psi with no applied axial load (simulating a compressive axial flight load of 1.1 kips/in) and the overpressure condition of 18.2 psi with 1.1 kips/in applied axial tension. During the first of these conditions, the test was stopped at approximately 11 psi due to unexpected discontinuities in the output of strain gages located on the OML surface directly opposite the gap between the stringer and the frame mousehole cutout. X-rays of the full length of each frame suggested two types of damage had formed during the test: (1) small delaminations in the skin (approximately 0.1 in^2) adjacent to some mousehole frame flange corners, and (2) a hairline matrix crack in the skin along the full width of the

frame at some mousehole frame-flange ends. No further indications of damage growth were observed during the completion of the 13.8 psi condition or during testing of the overpressure condition.

TCAPS-1 failed unexpectedly during a test to evaluate ultimate capability for internal pressure combined with the highest axial tension loads (i.e., 13.8 psi with 5.0 kips/in). Specifically, the panel failed at approximately 11 psi and 4.1 kips/in. Thorough evaluation, including finite element analyses and destructive inspections, indicated that failure was caused by unrepresentative stress concentrations at the intersections of the outer frames and the stringers induced by the large doublers bonded to the panel to introduce the high axial loads. Verified failure criteria do not exist to allow comparison of the test performance relative to that of a true fuselage.

Detailed finite element analyses were conducted of these panels configurations prior to test. Modeling techniques and comparison of predictions with experimental results are discussed for Panel 11b in [24]. Correlation of the predicted strains with the experimental results were reasonable for the hoop-direction. The observed stringer strains and radial deflections were significantly higher than predicted, suggesting differences between modeled and actual stiffnesses of the hoop restraints. Errors were subsequently found in the modeled stiffnesses of the skin reaction hardware, but updated analyses were not conducted.

Detailed discussions of modeling techniques and results for TCAPS-5 are contained in [23]. The errant skin-reaction stiffnesses had not been identified prior to the modeling of this panel, and analyses were not updated. Comparisons of predictions with experimental results are limited, but appear reasonable for a circumferential cut centered between frames. Predictions of strain distributions for TCAPS-1 and Panel 12 have not been extensively compared to experimental measurements due to resource constraints.

Several compression tests, primarily directed at stability issues, provided data regarding the ultimate strength capability of crown quadrant designs. The general configuration of curved 3-stringer, 2-frame compression panels were described in Section 5.1.1 and represented early crown designs with low skin axial stiffness. The test results indicated that the tested concepts met the ultimate compression loading requirements. Secondary stringer bending, initially driven by skin buckling, contributed to the final failure of the panels. The strength reductions due to the BVID were small (i.e., 7%), yet were likely influenced by the direction of the panel's secondary bending, which was in turn affected by the test panel boundary conditions.

Compression tests were also conducted on a single 5-stringer, 4-frame panel, previously described in Section 5.1.1, that represented early design concepts for the forward crown (see Section 5.1.1 and [19]). The panel successfully sustained 125% of the ultimate axial load without damage and failed at 185% of ultimate load with BVID located at two skin/stringer interface locations (and with a repaired circumferential frame).

6.1.2 Keel Quadrant

Uniaxial compression tests of two 2-frame specimens and a single 4-frame panel provided data supporting assessment of ultimate load capability of the aft keel design. As shown in Figure 6-6, the panel configurations were characterized by relatively thin facesheets and medium density core. BVID on the OML facesheet and separately on the IML facesheet were considered.

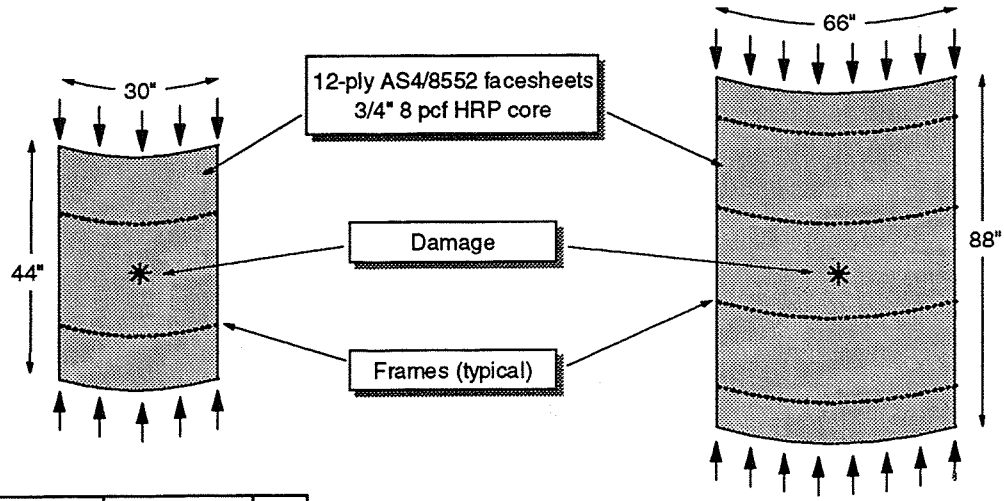

Specimen ID	Damage	Qty
AK22-1c	BVID on IML facesheet	1
AK22-2	BVID on OML facesheet	1

Specimen ID	Damage	Qty
AK25	BVID onOML facesheet	1

Figure 6-6. Aft-keel ultimate strength test matrix.

The 2-frame specimens, both obtained from a panel designated AK22, were tested in compression with impact damage on the IML and OML. The loaded specimen ends were potted and the unloaded edges were constrained by knife edge supports on each facesheet. No restraints were applied to the frames. Failure occurred at compression loads of 6.0 kips/in and 6.8 kips/in, respectively. These load levels were determined to be compatible with the requirements in the aft third of the keel (i.e., approximately 3.0 to 4.5 kips/in) since they required adjustment for environmental effects and statistical variation (i.e., an approximately 25% reduction). Failure of these specimens initiated away from the damage sites, in the inner skin at the edge of an attached frame flange. The frame at this location separated from the skin during failure.

It was surmised that the failure initiated at wrinkles in the inner skin (caused by frame sinkage during cure, and possibly made worse on the specimens due to a slight mismatch in the radii of the inner skin and attached frame flange). The stresses here may have been magnified by discontinuities in axial stiffness (skin vs. skin plus frame flange) and/or interaction with the global panel deformation, which varies across the width due to the presence of side edge restraints. (The edge restraints are needed since the frames are not continuous as they would be in a complete fuselage shell, and therefore cannot

develop hoop loads to resist out-of-plane deformation.) The frames twist in response to this deformation, creating inward (crushing) and outward (peeling) forces on opposite edges of the attaching flange, and adding to the local skin stresses. Just prior to specimen collapse, however, damage growth was observed at the impact sites, indicating imminent failure at those locations.

Prior to test, finite element analyses that incorporated strain softening laws developed from unconfigured tests (see [7] and Section 8.1.2) were conducted for these two-frame panels. Failure predictions agreed very well with measured failure loads. As shown in Figure 6-7, predictions ranged from approximately 1.3% below to 3.5% above the measured strengths. The tests also confirmed predictions that impacts on the OML are less critical than those on the IML due to the superposition of bending stresses from global panel deformation.

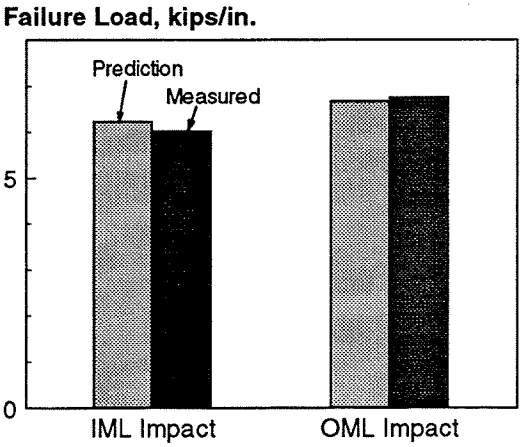

Figure 6-7. Comparison of measure failure loads of aft keel impact damaged tests with strain softening predictions.

The largest aft-keel panel, designated AK25, was tested in compression with the two frames nearest the panel center restrained at their ends from radial movement, and the unloaded edges of the panel constrained by knife edge supports on each facesheet. The initial test (subsequent tests are discussed in Section 8.1.2) was conducted to verify the ultimate allowable strain criteria. Prior to testing, the panel was impacted at its center to create BVID in the OML skin. The panel was then loaded to 367 kips — its capability based on the allowable strain for BVID, adjusted upward for room temperature test conditions. The panel successfully held this load without significant damage growth.

An identically sized mid-keel panel, designated MK1, was tested to evaluate sandwich repair concepts. The panel included significantly thicker facesheets (i.e., 30 plies each, t = 0.22 inch) and higher density core (i.e., 12 pcf) than the aft keel panels. The panel failed away from the repairs at 99% of the ultimate axial load (after adjusting to account for the room temperature, dry test environment) [25]. The failure mode was similar to that of the 2-frame specimens: compression failure of both skins across the full width of the panel at the edge of a frame flange. In this case, however, the frames did not

disbond. The test setup was also similar, and therefore may have contributed to the failure. At the time of this writing, cross-sections of the panel had not yet been taken to determine the presence of manufacturing anomalies such as skin wrinkles.

6.1.3 Side Quadrant

A detailed nonlinear finite element analysis of a side window-belt panel consisting of three frames, three full-depth window close-outs, and three windows was performed to evaluate design details in the region [12, 26]. Several significant findings resulted from these studies. The load case that combines shear with internal pressure was found to be dominant. The studies lead to an optimization of the facesheet padup scheme in the window-belt region, with several ±45° plies eliminated and the doubler extended several inches circumferentially. The upstanding leg of the window frame was also eliminated, since the full-depth close-out configuration provided the majority of the bending stiffness necessary to preclude buckling adjacent to the cutout. The material and configuration of the window close-out was also found to have only a very small influence on the strain distributions.

A detailed evaluation of the reinforcement structure around the passenger door cutout was conducted by Northrop Grumman Corporation, under an ATCAS subcontract [26, 27]. The study supported design refinement activities. Specifically, it identified a slight unconservatism in the edge frame, sill, and intercostal designs. It also identified a more structurally efficient distribution of the skin-doubler material. The design was not updated to address these findings, however, due to manpower constraints.

6.2 Outstanding Issues

A number of unresolved issues were identified as a result of the ATCAS development activities. General failure criteria able to address in-plane and through-thickness concentrations when subjected to combined loads do not exist. Such criteria are needed to accurately assess structural strength and to relate results of structural tests to the true fuselage response. Finite element models incorporating strain-softening material laws have demonstrated the ability to predict failure of structural configurations with impact damage located remote to complex design details. Addressing the more difficult locations, however, has not been accomplished, and requires significant advancements related to modeling the load transfer between structural elements, and its degradation.

Relatively simple design methodologies, developed for a constrained design space with the insight from this generalized failure analysis, are necessary for efficiently generating structural designs without excessive conservatism. Additional characterization of the effect of potential manufacturing anomalies (e.g., fiber waviness due to frame sinkage) on strength is required. A close link between this activity and manufacturing developments should be pursued, both to focus manufacturing efforts on important anomalies and to ensure predictive capability for the defects which are expected during production.

The effects of impact damage on ATCAS structural configurations have not been fully characterized. Damage events and states that reduce the structural strength below ultimate load need to be determined and characterized. Specifically, additional impact locations (e.g., closer to stiffening elements) and impactor geometries should be addressed. Criteria for determining damage levels associated with ultimate strength should also be reconsidered. An illustration of the interaction of these issues is contained in [28], where blunt impacts on the outer surface of skin/stringer panels were found to be capable of causing significant stringer and skin damage without any outer-surface visibility.

Additional testing is required to address a number of issues related to ATCAS materials and structural configurations. The effects of severe environment and statistical variation have not been adequately addressed. Only limited tests were conducted at temperatures and/or moisture contents other than ambient [7, 29], and most testing was limited to two or three replicates. Assumptions related to environmental and statistical knockdown factors for design values must be verified. In addition, design values for stanchions, floor beams, window frames, and intercostals, were engineering estimates based on little or no test data.

Strength improvements with increasing laminate thickness were not studied for small damage sizes associated with ultimate strength. The effects observed during material residual strength characterization [7] suggested that these improvements are also operative in the small-damage domain. In addition, strength reductions induced by ply terminations were only addressed in a limited manner. Comparisons of the only such test that included AS4/8552 facesheets with similar constant-gage results (i.e., Panels FK1 and AK10, respectively) provided no indication of ply drops adversely influencing the strength [30].

Scaling relationships between coupon and structural configurations are also required for all effects studied at the coupon scale. This capability allows cost-effective characterization while ensuring adequate, though not excessive, structural capability.

7.0 ATTACHMENT AND SPLICE STRENGTH

This section addresses the structural connections in the ATCAS fuselage study section for loadings associated with ultimate strength, damage tolerance, and durability. The attachments within the quadrants include the axial and circumferential stiffening elements to the skin or sandwich facesheets, the cargo and passenger floor elements to themselves and to the circumferential frames, and window/door cutout stiffening elements to the sandwich facesheets. All splices between quadrants and between fuselage sections, termed *longitudinal* and *circumferential splices*, respectively, are also addressed.

7.1 Related ATCAS Developments

7.1.1 Crown-Quadrant Attachments

Skin/Stringer Bondline. Eleven tests were conducted to assess skin/stiffener bondline strength in a simulated post-buckled environment [17]. The specimens, which consisted of a single stringer attached to a skin segment, were machined from six panels representing a range of crown-quadrant design options. The loading was similar to that used for 3-point bending, but the applied load at the specimen midspan was applied only to the skin segments extending beyond the stringer flanges, as shown in Figure 7-1. Separation failure of the specimens was characterized by a delamination between the first and second skin plies, not at the skin/stringer bondline. This behavior is consistent with that observed in the stability tests of 3-stringer panels (Section 5.1.1) and with findings from end-notch-flexure and double-cantilever-beam tests [7]. Results supported findings of reduced stiffness of AFP laminates when compared to hand-laid tape laminates (see Section 5.1.1 and [7]). Local bending-stiffness reductions resulting from stringer-cap impact damage were also observed. The skin/stringer separation failure mode of the larger stability panels suggest that these element tests may be suitable building-block tests, although scaling relationships have not been established.

Skin/Frame Bondline. The bonded-frame attachment strength in the crown was studied with a combination of element tests and global/local finite element analyses, as shown in Figure 7-2 [31 - 34]. The "global" model, representing a unit skin/stringer/frame cell, is shown in Figure 7-3, and included shear deformable laminate elements and symmetric boundary conditions. The three internal load cases shown in Table 7-1 were applied to this model. Geometrically nonlinear solutions were obtained for each.

Several important trends were identified with these skin/stringer unit cell analyses. The nonlinear aspects were found to significantly alter the bending moment distributions. In the mousehole gap (identified in Figure 7-4), membrane stiffening due to pressure-induced hoop loads tended to reduce the bending moments. Nonlinear effects were also important at the midbay flange tip (also identified in Figure 7-4) for load cases that include axial loading.

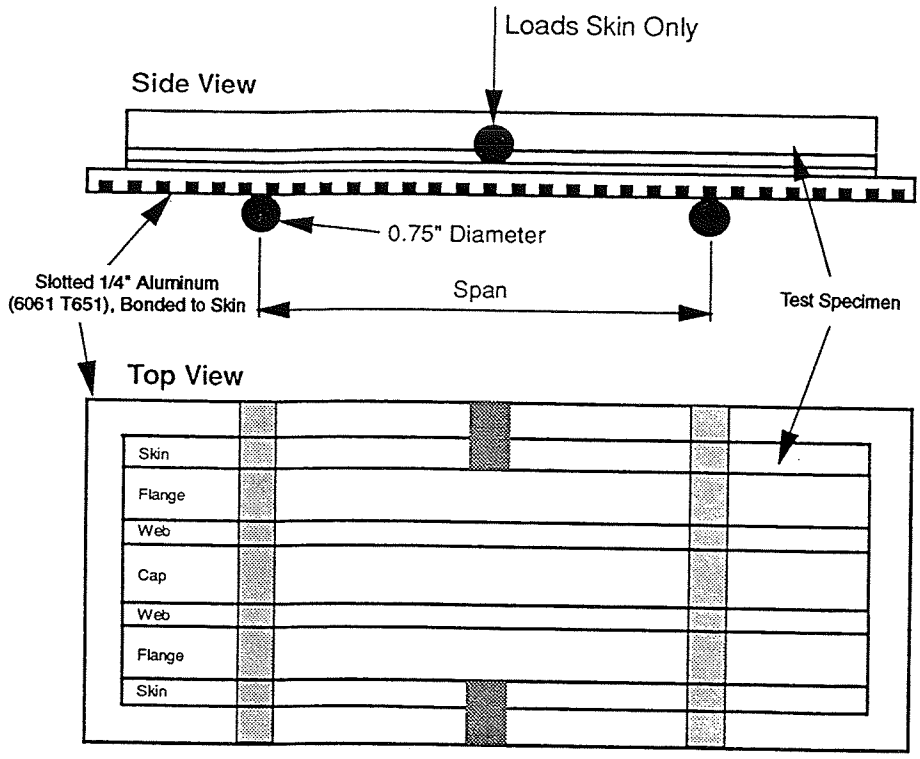

Figure 7-1. Skin/stringer bondline test configuration.

Large moments (about the frame axis) and transverse shear gradients were predicted at the flange tip near the frame-flange corner (identified in Figure 7-4), with the high axial load (i.e., the axial and ultimate load conditions) causing the most severe pull-off conditions. Fiber-direction strains for the two inner-most skin plies also peaked near the frame-flange corners, with values approaching 7000 με for the ultimate load condition. The axial load was found to result in compressive frame/skin bondline normal forces in the mousehole gap region. The ultimate and overpressure conditions resulted in large bending moments (about the stringer axis) in this region, with moment and transverse shear values peaking near the location of the frame web. At this location, the fiber-direction strains in the two inner-most skin plies approached 8000 με for the overpressure condition, although these values may be overpredicted due to the two-dimensional modeling approach.

Pull-off tests to address bondline strengths at the midbay flange tip included clamped and simply-supported boundary conditions for the skin, as shown in Figures 7-5 and 7-6, respectively [24]. Clamped test results indicated that the use of adhesive or braided inserts as the frame *noodle* (i.e., the triangular-shaped region at the base of the frame web) had little effect on failure. Damage was initially observed at the frame flange tip, but at higher loads, damage in the noodle became dominant. This shift may have been caused by membrane forces that developed in this clamped specimen configuration and/or by a curvature reduction near the flange tip as the damage progressed.

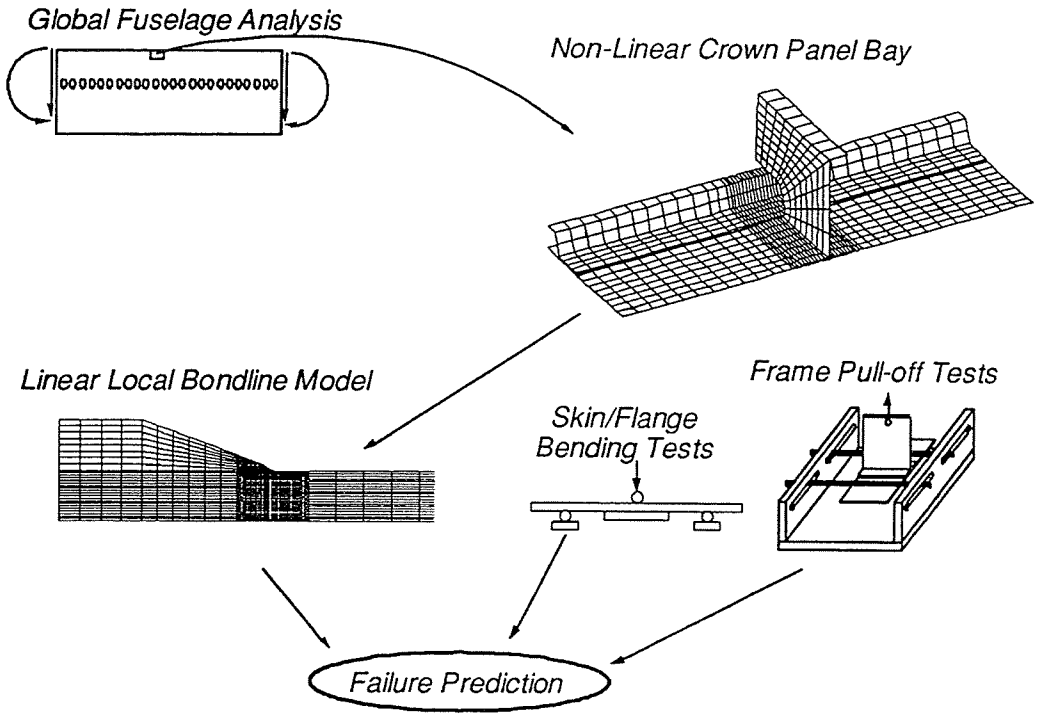

Figure 7-2. Methodology for evaluating frame/skin bondline strength.

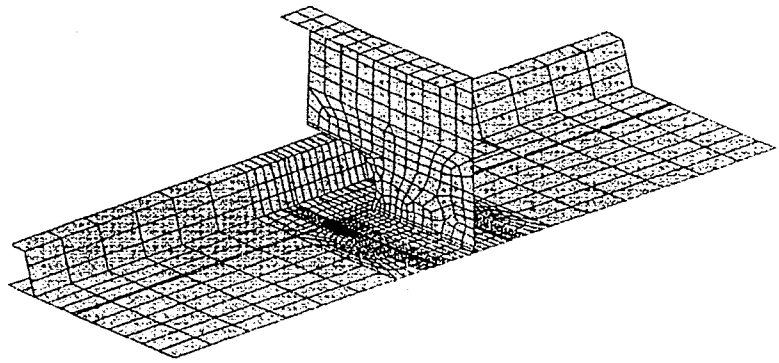

Figure 7-3. Skin/stringer unit cell finite element model for bondline analyses.

The simply-supported specimens exhibited failure due to damage growth from the frame edge (without significant noodle damage), but at lower loads than observed for the clamped specimens. In both specimen types, damage progressing from the frame edge typically traveled within the top three plies of the skin, although the damage extended deeper for specimens with evidence of cure-induced frame sinkage. Failure results of

thin-skin simply-supported specimens are shown in Figure 7-7, and suggest that the most important load resultant is the skin bending moment at the tip of the frame, not the frame pull-off load itself.

Table 7-1. Internal load cases for skin/stringer unit cell model.

Condition ID	Resultant Axial Load (kips/in)	Internal Pressure (psi)
Axial	5.0	0.0
Ultimate	5.0	13.8
Overpressure	0.0	18.2

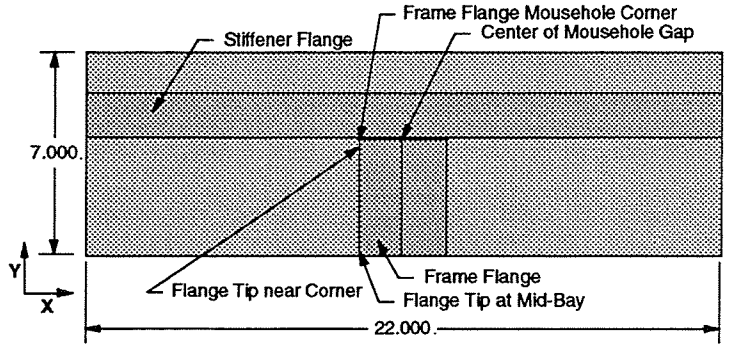

Figure 7-4. Locations of interest in bondline analysis.

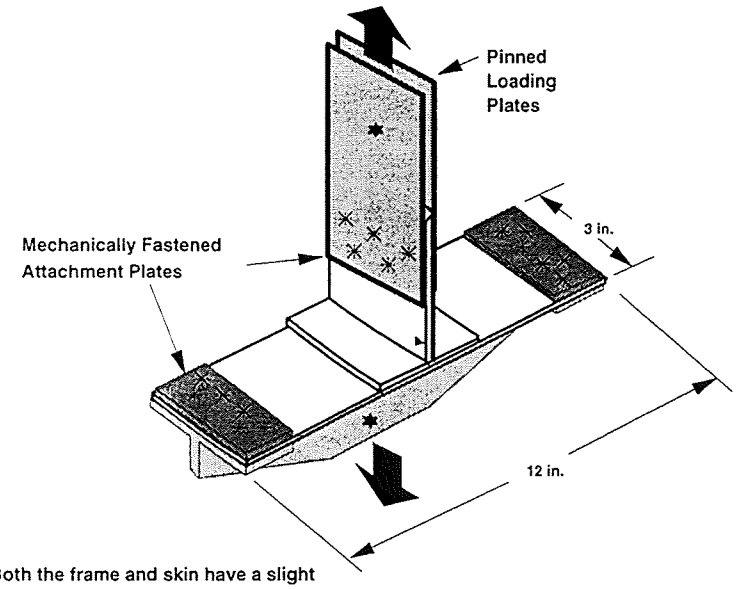

Note: Both the frame and skin have a slight curvature (122 in. radius) along frame axis

Figure 7-5. Clamped frame pull-off test specimen.

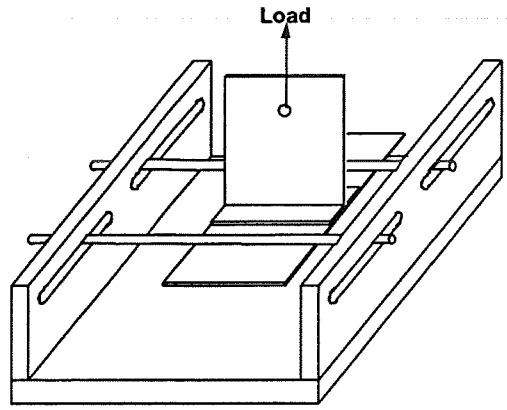

Figure 7-6. Simply-supported frame pull-off test specimen.

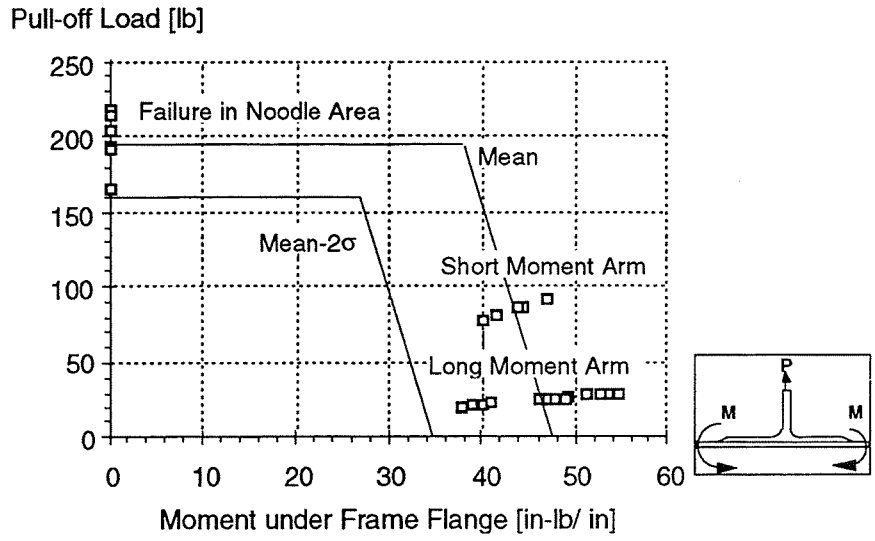

Figure 7-7. Failure envelope for ultimate load of simply-supported thin-skin pull-off specimens

A limited number of fatigue tests (R = 0.25) were performed in the simply supported frame pull-off fixture to develop a test method and observe failure mechanisms. High load levels (i.e., 80 to 95% of the static crack initiation force) were required to generate damage growth within relatively few cycles (e.g., 1000). As was the case for static tests, fatigue crack initiation and growth was seen to occur from both frame edges. After some growth, damage was also noted around the noodle. Final failure occurred at 10,000 to 20,000 cycles as one of the cracks starting from the edge became dominant and abruptly grew across the frame width. The tests suggest that the design's capability is likely adequate, since the test represented an extreme fatigue spectrum.

Additional tests of simplified specimens were conducted to more efficiently study the failure mechanisms of bonded skin/flange configurations loaded in bending and transverse shear [33]. Three- and four-point bending tests were conducted on specimens

with a simulated flange bonded onto a skin segment, as shown in Figure 7-8. Specimen variables included flange termination angle (i.e., 20° and 90°) and the layup of the skin and flange. Despite the use of a different material (i.e., IM6/3501-6) for both the skin and flange, the specimens exhibited similar failure mechanisms to the tests with the full frame segment. Some specimens, however, exhibited damage initiation within the flange — a failure mechanism not observed with the braided frames. These tests, in combination with the configured tests, demonstrated that strength of the bondline does not limit the skin/frame pull-off capability; failure typically occurs within the skin. In addition, specimens with a 20° taper to the flange tip exhibited significantly higher capability, as shown in Figure 7-9.

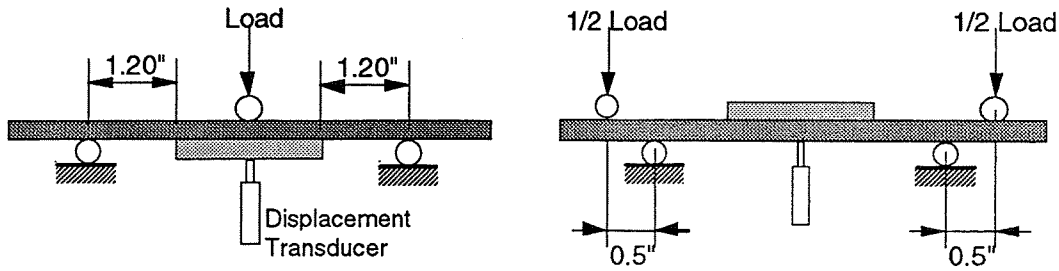

Figure 7-8. Three- and four-point bending configurations for bonded flange tests.

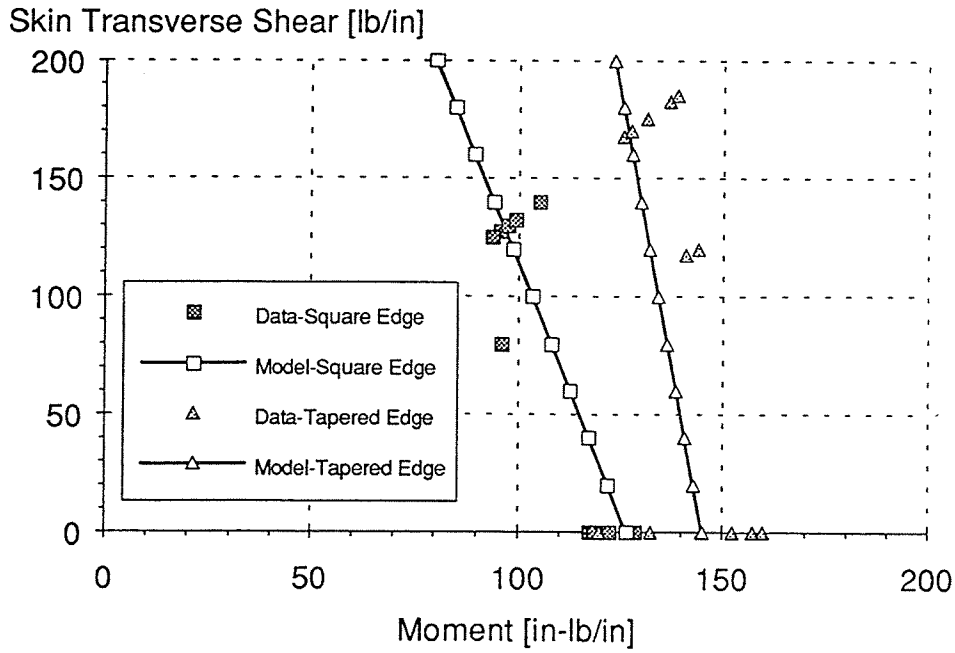

Figure 7-9. Typical three- and four-point flexure test results.

Detailed 2-dimensional plane-strain models were used to study the flange-tip region in the pull-off tests, the skin/flange flexure tests, and the actual fuselage conditions. A high degree of mesh refinement was used in these models, with up to three quadratic elements

per ply thickness, as illustrated in Figure 7-10. Linear analyses were used since deformations on this scale were expected to be small. For simulations of the tests, load and boundary conditions were simulated directly in the model. For simulations of the fuselage, three load components, obtained from the unit skin/stringer/frame cell model, were applied to the local flange-tip model: in-plane tension perpendicular to the frame axis (N_x), bending about the frame axis (M_x), and transverse shear (Q_{xz}). N_x loads were found to produce significant peel stresses along the frame/skin interface.

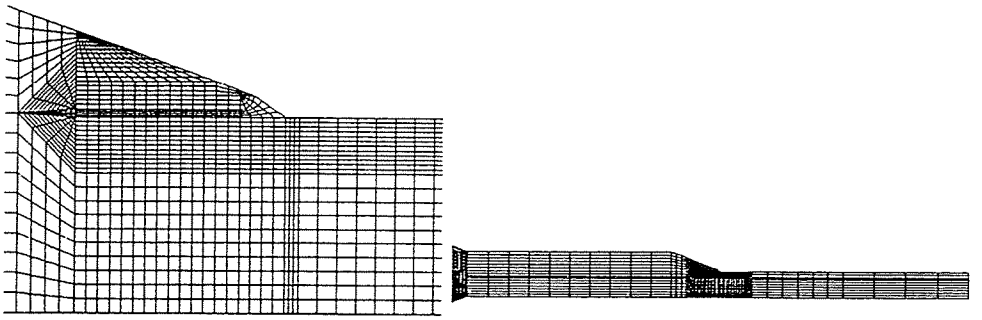

Figure 7-10. Typical local model of frame flange-tip region.

A strength-of-materials approach was used to predict initiation of the disbonding. A failure criterion based on the maximum transverse tensile stress within the top skin ply was relatively successful in predicting damage onset; transverse tensile strengths of 6500 to 7500 psi were typically observed in tests. As shown in Figure 7-11, this method predicts sufficient structural capability along the full frame length in the overpressure loading condition, but not, however, for the ultimate condition. It should be noted, however, that the tests for determining the strength values did not include any consideration of axial loads, limiting the credibility of this conclusion.

A fracture mechanics approach, considering only N_x and M_x loading, was used to evaluate disbond growth. Results indicated a strong interaction between these two loadings; the strain energy release rates (SERRs) for combined load cases were found to be much larger that the sum of the SERRs obtained for the individual cases. Limited results also showed that the calculated total SERR at failure in the pull-off and flexure tests was consistent with the value obtained in mixed-mode fracture tests of skin material (i.e., ranging from 700 to 900 J/m^2). Typical predictions of fuselage response based on this approach (considering only N_x and M_x load components) are shown in Figure 7-12. As was found using the strength-of-materials approach, adequate strengths were predicted for the overpressure loading condition, but not for the ultimate condition.

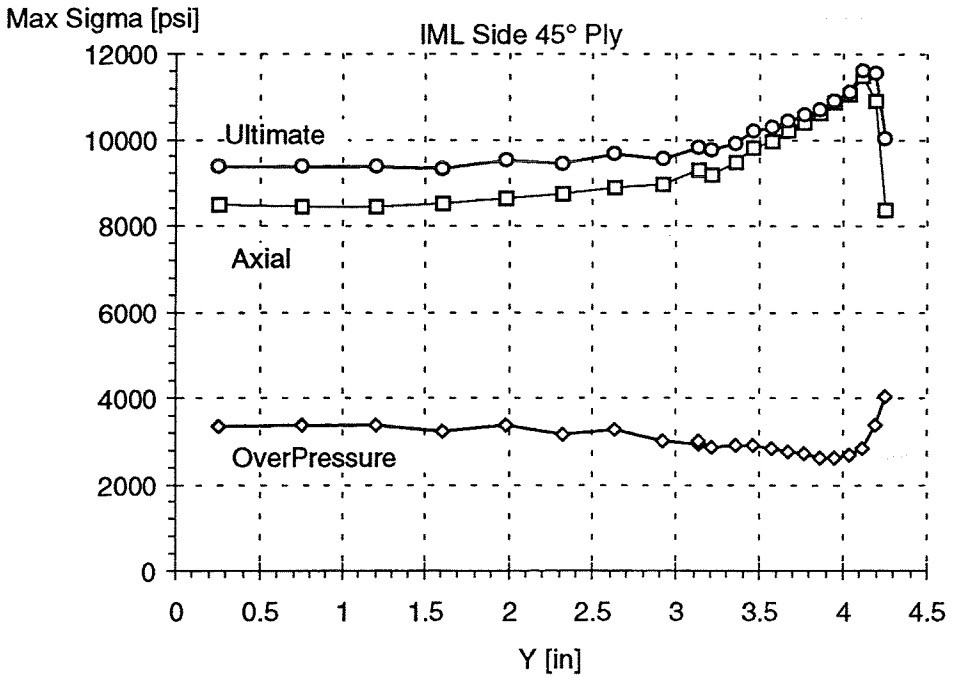

Figure 7-11 Maximum transverse tensile stresses in the surface skin ply at frame/skin interface.

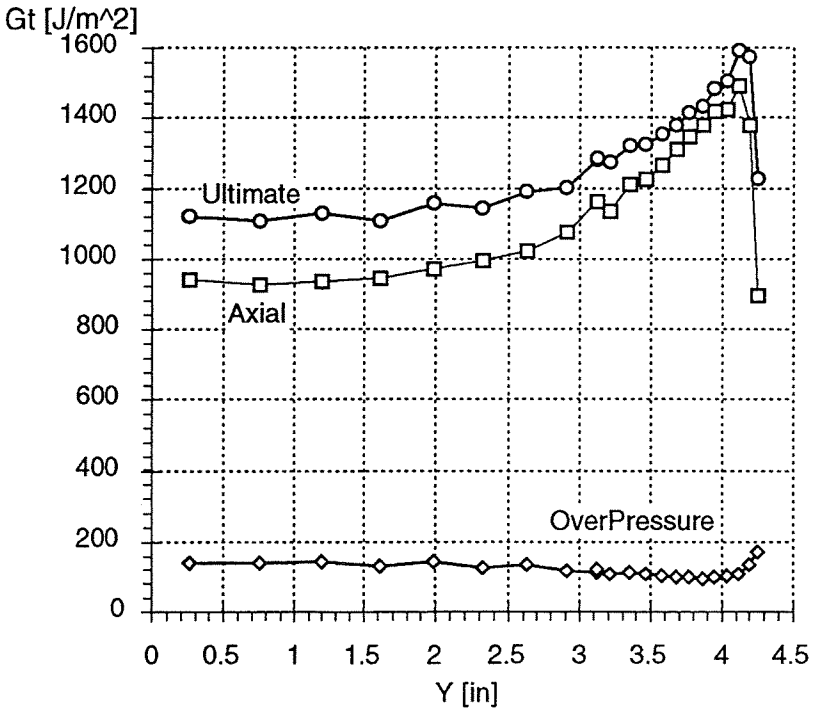

Figure 7-12. Strain energy release rates at frame/skin interface.

Pull-off tests of the mousehole design detail were also conducted, as shown in Figure 7-13 [24]. For these tests, failure originated under the frame noodle near the stiffener and propagated as a delamination under the frame. Predictions based on the global finite element analyses (i.e., unit skin/stringer/frame cell model) and the failure loads obtained in these tests indicate that frame disbonding in the mousehole gap will initiate below ultimate load. Energy-based predictions of a similar model indicate that the growth will be stable, and the damage extent at ultimate load will be small (e.g., 0.5 in). Neither the analyses nor the failure criterion, however, have been sufficiently developed to support firm conclusions. In fact, ultimate loadings applied to large, configured panels have demonstrated ultimate capability without any significant damage beneath the frames (see discussions below on Panel 12).

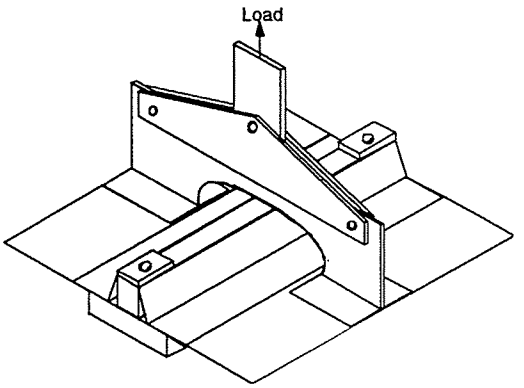

Figure 7-13. Simply-supported frame-mousehole pull-off test specimen.

Pressure-box tests of configured crown panels provided insights into the strength of the frame-skin attachments. The configuration of, and test results from, the two bolted-frame panels, Panel 11b and TCAPS-5, and the two bonded-frame panels, Panel 12 and TCAPS-1, are discussed more thoroughly in Sections 6.1.1 and 8.1.1. Discussions here are limited to results directly related to the skin/frame attachment. Geometry modifications were made to all but one of the Panel 12 mouseholes, previously shown in Figure 6-5, based on predictions of significantly reduced peeling moments.

Both bolted and bonded frame attachments were found to be adequate for the ultimate overpressure condition (i.e., 18.2 psi internal pressure with 1.1 kips/in. resultant axial load), despite some small skin damage near the mouseholes in the bonded-frame panel (i.e., Panel 12). There was no apparent difference between the original and modified mousehole geometries on Panel 12 relative to this damage formation. As discussed in Section 6.1.1, the bonded-frame panel tested with high applied axial load (i.e., TCAPS-1) did not successfully sustain the required loads (13.8 psi, 5.0 kips/in axial load), but failure appeared to result from unrepresentative stress concentrations near the outer frames caused by the close proximity of the axial-load introduction doublers. Detailed finite element analyses indicated that, for high axial load conditions, the low axial skin stiffness combined with the relatively high frame-flange transverse stiffness

resulted in high strain gradients in the skin near the frame-flange mousehole corner, even in regions not adjacent to the axial load doublers.

For hoop damage tolerance conditions with internal pressure only, the bolted frame attachment of Panel 11b provided sufficient load transfer from the skin to allow damage arrestment short of and underneath the unsevered frames. (Similar testing of TCAPS-5 did not tax the bolted attachment of the unsevered frames to the skin since significant damage growth did not occur.) The bonded frame attachment, however, did not provide sufficient load transfer capability to arrest damage in similar tests of Panel 12; delaminations accompanying the advancing damage appeared to separate the undamaged frame from the load path, allowing the damage to progress unchecked to the panel edge. Even without damage arresting at the frame, however, the strength of the bonded-frame panel was within 10% of the bolted-frame configuration.

7.1.2 Keel Quadrant Attachments

The keel frames must restrain pressure-induced skin expansion, provide nodal reactions for compression and shear stability, and transfer localized loadings into the sandwich skin (e.g., stanchion loads). Frame push-in loadings must be considered in addition to the pull-off conditions due to the potential for crushing of the honeycomb core. Pull-off tests, illustrated in Figure 7-14, and similar push-in tests were conducted for aft-keel configurations, while only pull-off data was generated for the mid-keel region.

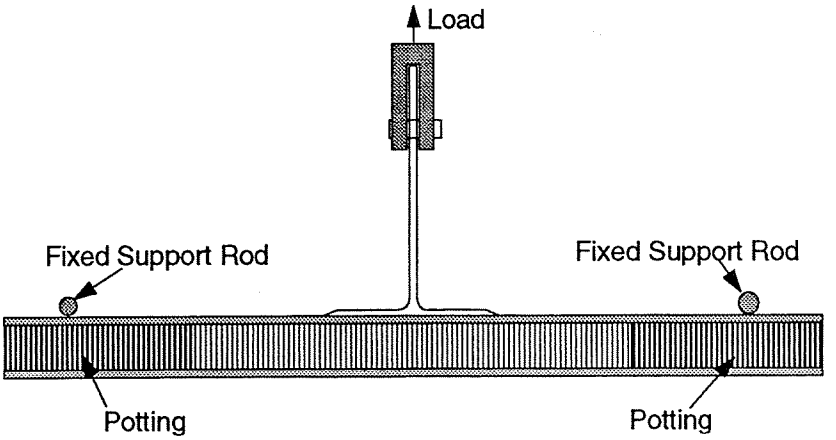

Figure 7-14. Keel frame pull-off test configuration.

The aft-keel pull-off specimens exhibited failures either within the top facesheet ply or at the facesheet/core interface. The mid-keel pull-off specimens, which contained a fabric ply on the inner and outer surface of both facesheets, exhibited failure along the interface between the fabric ply and the frame/skin bondline adhesive. In all cases, the failures were catastrophic, with few visual or audible indications prior to the failure event. For the push-in tests, the core exhibited transverse shear failures near the edges of the frame flange. Aft-keel pull-off and push-in test results are shown in Figure 7-15, and are several times higher than required.

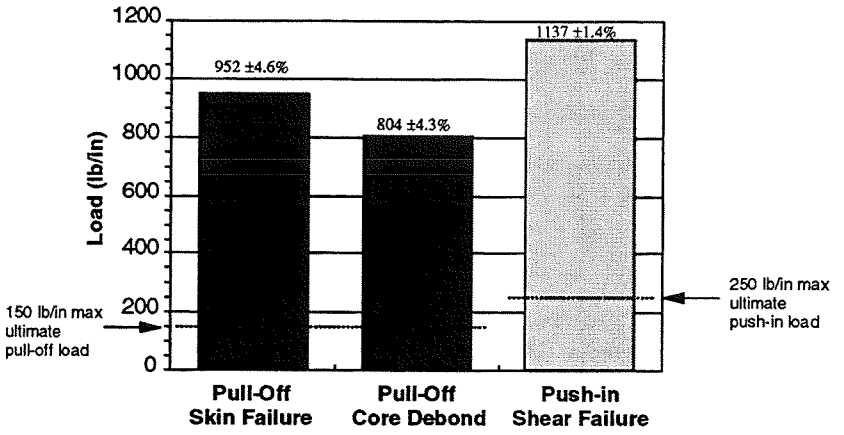

Figure 7-15. Aft keel pull-off and push-in test results.

The static and fatigue strength of mid-keel pull-off coupons with BVID were also experimentally measured. The impacts were created on the inner surface of the frame flange as close as possible to the web using 60 ft-lbs of energy and a 1-inch diameter impactor. One specimen was inspected using pulse-echo, and then sectioned to determined the extent of internal damage. As shown in Figure 7-16, multiple delaminations and transverse ply cracks were found in the upper facesheet. The extent of the delaminated area agreed very well with the inspection results, as was also found in [7]. A clear fracture line was also observed in the core under the impact. No attempts were made to quantify fiber failure occurring in the skin damage zone.

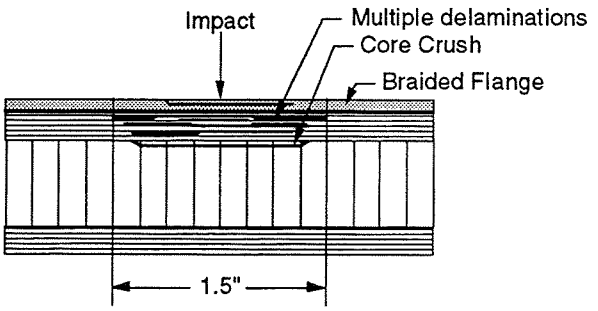

Figure 7-16. Impact damage in mid-keel specimens.

The statically-tested specimens failed within the scatter band of the undamaged failures, indicating that these specific impacts did not have a significant effect on pull-off strength. Specimens tested in tension-tension fatigue (up to 10^5 cycles) exhibited large scatter in the number of cycles to failure. The data, shown in Figure 7-17, suggest an endurance limit for impacted configurations significantly above the required capability, and approximately 45% of the static undamaged strength. As in the undamaged mid-keel tests, most of the impacted static and fatigue specimens failed at the interface between the film adhesive and the facesheet's fabric surface ply. This was in contrast to the failure of the undamaged aft-keel specimens, which occurred between the first two skin plies, both of which were tape.

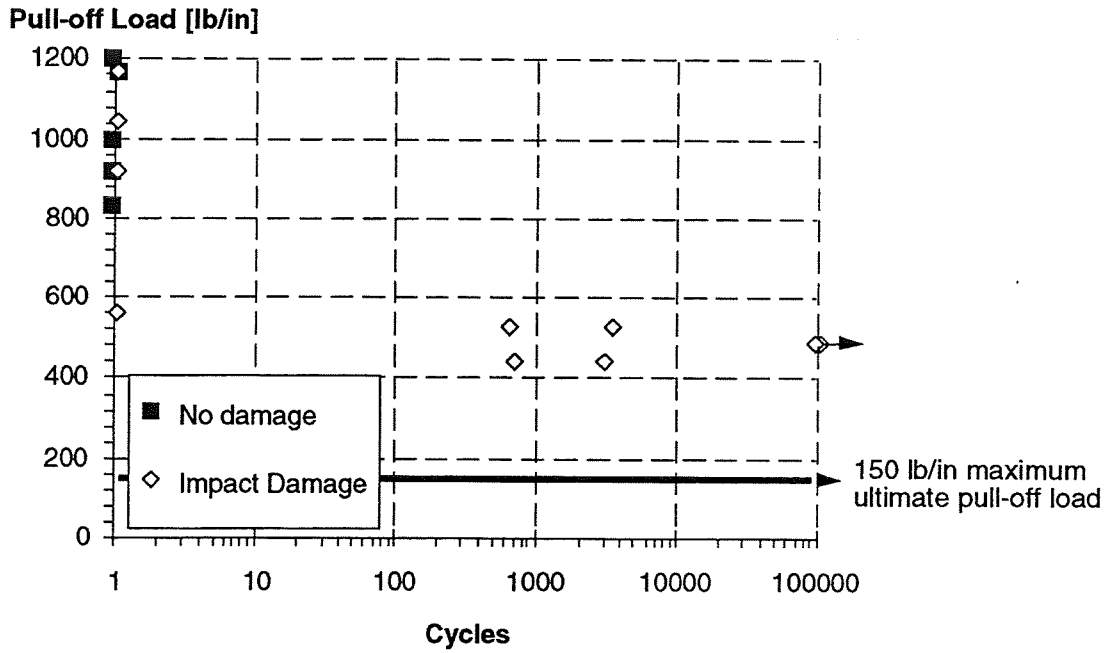

Figure 7-17. Static and fatigue pull-off strengths of mid-keel specimens.

Detailed finite element analyses of these specimen geometries were conducted to assess potential failure criteria. The model, shown in Figure 7-18, utilized one row of elements for each ply of the upper facesheet in order to accurately obtain interlaminar stress distributions in the vicinity of the frame-flange tip. The bondline thickness, frame-fillet geometry, frame-flange-tip thickness, and skin resin pocket beyond the frame-flange tip were all modeled based on typical dimensions obtained from microscopic measurements, thereby avoiding the numerical singularities associated with the sharp corners.

Comparison of test results to these analyses identified failure criteria that, in conjunction with the described modeling approach, provided good first-order predictions. Failure within the facesheet surface ply, or between that ply and the adjacent facesheet ply, can be estimated by comparing the predicted maximum interlaminar tension stresses with experimentally-measured strengths (e.g., from flatwise tension tests). Failure at the facesheet/core interface can be predicted by comparing the maximum interlaminar tension stress at that interface with strengths measured from flatwise tension tests of sandwich configurations. The transverse-shear core failures can similarly be predicted using the maximum transverse shear stress in the core and associated ribbon-direction strengths, as typically reported by core manufacturers.

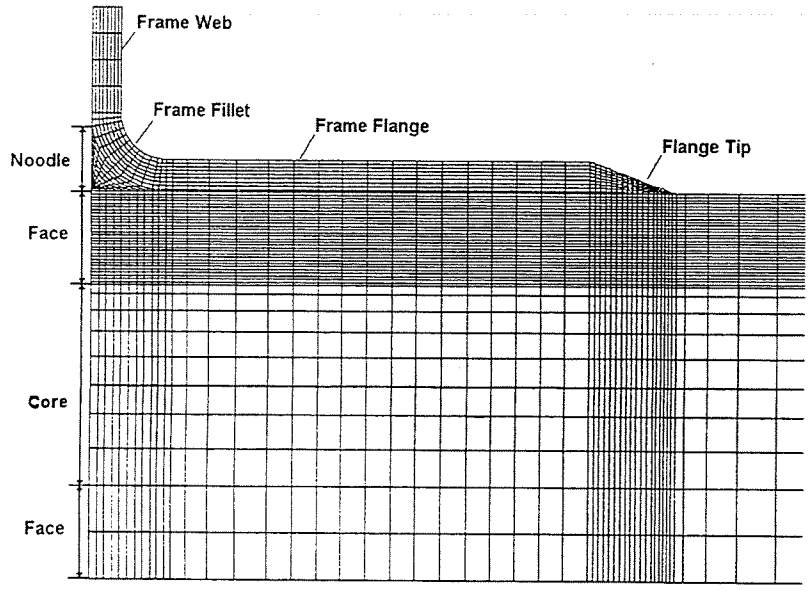

Figure 7-18. Finite element model of keel frame pull-off and push-in tests.

7.1.3 Panel Splices

Coupon tests supporting splice analyses are reported in [7]. Included are coupon tests of full-depth sandwich splice close-out configurations representative of the circumferential and longitudinal splices of the side and keel. Some of these results are also applicable to system attachments, where the use of close-outs is also anticipated.

Splice analyses developments were conducted at United Technologies - Sikorsky Aircraft under an ATCAS subcontract [35, 36]. The effort was focused on developing simplified, closed-form methods compatible with optimization analyses. The resulting software addresses four splice configurations, three fastener patterns, and five failure modes. The design configurations addressed include (1) skin/stringer to skin/stringer, (2) skin/stringer to sandwich with rampdown, (3) sandwich with rampdown to sandwich with rampdown, and (4) full-depth sandwich to full-depth sandwich. The fastener patterns on each side of the splice that are considered are (1) one row, (2) two aligned rows, and (3) two staggered rows. Failure modes considered are (1) fastener shear failure, (2) panel and splice-plate bearing/bypass, (3) panel and splice-plate inter-fastener buckling, (4) sandwich rampdown compression buckling, and (5) sandwich rampdown core failure. Fastener countersink is addressed through modified fixity for inter-fastener buckling. Empirical correction factors for reduced fastener clamp-up, oversize fastener holes, and off-axis loading are also included to approximately address manufacturing anomalies and durability issues. These methods, in combination with parallel cost-prediction methods, were used to perform preliminary assessments of the importance of splice design variables [35].

An investigation of thick laminate joints subjected to compressive loads, both representative of the forward keel splice, was conducted by Hercules Aerospace and Hercules Advanced Materials and Systems Companies, under an ATCAS subcontract [37]. The experimental results obtained from coupon tests are discussed in [7]. The analytical portion of the study addressed the effect of joint parameters on fastener load sharing within the joint. Specifically, bolt diameter, bolt spacing, row spacing, fastener pattern, hole clearance, and transverse bolt torque-up were evaluated through detailed finite element analyses. The results indicated that the fastener diameter and fastener spacing variables had only a small effect on the load distribution between the fasteners in a three-row joint. Increased fastener diameter, however, was found to decrease the already proportionately small load carried by the middle row. Increasing the fastener diameter of only the middle row was unexpectedly found to reduce the load carried in that row.

7.2 Outstanding Issues

7.2.1 Attachments

Several bonded attachment issues require additional development. Most importantly, bondline failure-prediction methods must be validated, (and further developed if necessary) by comparison with test results. This is particularly true of the mousehole gap region in the crown, where detailed analyses have not been conducted to support preliminary failure criteria development.

A significant database of failure and non-failure conditions has been developed for a range of ATCAS designs, providing a good basis for failure-criteria development. The database, however, must be extended to address a wider range of configurations, particularly the forward keel, the axially-hard crown skin laminates, and the side. Long-term durability tests are needed to quantify the effects of load frequency, environment, and initial damage conditions on bondline strengths. The ability of a frame bondline discontinuity (e.g., stringer mousehole in the crown, drain mousehole in the keel) to arrest frame debonding should also be experimentally assessed. Additional bonded-frame specimens can be obtained, as necessary, from a large, untested pressure-box panel (i.e., TCAPS-2).

The validated bondline failure criteria must also be integrated into a generalized methodology. Interactions between bondline stresses and skin concentrations (both in-plane, caused by cutouts, etc., and out-of-plane, caused by thickness discontinuities) must be addressed. For example, the skin damage observed near the frame-flange corner at the mouseholes was likely a result of these combined effects. Pressure-box test results should be used to verify detailed modeling schemes for the mousehole, and, if necessary, modify the design of the single mousehole element test fixture to better simulate pressure loads.

Additionally, frame pull-off load levels are needed from the composite loads model to allow accurate assessment of observed capability versus requirements; current modeling strategy does not provide accurate representation in this area.

Bolted attachments within each quadrant are reasonably-well characterized. The most important of these is the floor attachment to the circumferential frames. Detailed sizings of these connections should be performed; sufficient braided-element data exists for additional refinement, but little or no data exists for the pultruded elements. Additional verification of the window-frame attachments and the associated close-outs are also required.

7.2.2 Panel Splices

A large number of splice-related issues remain unresolved. The damage tolerance of splice configurations must be evaluated. Damage tolerance considerations have been included in splice designs only indirectly; the skin laminates at the splices maintained layups and total thicknesses comparable to the far-field panel, which were developed considering damage tolerance requirements. A consistent approach must be defined, tested, and related to experience in metal or composite structure.

Fatigue and creep are expected to have a significant impact on splice designs and performance, particularly for full-depth sandwich splices with non-solid close-outs. An approach assuming a reduced fastener clamp-up and associated lower bearing strengths appears feasible and practical. Experimental data is necessary, however, to (a) properly select a conservative clamp-up value and (b) provide bearing strengths for that clamp-up. Full-depth sandwich splice configurations are particularly lacking in a historical database.

Experimental data is required for verification and refinement of methods addressing a variety of other issues. In many instances, large-scale tests are necessary to address the load-sharing issues inherent in structural splices. Fastener and fastener-pattern variables (e.g., spacing, diameter, thickness-to-diameter ratio) require additional characterization, particularly for the high loads and thick facesheet thicknesses present in the forward keel. Thick-laminate analysis methods must be verified; inclusion of material nonlinearities may be required to properly model the joint response. Additional characterization of splice configurational details, such as rampdown/joggle angles and splice intersections, is also needed. Element splices have not been significantly addressed from a characterization standpoint. The effectivity of core close-outs as moisture barriers, particularly when exposed to cyclic loading, must be determined. Fabrication process effects (e.g., increased splitting of AFP laminates), and composite-to-metal splice issues also require additional experimental results. A close relationship should be maintained between structural and manufacturing developments to ensure proper consideration of the interactions between structural configuration, panel tolerances, assembly pull-up, and splice performance. Increased understanding of these issues and effects would allow reduced conservatism and higher confidence in splice design concepts.

8.0 DAMAGE TOLERANCE

Damage tolerance evaluations were performed to ensure adequate structural performance in the presence of potential large-scale damages. In contrast to ultimate strength evaluations, damage tolerance assessments must address relatively infrequent, but large damages in combination with maximum expected load levels. In these discussions, damage tolerance refers to residual strength in the presence of large notches, and does not address the remaining two issues typically associated with structural damage tolerance: damage growth with fatigue loading and appropriate inspection procedures and schedules to ensure the damage does not become critical prior to detection.

8.1 Related ATCAS Developments

8.1.1 Crown Quadrant

Damage tolerance evaluations of the crown focused on early designs developed to meet 80% of limit flight loads with a failed structural unit. The reduced severity of the axial damage tolerance condition resulted in skin laminates that were significantly stiffer in the hoop direction than in the axial direction (i.e., 9.11 vs. 5.37 msi).

Axial Damage Tolerance. Axial damage tolerance testing included coupons and large unstiffened panels [7], tear strap panels, and 5-stringer panels, as shown in Figure 8-1. Flat panels were assumed to be sufficient for this condition due to small predicted curvature effects.

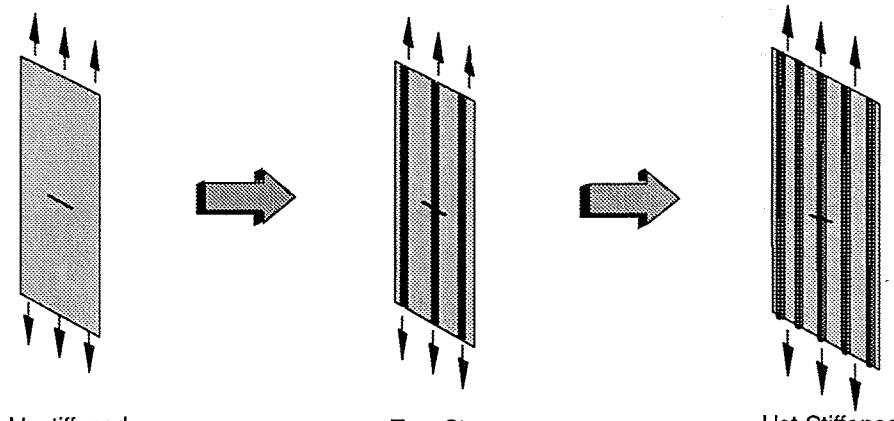

Figure 8-1. Crown axial damage tolerance tests.

Tension tests of tear-strap panels confirmed expectations that, in the presence of sufficient discrete stiffening, damage growth within the skin will arrest [38]. Specifically, two identical 5-tear-strap panels with straps providing 58% of the panel's axial stiffness, shown in (Figure 8-2) were tested with two different notch lengths. The panel failure loads were within several percent of each other. Damage growth plots

constructed from intermediate x-ray measurements of damage extent, shown in Figure 8-3, indicated stable damage growth in both cases, and a convergence into the residual strength curve. This convergence is surmised to result from development of a relatively large damage zone emanating from the notch tips, and is analogous to slow crack growth exhibited in similar tests with metallic panels [39].

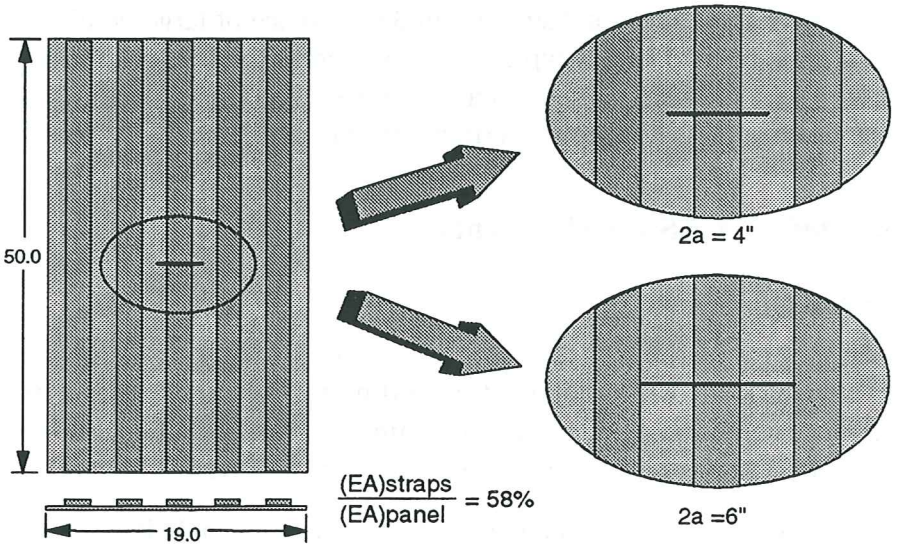

Figure 8-2. Tear-strap panel configurations.

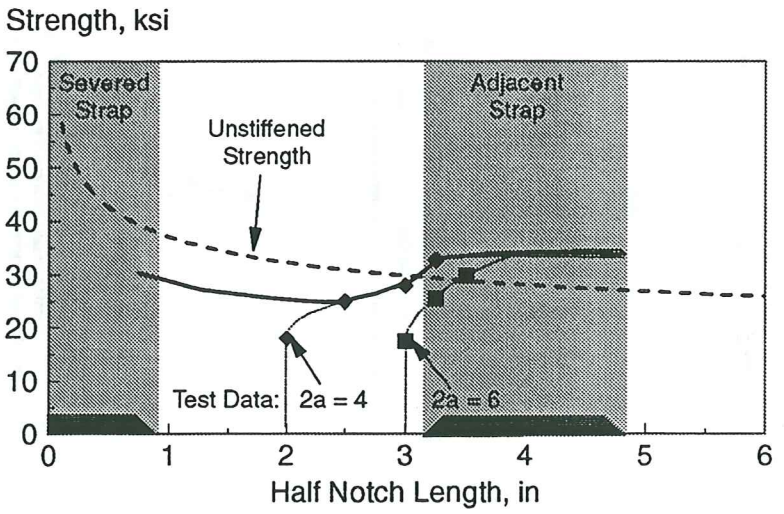

Figure 8-3. Tear-strap panel residual strength.

Tension tests of two 5-stringer panels were also conducted [38]. The panels, identical except for material, were 63 by 137 inches, and had 5 cocured hat stringers spaced at 14 inches, as shown in Figure 8-4. The first panel was fiber placed from AS4/938, and

had the compliant skin and stiff stringer (E_x = 6.9 and 13.3 msi, respectively) contained in early crown designs which considered only 80% of limit flight loads for damage tolerance conditions, as opposed to 100% in later designs. The layups and dimensions of the second panel were identical to the first, but the skin and stringer material was changed from AS4/938 to a fiber-placed intraply hybrid of 75% AS4/938 and 25% S2/938. In both cases, a 14-inch notch severed a full skin bay and the central stringer.

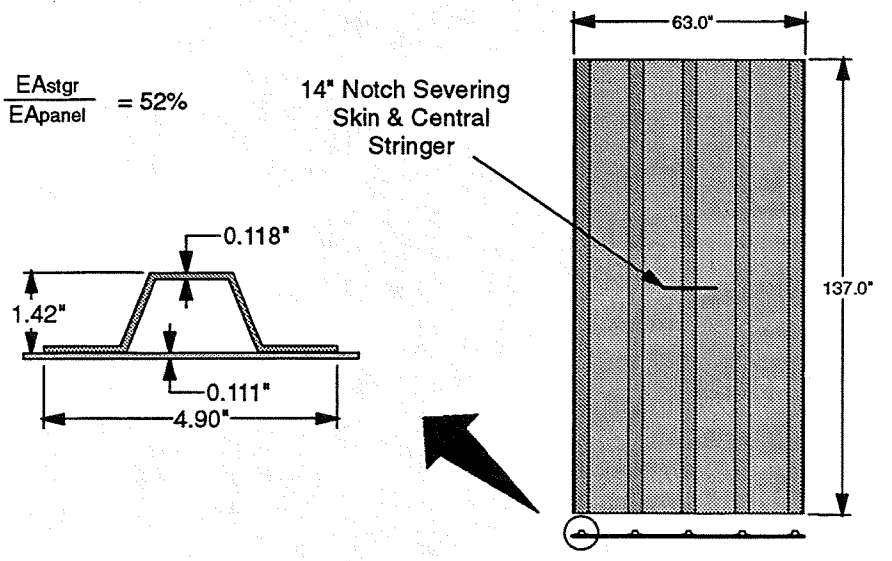

Figure 8-4. Flat 5-stringer panel configuration.

Similar failures were observed in both panels, although damage in the hybrid panel initiated at lower load levels and was more extensive prior to failure than the all-graphite panel. Damage grew asymetrically from the notch tips in a stable manner within the skin to the adjacent stringers. Strain gages on adjacent stringers showed higher strains as skin damage approached, indicating increased load sharing that helped arrest the damage. A review of all evidence suggests that the final failure sequence was caused by extension of the fiber failure within the skin beyond the adjacent stringer. The damage state beneath the stringer prior to initiation of the final failure sequence included a combination of fiber failures and delamination. The delaminations locally reduced the load transfer from the skin into the stringer, decreasing the relief of the damage-driving forces in the skin. Further reduction of the skin-to-stringer load transfer, caused by delamination growth which accompanied extension of skin fiber failure beyond the stringer, provided additional driving force during the failure sequence. The failed all-graphite panel is shown in Figure 8-5.

Predictions based on material characterization results and metallic elastic-plastic correction factors provided excellent agreement with measured damage-growth data. Damage growth results from the AS4/938 panel are compared with predictions in Figure 8-6. This excellent correlation is at least partially circumstantial, since the actual and assumed configurations differed in the orientation of the hat stringers (i.e., open vs. closed) and their attachment to the skin (i.e., riveted vs. cocured). It demonstrates,

however, that the degradation of the load transfer between the skin and the undamaged, adjacent stiffening element must be considered to accurately predict structural failure.

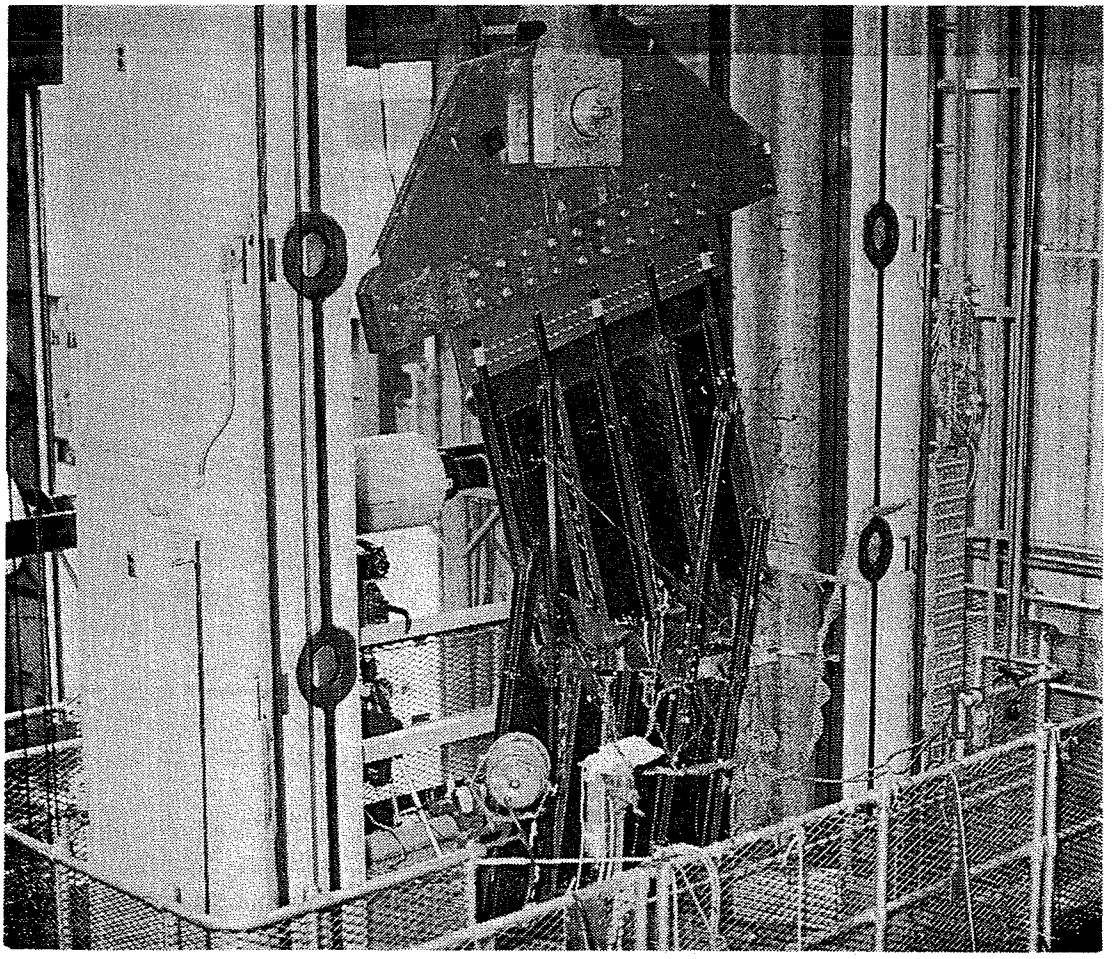

Figure 8-5. Failed flat five-stringer AS4/938 axial damage tolerance panel.

The strength results from the two 5-stringer panels are compared with the limit axial loads in Figure 8-7. The strength of the non-hybrid panel was approximately in the middle of the load range required for the crown quadrant. (It was originally designed for the forward end, but using the 80%-of-limit-load criterion.) The hybrid panel demonstrated a 25% increase in load-carrying capability over the non-hybrid panel, despite its reduced modulus. This increase is nearly identical to that observed in the unstiffened panels [7]. The gross-area failure strain of 4000 με was an approximately 45% increase.

Techniques for including strain-softening material laws into detailed finite element analyses were developed to support prediction of structural response [40]. The test and analysis developments related to this approach identified the importance of progressive fiber failure in predicting damage progression. The developed methods were successful

at tracking the damage growth to the point it reached the adjacent, undamaged stiffener [41, 42]. The analysis was discontinued at that point since strain-softening laws had not been determined for the stringer material, and methodologies did not exist to address the degradation of skin-to-stringer load transfer capability associated with the surface ply delaminations observed in the test.

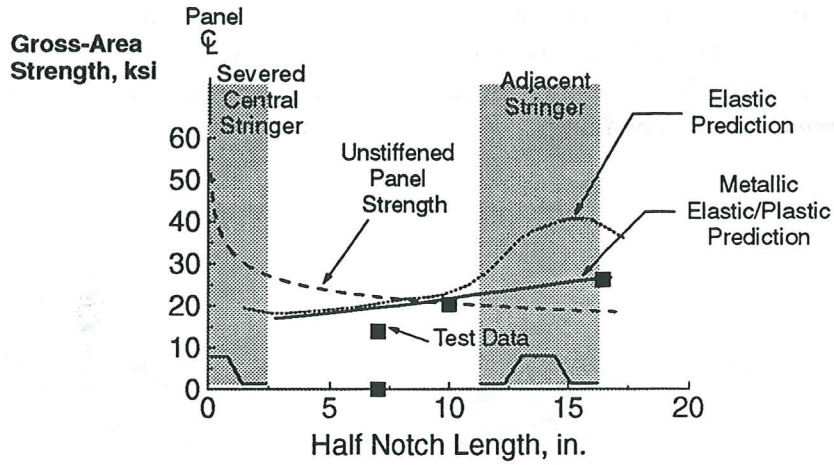

Figure 8-6. Comparison of crown 5-stringer tension damage tolerance results with predictions.

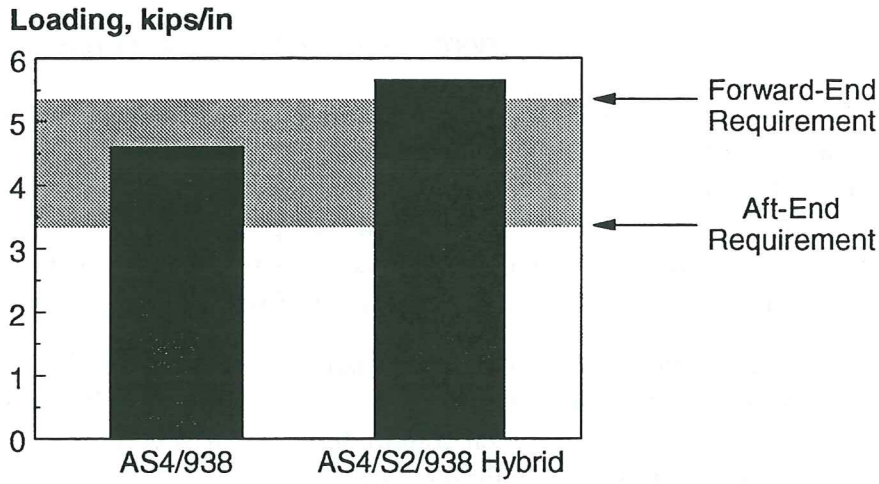

Figure 8-7. Crown axial damage tolerance results relative to requirements.

An R-curve approach for scaling tensile strengths of unstiffened panels to tear-strap and 5-stringer panels was pursued at NASA LaRC under non-ATCAS funding [43]. R-curve methods have been successfully used for metallic structure to account for material plasticity while avoiding rigorous analyses. In the current work, crack driving forces for the stiffened panel were determined using approximate elasticity equations modified by empirical correction factors. Material toughnesses were similarly determined from unconfigured test results. Self-similar crack growth was assumed in both cases. It was

found that traditional R-curves based on *crack growth* of unconfigured tests varied with initial notch length and were unsatisfactory. Predictions using R-Curves determined from unstiffened *strengths*, however, were reasonably accurate.

Hoop Damage Tolerance. Unlike the axial damage tolerance case, curvature effects are predicted to be large for the hoop damage tolerance condition, and were therefore considered in structural tests. As shown in Figure 8-8, flat unstiffened tension tests [7, 44] as well as a tear-strap-stiffened pressure-box panel provided building-block data to complement the eight fully-configured pressure-box test panels, which spanned a range of design variables and test conditions.

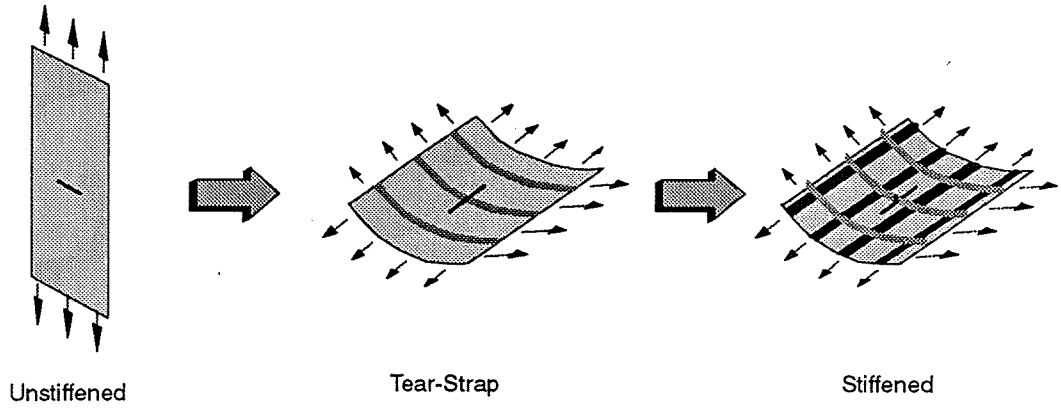

Figure 8-8. Crown hoop damage tolerance tests.

The test of the tear-strap panel provided little insight into structural damage effects since the axial and bending stiffness of the straps along their length were very low (the straps were intended to simulate frame flanges). The damaged panel (22-inch central notch severing the central strap) was tested to an internal pressure of 4.5 psi (90% of predicted failure). Mechanical tests and deply of the approximately 1-inch damaged regions provided physical evidence supporting the pursuit of strain-softening models [7, 44].

During the contract, three configured crown panels with damage, designated Panel 11b, Panel 12, and TCAPS-5, were tested in the pressure-box fixture. These panels contained 3 frames, 4 stringers, and a 22-inch longitudinal notch severing skin and the central frame, as was previously shown in Figure 6-1.

The panel configurations were discussed in Section 6.1.1, but will be reviewed here for convenience. Differences in design detail were previously highlighted in Figures 6-2, 6-3, and 6-4. Panel 11b included all-graphite skins with a relatively high hoop modulus, and mechanically-fastened frames with mouseholes that extend beyond the full width of the stringers. Panel 12 was identical to 11b, except that the stringers had a lower axial modulus, the frames were cobonded instead of mechanically fastened, and the mousehole geometry had been slightly modified, as was shown in Figure 6-5 and 7-14. TCAPS-5 featured a graphite-glass intraply hybrid skin with a relatively low hoop modulus and higher-stiffness bolted frames. Glass-fabric pads beneath the frame on TCAPS-5

allowed a direct mechanical attachment between the frame and the stringer flange, and the mousehole configuration to be significantly narrower.

All panels were subjected to internal pressure only. Detailed discussions of the Panel 11b and TCAPS-5 tests are contained in [23] and [38], respectively. Figures 8-9, 8-10, and 8-11 illustrate the damage state in each panel after completion of the tests. Panel 11b exhibited damage growth from 22 to 36 inches at 9.3 psi, then an additional growth event at 10.0 psi that resulted in the damage extending to, and slightly beyond, the adjacent unsevered frames. Panel 12 also exhibited a damage growth event at 9.3 psi, but unlike Panel 11b, the damage continued well beyond the unsevered frames to the fasteners that attached the axial load introduction doublers to the panel edge. The damage in both panels was characterized by extensive delamination and a region of intense fiber failure. TCAPS-5 reached a maximum pressure of 15.5 psi, when pressure-box air supply limitations precluded further loading. Its final damage state was characterized by delaminations and fiber failure regions on the order of only 3 to 4 inches, despite sustaining 55% higher pressure than Panel 11b.

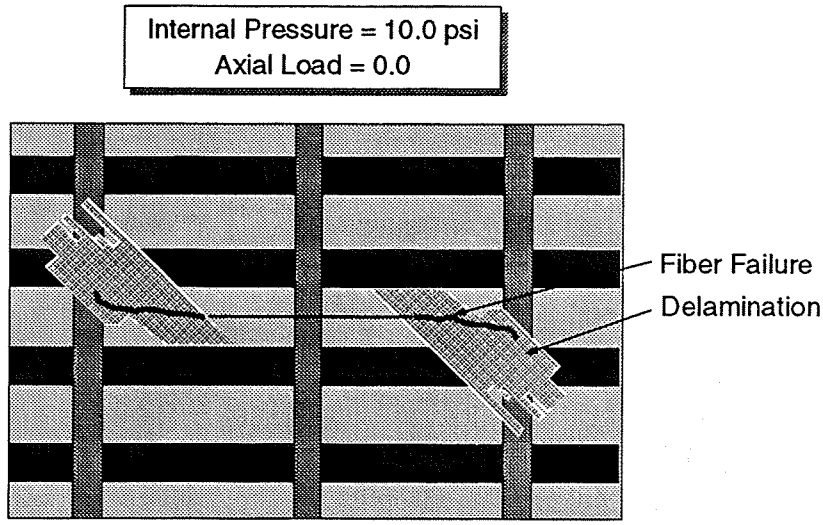

Figure 8-9. Panel 11b final damage state.

Residual strength response was predicted for these panels using power-law extrapolations of notched strength data from flat unstiffened laminates in combination with metallic elastic-plastic configurational correction factors that were modified to account for modulus differences. These predictions are compared with the actual damage growth in Figure 8-12. The prediction for Panel 11b was reasonably accurate for damage growth in the skin, but overpredicted the load transfer to, and hence the beneficial effect of, the undamaged adjacent frames. Deviations from these predictions were not unexpected due to differences between composite and metallic damage localization and structural configurations. Similar comparisons are seen with Panel 12, except without the arrest either prior to or at the adjacent frame. In this case, the skin-to-frame load transfer was additionally reduced by the skin delaminations that accompanied the advancing damage. Predictions of TCAPS-5 response were not as accurate. The response, however,

exceeded its much higher predicted capability, providing further evidence of the superior toughness of the hybridized laminates.

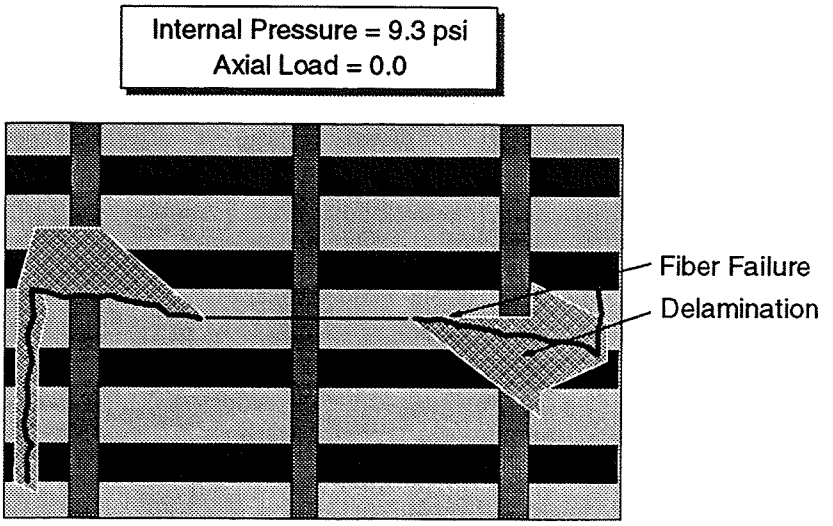

Figure 8-10. Panel 12 final damage state.

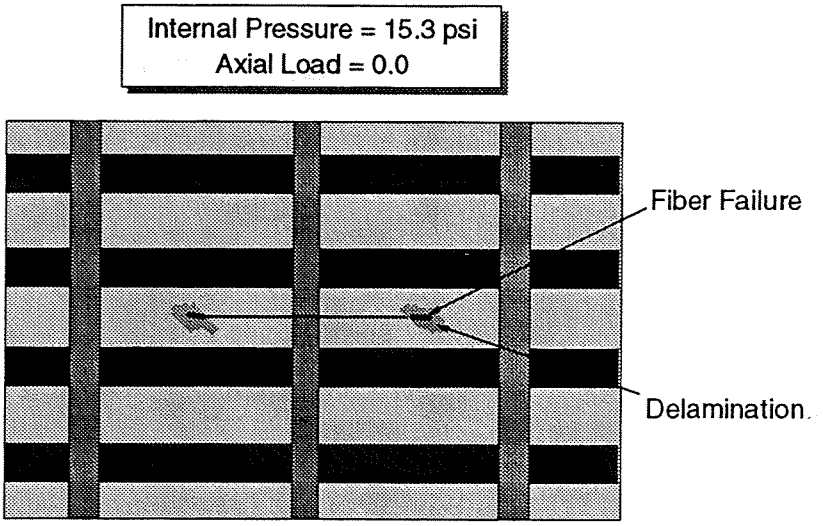

Figure 8-11. TCAPS-5 final damage state.

The R-curve approach was also applied to the prediction of TCAPS-5 under non-ATCAS funding [45]. The material toughness was obtained from unstiffened tests, as previously described. The complexity of the structural configuration (i.e., frames, stringers, and curvature) necessitated the crack driving forces to be determined using finite element analyses with varying notch lengths. Self-similar crack growth was again assumed. Comparison of this method with experimental observations are contained in [45]. The usefulness of this method is reliant on computation advantages relative to strain-softening

approaches to counteract the added assumption of self-similar crack growth. These advantages, if any, have not been determined.

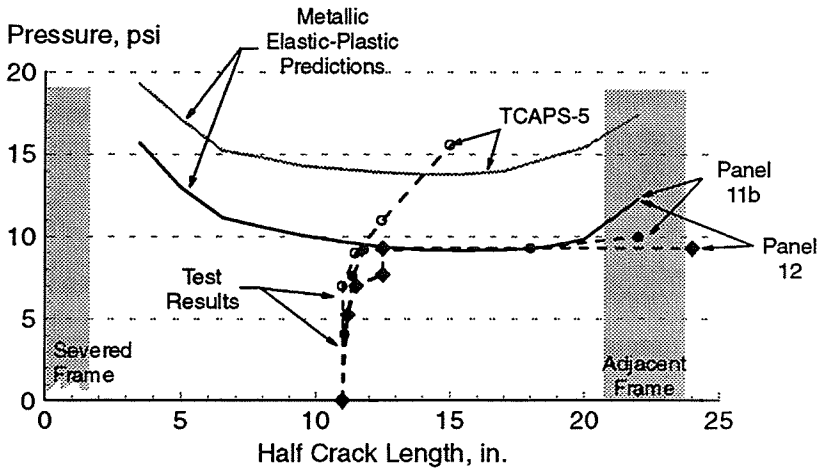

Figure 8-12. Comparison of predicted and measured damage growth in crown pressure-box test panels.

A comparison of the Panel 11b, Panel 12, and TCAPS-5 test results with the limit loading requirements is shown in Figure 8-13. Panel 11b exceeded by 13% the limit *pressure plus flight loads* condition that was tested. A positive slope to the interaction curve is expected [46], and this margin provides some confidence that the design could meet the highest axial compression condition. A strong argument can also be made that such a design would meet the limit *overpressure* requirement, since only a 1% improvement is needed as the resultant axial load relating to the bulkhead reaction of the pressure is applied. The pressure level withstood by Panel 12 was above the 8.85 psi requirement for the limit *pressure plus flight load* case. Its ability to meet the *overpressure* requirement, however, is in doubt. The TCAPS-5 result exceeded all requirements by a substantial margin.

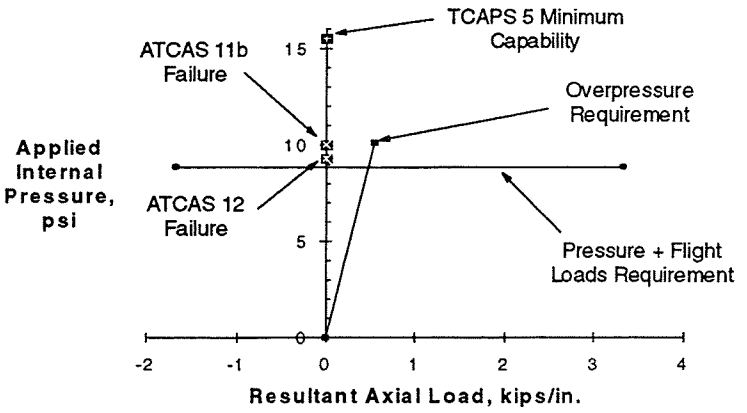

Figure 8-13. Comparison of crown hoop damage tolerance results relative to regulatory requirements.

The absence of damage arrest at the unsevered frames raises concerns relative to the performance of bonded frame concepts in damage tolerance scenarios. Visual inspection of the frames after failure revealed nearly complete separation from the majority of the skin, with one or two surface plies still attached to the frame. It is hypothesized that surface-ply delaminations associated with the advancing damage decoupled the frame from the load-carrying skin plies, effectively eliminating its ability to arrest the advancing damage. Differences in stringer stiffness, axial load introduction doublers, and test pressure control procedures between Panels 11b and 12 might also have contributed to the differences in damage arrestment at the frames.

Compression damage tolerance of the crown was not addressed relative to skin notches. A large configured compression panel was tested with a simulated 1-bay frame disbond, as discussed in Section 5.1.1 and [19]. The panel successfully sustained limit load levels without failure.

8.1.2 Keel Quadrant

Testing to support damage tolerance evaluations of the keel quadrant were limited to the configurations representative of the aft end. Unconfigured sandwich coupons [7], two 2-frame specimens, and a 4-frame panel were tested in uniaxial compression. As shown in Figure 8-14, machined slits through the OML facesheet and both facesheets were considered.

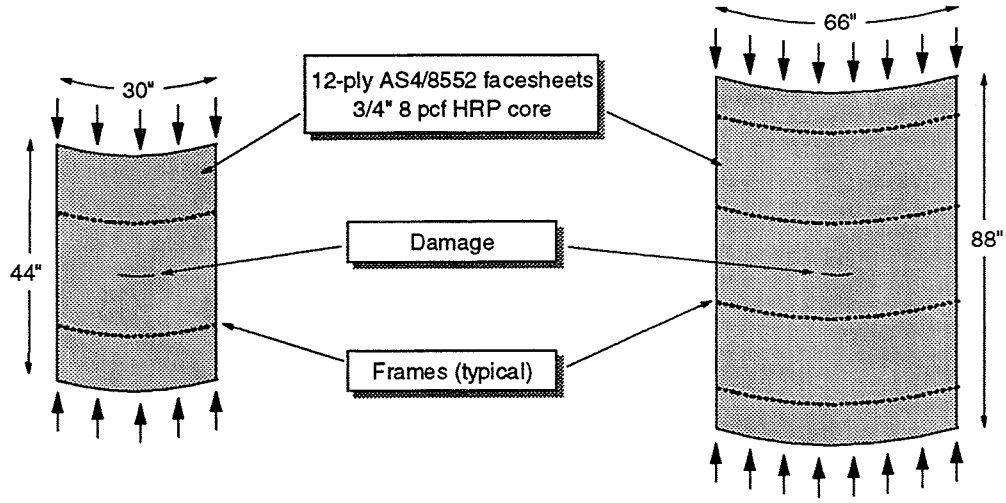

Source Panel	Damage	Qty
AK23	4" notch through both facesheets	2

Panel ID	Damage	Qty
AK25	4" notch through OML facesheet	1
AK25	8.8" notch through both facesheets	1

Figure 8-14. Structural damage tolerance test matrix for aft keel.

The 2-frame specimens, both obtained from a Panel AK23, were tested to failure in compression with 4-inch notches. The loaded specimen ends were potted and the

unloaded edges were constrained by knife edge supports on each facesheet. No restraints were applied to the frames. Immediately prior to failure, small regions of short-wavelength buckling extended approximately 1 inch from each notch tip. Failure was characterized by catastrophic damage growth in both facesheets to the panel edges.

The largest panel, designated AK25, was tested in compression with the two frames nearest the panel center restrained at their ends from radial movement, and the unloaded edges of the panel constrained by knife edge supports on each facesheet. The first notched test was conducted after machining a 4-inch-wide notch through the OML facesheet at the same location as a BVID that was imparted for a previous test (discussed in Section 6.1.2). The panel was loaded to 174 kips, approximately the maximum load expected in the final test. Strain data available from this test provided useful comparisons to similar data from the tests of smaller panels with 4-inch notches through both facesheets; these comparisons, however, were not accomplished during the program.

For the final test, an 8.8-inch-wide notch was machined at the panel center through both facesheets, and the panel tested to failure. The expected failure load based on a power-law curve fit through small (1 to 3 inches) notch data for the same materials and layup was 172 kips. Actual failure occurred at 165 kips, 4% below the power-law curve. The AK25 large notch data point is plotted along with the smaller unconfigured and configured test data in Figure 8-15. Note that the curve is based only on the data from flat unconfigured sandwich coupons.

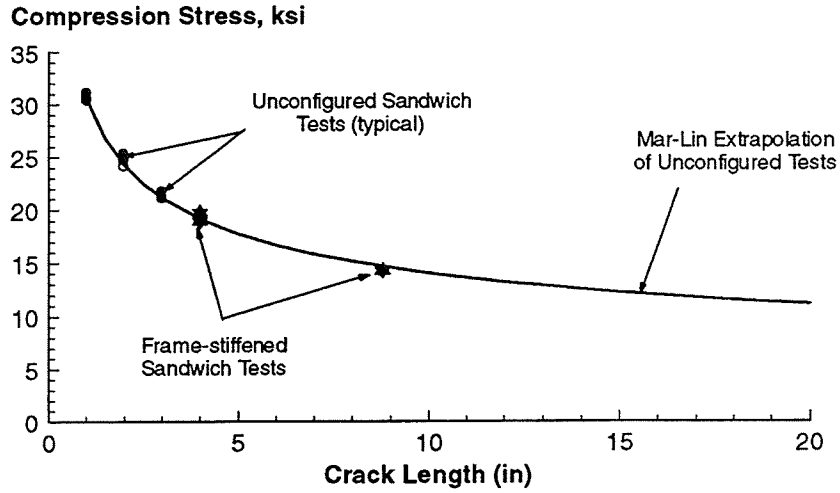

Figure 8-15. Comparison of configured aft keel test result with predictions from unconfigured coupon tests.

Prior to test, finite element analyses that incorporated the strain softening laws developed from the unconfigured tests were conducted for the configured panels. The model for AK25 is shown in Figure 8-16; similar modeling strategies were used for the 2-frame tests. Predicted and measured strain distribution along the symmetry planes of the notched 2-frame specimens are shown in Figure 8-17. The distribution along the loading

axis of the specimen was predicted well, with the exception of the end effects at the potting. Correlation along the panel width was also very good.

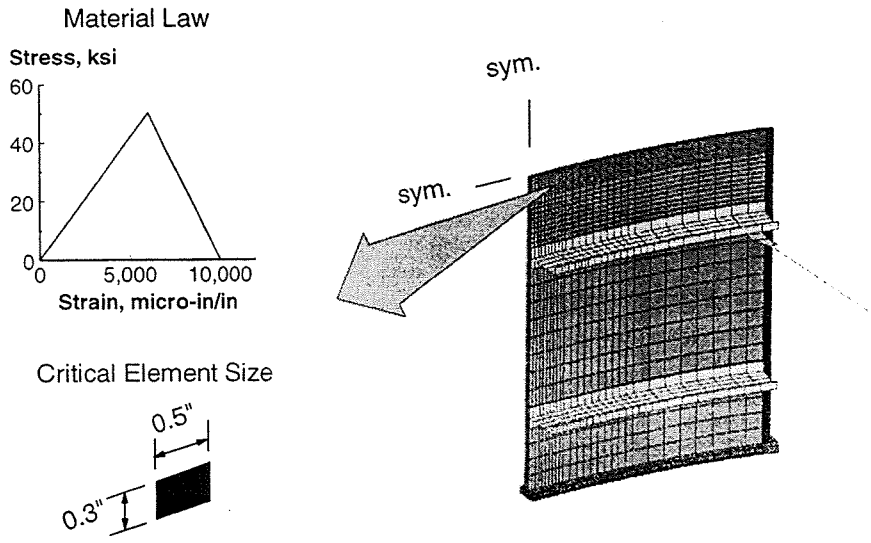

Figure 8-16. Finite element model and strain softening law for 4-frame aft keel damage tolerance simulations.

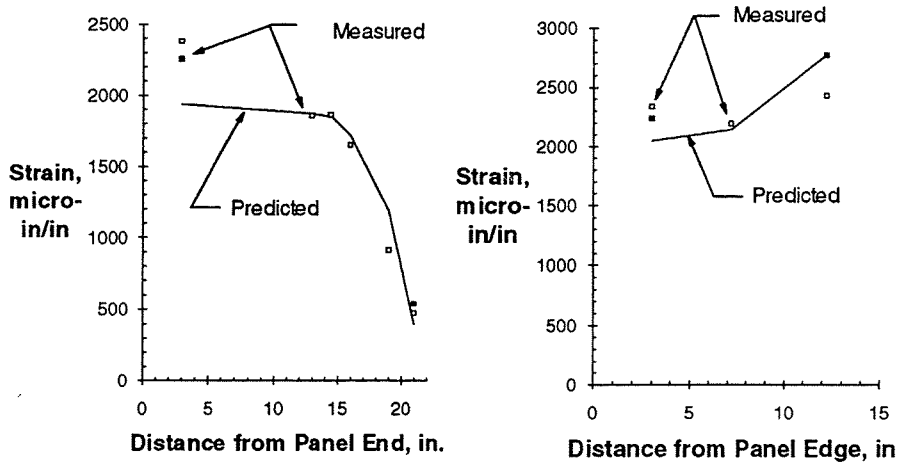

Figure 8-17. Comparison of predicted and measured strain distributions for 2-frame aft keel notched tests.

Failure predictions of these configured panels, in combination with those for similar tests with BVID (discussed in Section 6.1.2), demonstrated the power of the strain softening approach in scaling coupon results to a range of damage sizes and types in configured structure. Excellent agreement was observed between the failure predictions and notched experiments. As shown in Figure 8-18, predictions ranged from approximately 4% to 10% below the measured strengths.

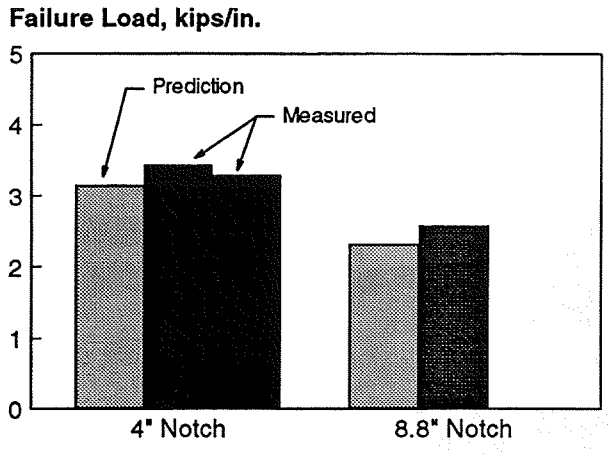

Figure 8-18. Comparison of measure failure loads of aft keel notched compression tests with strain softening predictions.

The large-notch configured test substantiated the damage tolerance methodology used in the keel design, described in Section 3.3.2. Figure 8-19 contains a comparison of the requirements with the capability predicted by the power-law extrapolations of test results, both with and without consideration of the thickness-related strength improvements identified in [7]. (Note that the requirement for the forward and middle keel panel areas addresses smaller damage sizes than the aft end. See Section 3.1.6 for further discussions.) Throughout the length of the keel, the damage tolerance capability aligned well with its requirements. The estimated strength improvements related to increased thickness are strongest in the middle and forward regions, and would provide a maintenance advantage for this design; higher strengths result in larger damage sizes being necessary to reduce structural strength below the required capability, thereby reducing the frequency and/or intensity of inspections necessary to detect such damages. These strength improvements also suggest reduced panel thicknesses may be possible.

8.2 Outstanding Issues

The developments accomplished in ATCAS identified a number of issues relating to structural damage tolerance that remain unresolved. Methods for extending unconfigured notched-strengths to strength predictions for configured composite structural concepts are not well defined. For skin/stringer composite designs, configuration factors derived from metal damage tolerance methodology provided relatively good predictions and strong insights into the need for considering material nonlinearities. However, the configurational and structural response differences between metallic and composite designs (particularly sandwich) make their use for accurate assessments unacceptable. The approach used to obtain these metallic configuration factors, however, offers a good model for composites development (i.e., finite element analyses supported by structural tests).

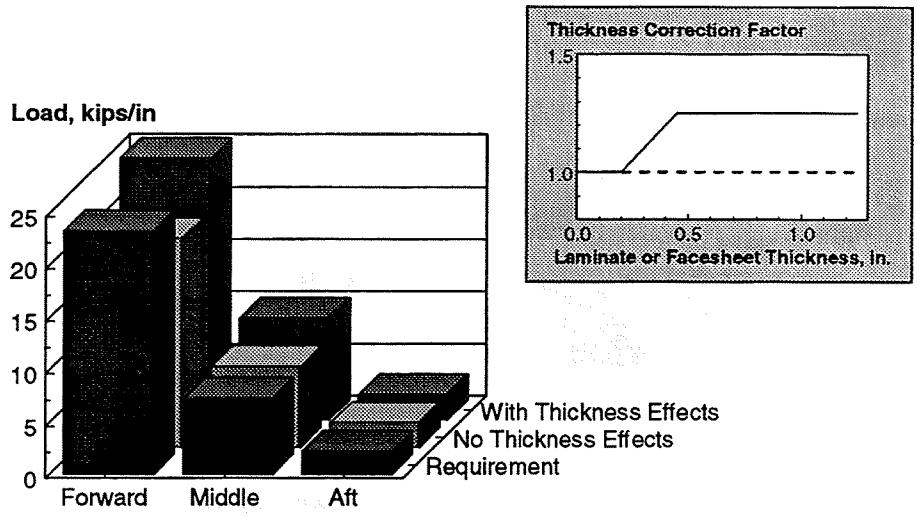

Figure 8-19. Comparison of predicted keel axial compression damage tolerance capability with requirements.

Accurate prediction of load distribution and redistribution is an essential ingredient to successful analytical damage tolerance methodologies. Strain softening material laws appear to capture the aspects of damage-induced material degradation necessary to address the associated load redistribution at a sufficiently high level that it remains computationally compatible with the large finite element models necessary to address structural configurations. Procedures for degrading the skin/stiffener load transfer due to approaching damage are necessary for further application of finite element analyses that use strain-softening laws. The use of non-local material behavior in finite element analyses should also be explored in efforts to improve predictions of strain distributions near damage and eliminate the dependence of strain-softening laws on element mesh due to classical formulations [47].

These methods and supporting tests are needed to properly account for configurational issues specific to composite designs. Specifically, the following aspects require additional consideration: (a) bonded element effectivity in arresting damage growth in skin/stringer and sandwich configurations; (b) effects of damage variables, including shape, location, and orientation; and (c) combined load effects.

The ability of bonded elements to arrest damage was not clearly demonstrated for the developed designs. In the skin/stringer crown, the damage in the pressure-box tests was not arrested at the adjacent frame for the bonded-frame configuration, although the panel was not sufficiently large to allow confident extension of this finding to the true fuselage shell. In the axial damage tolerance 5-stringer panel tests, the damage *was* arrested at the adjacent, undamaged stringers. These panels, however, contained stringers that were very stiff relative to the skin. The smaller relative stiffness difference between the skin and stringers in later crown designs might make arrest less likely. Furthermore, internal pressure, which was not present in these tests, would tend to provide a mode 1 driving

force on significant delaminations in the skin, further reducing load transfer into the stringers. In sandwich structure, the physical distance between the bonded frames and the outer facesheet might also reduce their effectivity in arresting damage there. However, the sandwich construction greatly reduces the pressure-induced local bending at the notch tip. Addressing this issue for sandwich structure is of additional importance since no data exists to justify the use of metallic skin/stringer configuration factors in ATCAS development of composite sandwich designs.

Consideration of additional notch variables is also necessary. Limited evidence collected during crown tension-fracture studies [29] suggested that, compared to machined slits of comparable dimension, sharp penetrations created by an impact event displayed similar strengths (i.e., ±10%) for thin AS4/938 laminates, 25% higher strengths for thicker AS4/938 laminates, and 22% lower strengths for toughened-resin laminates [7]. Sharp penetrations, holes, and other notch shapes should be considered to bound the effects of potential damage threats. Notch shape is expected to have a particularly significant affect on compression strength due to the local-instability failure mechanism suggested by unstiffened results [7].

Neither notch orientation or location have been significantly addressed, either through analysis or test. Simple, estimated methods used to develop the side design indicated that 45° damage tolerance was a critical design driver. Only notches located centrally between elements have been considered. Notches parallel to stiffening elements and either adjacent or beneath them may prove to be more critical than those considered.

Combined load effects on damaged strength must also be more thoroughly evaluated, including axial tension, axial compression, and in-plane shear. This is of particular importance to the side quadrant, where large shear loads are combined with pressure-induced hoop tension and either axial tensile or axial compressive loads. Appropriate interaction relationships are necessary to address the full compliment of potential conditions.

Several material-related issues with structural implications also require additional consideration. Thickness effects on notched compression strength, their scaling to the structural regime, and their resulting influence on the keel and side quadrant designs should be addressed. Environmental effects should be explored for compression, since they are likely to have strong influences on the local-instability failure mechanism suggested by unconfigured tests. Rate-dependent fracture response needs to be quantified, both at a material and structural scale, to address damage containment of discrete penetration events which occur while the fuselage is pressurized.

Finally, investigations of damage states that reduce the structural capability to limit load but are most difficult to detect (i.e., critical damage states) should be pursued. Such damage states should be identified and characterized, and the static and fatigue growth behavior assessed.

9.0 CONCLUDING REMARKS

Activities performed within the ATCAS program have identified and, to varying degrees, addressed critical structural performance issues for composite fuselage concepts. The program's central design process forced the development and implementation of an acceptable design methodology, including criteria and sizing methods. Structural tests of the developed designs, and of attractive alternatives, have provided a large database for validating the design methodology, and assessing the accuracy of detailed predictive methods over a representative design space. The structural evaluations were closely coupled with the manufacturing assessments to ensure consideration of process-induced performance characteristics.

Design Criteria. In general, acceptable design criteria for composite fuselage structure exist, and are extensions of those developed for previous composite applications. However, improvements in several areas are needed. Specifically, major developments are needed to determine appropriate criteria for (a) stiffness and weight effects on vehicle handling and flutter, (b) ultimate strength and stability with partially disbonded frames and sandwich facesheets, (c) shimming and pull-up requirements, and (d) damage-size requirements for damage tolerance of sandwich configurations. Relatively minor developments are necessary to address criteria for (a) skin postbuckling and stringer column buckling of skin/stringer configurations, and (b) critical damage conditions associated with ultimate strength.

Internal Loads. Analysis methods for predicting general internal load distributions in fuselage structure are well established for metallic materials, and no major obstacles are expected in extending these methods to composite fuselage structure. Large-scale verification of these methods is necessary. Simplified methods and modeling guidelines for simulating the effects of nonlinear phenomenon on internal load distributions (e.g., reduced effective skin stiffness due to postbuckling, distance over which added plies become fully effective) that are compatible with the computationally-intensive preliminary design environment have not been developed. Similarly, the effect of non-local material response on load distributions in the vicinity of cutouts must be experimentally assessed, and appropriate methods developed as necessary for including these effects in loads modeling activities.

Stability. Detailed analysis methods for addressing compression stability of composite structures are well established and verified. These methods accurately predicted the experimental load levels at the onset of instability and the associated mode shapes for a range of scales and configurations. Similar approaches for addressing shear and combined compression/shear stability must be developed and verified. Methods for including the effect of impact damage on stability response must also be developed and verified. Modeling of the damage as a soft inclusion, either explicitly or through a strain-softening approach, appears to be attractive in this regard. Closed-form methods addressing idealized boundary conditions also exist, and are compatible with the needs of design sizing activities. However, calibration of these methods to reflect actual response

of fuselage structural arrangements is needed. This calibration can likely be accomplished primarily through detailed structural analyses, augmented by limited experiments.

Ultimate Strength. Detailed predictive methods for ultimate strength are not as well developed. General criteria for predicting damage onset and growth are needed for in-plane and through-thickness concentrations, and combined loadings. Prediction of load redistribution caused by the damage is an essential component to accurate predictions of structural failure. Finite element models incorporating strain-softening material laws have demonstrated the ability to predict structural failures, although only with initial damage located remote to complex design details. Similar capability is needed for the more difficult locations.

In general, structural tests have demonstrated adequate ultimate load capability for the ATCAS design concepts, within the bounds of the conditions tested. The premature failure of the pressure-box panel subjected to high axial loads with internal pressure was strongly influenced by load introduction effects. This emphasizes the importance of extending these test responses to the behavior within the true fuselage shell. Within these limitations, however, the successful demonstration of ultimate strength has validated the methodologies used in developing the designs. Conditions requiring more rigorous validation include impact damage, environment, and the statistical variation of structural failure.

Attachment and Splice Strength. Structural tests have demonstrated the integrity of the bonded attachment of the circumferential frames and stringers to the skin, although the effects of impact damage, environment, and cyclic loading have not been adequately addressed. Specifically, failures only occurred along the bondline when the skin contained a fabric surface ply; otherwise, element separation was controlled by the transverse strength of the skin laminate. Strength-of-materials criteria provide a first approximation of damage initiation. Detailed finite element models in conjunction with energy-based failure criteria can be used to predict bonded element separation, but are costly and/or of limited scope. Approaches are needed for addressing (a) damage propagation through the skin laminate thickness and (b) loading/geometry changes along the length of the element. Failure criteria must also be validated, and integrated into a generalized methodology addressing interactions between bondline stresses and skin concentrations. Methods for sizing mechanical connections within quadrants appear adequate.

Detailed methods for assessing performance of splices exist, though no splice tests of significant size have been conducted to verify the ATCAS structural arrangements. Design details of specific concern include the splicing of closed-section hat stringers and full-depth sandwich close-outs. Methods for predicting load distribution exist, but must be verified for ATCAS configurations. Moreover, methods to address the redistribution associated with local damage formation are needed. Splice development efforts must remain closely tied to manufacturing progress to ensure consideration of expected part tolerances.

Damage Tolerance. Extensive experimental data has augmented the development of damage tolerance predictive methods. This data suggests that strain-softening and non-local material responses are active in damage tolerance scenarios. The success of strain-softening analytical models in accurately scaling coupon results to structural configurations, and the dependency of these laws on element size, provide strong support for this conclusion. Additional development, however, is needed to address efficient determination of the material laws and the degradation of load transfer to undamaged structural elements. Development of analytical capability to address non-local material response is also needed to improve predictions of damage-induced load gradients.

Axial damage tolerance was experimentally demonstrated for both the crown and the aft keel. Hoop damage tolerance was demonstrated for the perceived critical loading condition (i.e., internal pressure only) for the skin-stiffened crown with a bolted frame/skin attachment; however, the ability of bonded frames to arrest damage under these conditions was not clearly demonstrated for the crown designs. The effectivity of bonded elements in arresting damage growth, therefore, requires additional analytical and experimental evaluation. Graphite-glass intraply hybrid skin concepts were also demonstrated to have vastly superior damage tolerance performance, which can potentially eliminate damage tolerance as a design driver and increase inspection intervals. Major issues requiring additional experimental data include the effects of damage variables (e.g., shape, location, and orientation), combined loads, dynamic events, cyclic loading of large damage, and environment.

10.0 REFERENCES

1. Ilcewicz, L., et al: "Advanced Technology Composite Fuselage - Program Overview," NASA CR-4734, 1997.

2. Ilcewicz, L., et al: "Application of a Design-Build Team Approach to Low Cost and Weight Composite Fuselage Structure," NASA CR-4418, 1991.

3. Flynn, B., et al: "Global Cost and Weight Evaluation of Fuselage Keel Design Concepts," NASA CR-4541, 1993.

4. Polland, D., et al, "Global Cost and Weight Evaluation of Fuselage Side Panel Design Concepts," NASA CR-4730, 1997.

5. Hanson, C., et al: "Design Integration of a Composite Aft Fuselage Barrel Section," *Sixth NASA Advanced Technology Conference*, NASA CP-3326, pp. 461-480, 1996.

6. Ilcewicz, L., et al: "Advanced Technology Composite Fuselage - Design Cost Methods," NASA CR-4737, 1996.

7. Scholz, D., et al: "Advanced Technology Composite Fuselage - Materials and Processes," NASA CR-4731, 1997.

8. Mabson, G., et al: "Cost Optimization Software for Transport Aircraft Design Evaluation (COSTADE) - User's Manual," NASA CR-4738, 1996.

9. Swift, T.: "Fracture Analysis of Stiffened Structure," *Damage Tolerance of Metallic Structures: Analysis Methods and Application, ASTM STP 842*, J. Chang and J. Rudd, eds., ASTM, pp. 69-107, 1984.

10. Niu, M.: *Airframe Structural Design*, Conmilit Press, Ltd., 1988

11. Finn, S., et al: "Analysis of a Pathfinder Shell Subjected to Internal Pressure and Mechanical Loads," *Fifth NASA Advanced Composites Technology Conference*, NASA CP-3294, pp. 33-72, 1995.

12. Carbery, D., et al: "Global /Local Analysis of Internal Load Paths in Support of Composite Fuselage," *Sixth NASA Advanced Composites Technology Conference*, NASA CP-3326, pp. 603-650, 1996.

13. Mar, J., and Lin, K.: "Fracture Mechanics Correlation for Tensile Failure of Filamentary Composites with Holes," *J. of Aircraft*, Vol. 14, No.6, pp.703-704, 1977.

14. Russel, S., et al: "A Weight-Efficient Design Strategy for Cutouts in Composite Transport Structures," *Third NASA Advanced Composite Technology Conference*, NASA CP-3178, pp. 879-898, 1993.

15. Russell, S., "A Unified Methodology for Analysis and Design of Cutouts in Composite Aircraft Structures", NASA CR-201640, 1997.

16. Ambur, D., et al: "Analysis of a D-box Fixture for Testing Curved Stiffened Aircraft Fuselage Panels in Axial Compression and Internal Pressure," *35th SDM Conference,* AIAA Paper 94-1345, 1994.

17. Swanson, G., et al: "Compression Test Results for Stiffened Composite Fuselage Structure," *Fourth NASA Advanced Composites Technology Conference,* NASA CP-3229, pp. 125-180, 1994.

18. Anderson, M., et al: "PASCO: Structural Panel Analysis and Sizing Code - User's Manual," NASA TM-80182, 1981.

19. McGowan, D., et al: "Compression Tests and Nonlinear Analyses of a Stringer- and Frame-Stiffened Graphite-Epoxy Fuselage Crown Panel," *Fifth NASA Advanced Composites Technology Conference*, NASA CP-3294, pp. 321-350, 1995.

20. Avery, W., et al: "Design and Structural Development of a Composite Fuselage Keel Panel," *Fifth NASA/DoD Advanced Technology Conference*, NASA CP-3294, pp. 463-496, 1995.

21. Caiazzo, A., "Tapered Facesheet Sandwich Analysis," Material Science Corporation Technical Final Report, MSC FRP 3208/2206, October, 1992.

22. Smith, P., et al: "Design, Analysis, and Fabrication of a Pressure Box Test Fixture for Tension Damage Tolerance Testing of Curved Fuselage Panels," *Third NASA Advanced Composite Technology Conference*, NASA CP-3178, pp. 789-806, 1993.

23. Rouse, M., and Ambur, D.; "Fuselage Response Simulation of Stiffened Panels Using A Pressure-Box Test Machine," *36th SDM Conference*, AIAA Paper 95-1362, 1995.

24. Walker, T., et al: "Benchmark Panels," NASA CR-194969, 1994.

25. Flynn, B., et al: "Advanced Technology Composite Fuselage - Repair and Damage Assessment Supporting Maintenance," NASA CR-4733, 1997.

26. Polland, D., et al: "Structural Development of Composite Fuselage Cutouts: Window Belt and Door Reinforcements," *Sixth NASA Advanced Technology Conference*, NASA CP-3326, pp. 339-368, 1996.

27. Russell, S., et al: "Design Cost Modeling of Fuselage Door Cutout Structure," *Fifth NASA Advanced Technology Conference*, NASA CP-3294, pp. 127-162, 1995.

28. Dost, E., et al: "Impact Damage Resistance of Composite Fuselage Structure", NASA CR-4658, 1997.

29. Walker, T., et al: "Tension Fracture of Laminates for Transport Fuselage - Part I: Material Screening," *Second NASA Advanced Technology Conference*, NASA CP-3154, pp. 197-238, 1992.

30. McGowan, D., and Ambur, D.: "Compression Response of a Sandwich Fuselage Keel Panel With and Without Damage," *Fifth NASA/DoD Advanced Technology Conference*, NASA CP-3294, pp. 321-350, 1995.

31. Minguet, P. J., et al: "Development of Structural Test Simulating Pressure Pillowing Effects in a Bonded Skin/Stringer/Frame Configuration," *Fourth NASA Advanced Technology Conference*, NASA CP-3229, pp. 863-880, 1994.

32. Minguet, P.J., O'Brien, T.K., "Analysis of Test Methods for Characterizing Skin/Stringer Debonding Failures in Reinforced Composite Panels," Composite Materials: Testing and Design (twelfth Volume), ASTM STP 1274, R.B. Deo and C.R.Saff, EDS., American Society for Testing and Materials, 1996, pp. 105-124.

33. Minguet, P.J., O'Brien, T.K., "Analysis of Skin/Stringer Bond Failure Using a Strain Energy Release Rate Approach," Proceedings of ICCM-10 Conference, Vol.1, pp.245-252, Whistler, B.C., Canada, August 1995.

34. Minguet, P.J., O'Brien, T.K., "Failure Mechanisms around the Interface between a Sandwich Skin and a Bonded Frame," Paper 96-1134, Proceedings of the 37th AIAA Structures, Dynamics and Materials Conference, Salt Lake City, April 1996.

35. Kassapoglou, C., et al: "Design Cost Modelling of Fuselage Splices," *Fifth NASA Advanced Technology Conference*, NASA CP 3294, pp. 163-182, 1995.

36. Kassapoglou, C., et al: "Design of Composite Fuselage Splices for Minimum Weight and Cost," United Technologies Sikorsky Aircraft Final Report, SER-510455, March, 1995.

37. Cohen, D., et al: "Analysis and Testing of Thick Automated Tow Placed (ATP) Joint Structures," *Fourth NASA Advanced Technology Conference*, NASA CP-3229, pp. 181-204, 1994.

38. Walker, T., et al: "Tension Fracture of Laminates for Transport Fuselage - Part III: Structural Configurations," *Fourth NASA Advanced Technology Conference*, NASA CP-3229, pp. 243-264, 1994.

39. Swift, T.: "The Influence of Slow Growth and Net Section Yielding on the Residual Strength of Stiffened Structure," *13th Symposium of the International Committee on Aeronautical Fatigue*, pp. 511-550, 1985.

40. Dopker, B., et al: "Damage Tolerance Analysis of Composite Transport Fuselage Structure," *35th SDM Conference*, AIAA Paper 94-1406, 1994.

41. Ilcewicz, L., et al: "Tension Fracture of Laminates for Transport Fuselage - Part IV: Damage Tolerance Analysis," *Fourth NASA Advanced Technology Conference*, NASA CP-3229, pp. 265-298, 1994.

42. Dopker, B., et al: "Composite Structural Analysis Supporting Affordable Manufacturing and Maintenance," *Sixth NASA Advanced Technology Conference*, NASA CP-3326, pp. 577-602, 1996.

43. Poe, C., et al: "Tension Strength with Discrete Source Damage," *Fifth NASA Advanced Technology Conference*, NASA CP-3294, pp. 369-437, 1995.

44. Walker, T., et al: "Tension Fracture of Laminates for Transport Fuselage - Part II: Large Notches," *Third NASA Advanced Technology Conference*, NASA CP-3178, pp. 727-758, 1993.

45. Wang, J., et al: "Residual Strength Prediction of Fuselage Panel with Discrete Source Damage," *Sixth NASA Advanced Technology Conference*, NASA CP-3326, pp. 701-722, 1996.

46. Smith, P., "Development of Pressure Containment and Damage Tolerance Technology for Composite Fuselage Structures in Large Transport Aircraft," NASA CR-3996, 1986.

47. Bazant, Z., and Cedolin, L., *Stability of Structures*, Oxford University Press, 1991.

48. Wang, J., et al: "Crown Panel Stiffener-Frame Intersection Structural Integrity Analysis," *Fifth NASA Advanced Technology Conference*, NASA CP 3294, pp. 351-368, 1994.

REPORT DOCUMENTATION PAGE

Form Approved
OMB No. 0704-0188

1. AGENCY USE ONLY *(Leave Blank)*	2. REPORT DATE	3. REPORT TYPE AND DATES COVERED
	April 1997	Contractor Report

4. TITLE AND SUBTITLE
Advanced Technology Composite Fuselage - Structural Performance

5. FUNDING NUMBERS
C NAS1-18889
C NAS1-20013 (Task 2)
WU 510-02-13-01

6. AUTHOR(S)
T.H. Walker, P.J. Minguet, B.W. Flynn, D.J. Carbery, G.D. Swanson, and L.B. Ilcewicz

7. PERFORMING ORGANIZATION NAME(S) AND ADDRESS(ES)
The Boeing Company
P.O. Box 3707
Seattle, WA 98124-2207

8. PERFORMING ORGANIZATION REPORT NUMBER

9. SPONSORING / MONITORING AGENCY NAME(S) AND ADDRESS(ES)
National Aeronautics and Space Administration
Langley Research Center
Hampton, VA 23681-0001

10. SPONSORING / MONITORING AGENCY REPORT NUMBER
NASA CR-4732

11. SUPPLEMENTARY NOTES
Langley Technical Monitor: W.T. Freeman, Jr.

12a. DISTRIBUTION / AVAILABILITY STATEMENT
~~FEDD~~ Publicly Available
Subject Category 24

12b. DISTRIBUTION CODE

13. ABSTRACT *(Maximum 200 words)*

Boeing is studying the technologies associated with the application of composite materials to commercial transport fuselage structure under the NASA-sponsored contracts for Advanced Technology Composite Aircraft Structures (ATCAS) and Materials Development Omnibus Contract (MDOC). This report addresses the program activities related to structural performance of the selected concepts, including both the design development and subsequent detailed evaluation.

Design criteria were developed to ensure compliance with regulatory requirements and typical company objectives. Accurate analysis methods were selected and/or developed where practical, and conservative approaches were used where significant approximations were necessary. Design sizing activities supported subsequent development by providing representative design configurations for structural evaluation and by identifying the critical performance issues.

Significant program efforts were directed towards assessing structural performance predictive capability. The structural database collected to perform this assessment was intimately linked to the manufacturing scale-up activities to ensure inclusion of manufacturing-induced performance traits. Mechanical tests were conducted to support the development and critical evaluation of analysis methods addressing internal loads, stability, ultimate strength, attachment and splice strength, and damage tolerance. Unresolved aspects of these performance issues were identified as part of the assessments, providing direction for future development.

14. SUBJECT TERMS
Advanced Composite Technology Program; Transport fuselage; Structural performance; Damage tolerance; Design criteria; Analysis methods; Test results

15. NUMBER OF PAGES
101

16. PRICE CODE

17. SECURITY CLASSIFICATION OF REPORT	18. SECURITY CLASSIFICATION OF THIS PAGE	19. SECURITY CLASSIFICATION OF ABSTRACT	20. LIMITATION OF ABSTRACT
Unclassified	Unclassified	Unclassified	